University of Florence

School of engineering - Department of industrial engineering of Florence "DIEF"

Thesis submitted in fulfilment of the requirements for the award of degree of:

Doctor of Philosophy in

Energy Engineering and Innovative Industrial Technologies

PhD School in Industrial Engineering – XXVII Cycle (2012-2014)

Settore disciplinare ING-IND/09

A hybrid model for reciprocating compressor with FEM acoustic characterization

Tutor

Prof. *Giovanni Ferrara*

Candidate

Dr. *Isacco Stiaccini*

Co-Tutor

Ing. *Lorenzo Ferrari*

PhD Course Coordinator

Prof. *Maurizio De Lucia*

Florence, Italy, December 2014

Declaration

I hereby declare that this submission is my own work and, to the best of my knowledge and belief, it contains no material previously published or written by another person, nor material which to a substantial extent has been accepted for the award of any other degree or diploma at University of Florence or any other educational institution, except where due references are provided in the thesis itself.

Any contribution made to the research by others I have been working with is explicitly acknowledged in the thesis.

_____

Isacco Stiaccini

December 2014

Ringraziamenti

Innanzi tutto desidero ringraziare i Prof. Ennio Carnevale e Giovanni Ferrara per la possibilità concessami di poter intraprendere e seguire il percorso del dottorato di ricerca, percorso non solo di alta formazione scientifica e professionale, ma soprattutto di crescita personale. In particolare, ringrazio il Prof. Giovanni Ferrara nella figura di tutor, sempre pronto ad indirizzarmi sia professionalmente sia nella maturazione come individuo e membro di un gruppo di lavoro. Un sentito ringraziamento all'Ing. Lorenzo Ferrari, che con pazienza e dedizione mi ha seguito e supportato nelle attività cui ho partecipato in questi tre anni.

Un particolare ringraziamento a tutti i colleghi del gruppo di ricerca REASE, Alessandro, Alfonso, Andrea F., Andrea T., Davide, Francesco, Fabio, Furio, Giovanni G., Giovanni V., Giulio, Luca e Michele che quotidianamente hanno contribuito nel rendere piacevoli e costruttive tutte le giornate passate in Facoltà. Un ringraziamento speciale a Giovanni G. e Luca R. per il contributo alla realizzazione di questo lavoro di Tesi, e soprattutto per aver condiviso e superato assieme le difficoltà incontrate durante l'attività.

Una persona speciale che non posso non menzionare, Fabio T., che ringrazio per il contributo sia alla scrittura della Tesi, ma soprattutto per aver arricchito con la sua conoscenza sconfinata il mio percorso formativo.

A questo punto impossibile non ringraziare Fabio, l'amico di sempre, compagno di tutte le avventure degli ultimi venti anni, sostegno e riferimento costante.

Un ringraziamento speciale a Valentina, che con pazienza mi ha supportato in ogni momento di questo percorso formativo.

Infine, ultimi ma non meno importanti, ringrazio i miei genitori e tutta la famiglia, senza i quali niente di tutto questo sarebbe stato possibile.

Contents

List of figures

List of tables

List of symbols and acronyms

a	Sound speed	[m/s]
A	Passage area	[m^2]
	Forward acoustic wave amplitude	[Pa]
b	Dynamic damping	[N s/m]
B	Backward acoustic wave amplitude	[Pa]
C	Gas volumetric capacity	-
	Coefficient	-
d	Diameter	[m]
D	Piston diameter	[m]
F	Force	[N]
i	Imaginary part	-
k	Stiffness	[N/m]
	Wavenumber	[rad/m]
K_s	Flow coefficient	-
l	Rod length	[m]
	Duct length	[m]
m	Mass	[kg]
$\dot{m}$	Mass flow	[kg/s]
M	Mass	[kg]
p	Pressure	[Pa]
q	Acoustic source distribution	[kg/(m3 s)]
$\dot{Q}$	Heat flow	[W]
r	Compression ratio	-
	Crank Radius	[m]

	Reflection coefficient	-
R	Reflection coefficient	-
s	Displacement	[m]
S	Surface	[m^2]
t	Time	[s]
	Transmission coefficient	-
T	Temperature	[K]
u	Specific internal energy	[J/kg]
v	Gas flow velocity	[m/s]
	Acoustic particle velocity	[m/s]
$\bar{v}$	Average velocity	[m/s]
V	Volume	[m^3]
x	Displacement	[m]
$\dot{x}$	Velocity	[m/s]
$\ddot{x}$	Acceleration	[m/s^2]
W	Work absorbed per cycle	[J/cycle]
Y	Characteristic impedance	[kg/(m^2 s)]
Z	Acoustic impedance	[kg/(m^2 s)]

Greek symbols

α	Attenuation constant	-
Δp	Pressure drop	[Pa]
λ	Filling coefficient	-
	Thermal conductivity	[W/(m K)]
ξ	Valve loss coefficient	-
γ	Specific heats ratio	-
μ	Dynamic viscosity	[Pa s]
ρ	Gas density	[kg/m^3]
σ	Clearance volume ratio	-
ψ	Loss factor	-
ω	Pulsation frequency	[rad/s]
Ω	Area	[m^2]

Subscripts

0	Average
01	Total upstream
1	Upstream
2	Downstream
$anec$	Anechoic termination
cyl	Cylinder
d	Downstream
D	Drag
$disch$	Discharge
exp	Experimental
f	Gas Flow
$hole$	Valve plate hole
H	Heating
L	Leakage
n	Normal to a surface
p	Piston
	Preload
r	Reed
	Rebound
$rigid$	Rigid termination
sim	Simulation
$suct$	Suction
u	Upstream
v	Valve

Acronyms

BC	Boundary Condition
BDC	Bottom Dead Centre
CA	Crank Angle
CAC	Crank Angle Calculator
FEM	Finite Element Method
FFT	Fast Fourier Transform
ICE	Internal Combustion Engine

IFFT	Inverse Fast Fourier Transform
Re.Co.A.	Reciprocating Compressor Analysis
TDC	Top Dead Centre

Introduction

Reciprocating compressors are a specific type of machinery designed to increase the pressure of a gas. Because of their very efficient method of compressing almost any gas mixture in wide range of pressures, they are a vital component for both industrial plants and civil applications. The large diffusion of reciprocating compressors and their high maintenance costs, together with the increasing worldwide demand for higher efficiency, require more accurate and detailed design processes, which are oriented both to performance optimization and increased reliability. Up to now, the development of reciprocating compressors was mainly focused on reliability and effectiveness. Nowadays, particular attention is currently paid to efficiency increase, noise reduction and vibration control.

In the design of reciprocating compressors and their plants, numerical simulations have an important role in the preliminary phases. In order to increase the design accuracy, the simulation tools used in the earliest phases of the design play a key role. These tools need to be as accurate as possible and meet the demands of engineers for usability and short computation times. For this purpose, several simulation tools can be adopted, according to the type of the analysis that need to be carried out. For example, the 0D models give results quickly and allow a global prediction of the compressor performance [1], whereas 3D Computational Fluid-Dynamics (CFD) analyses give the most detailed results [2] but lead to long computation times that cannot be accepted in a preliminary design phase.

A simplified model focusing on the evaluation of a compressor performance with improved description of physical phenomena is presented by R. Aigner et al. [3]. This work deals with the internal flow in a reciprocating compressor and the analysis of the

automatic valves motion. R. Aigner et al. presented both a one-dimensional and a two-dimensional numerical model for the prediction of valve motion and wave propagation inside the cylinder. The simulation results are compared with experimental measurements. A higher model complexity leads to an increase of the computation time, but does not provide any improvements on performance prediction.

In the works by E.Winandy et al. [4] and M. Elhaj et al. [5] simplified tools for the estimation of compressor performance are described and compared with experimental data. Both these works confirm the good predictability of the simplified numerical models.

The coupling of the reciprocating machine to the line is a recurrent topic [6] in industrial applications. The interaction between the machine and the pipelines can entail noise issues, vibrations and mechanical failures. An exemplifying work examining in detail these phenomena is the study by M. G. Nored et al. [7]. In their report, a detailed analysis of pressure wave propagation in the pipelines is shown. The strong influence of pressure wave propagation on failures and mechanical issues of pipeline structures is also reported.

In most cases both compressor and pipeline analyses are performed without considering their reciprocal interaction. Therefore, the influence of the pipeline acoustic response on the compressor thermodynamic cycle is neglected. The interaction between compressor and pipelines has strong influence on valve dynamics, and consequently on the thermodynamic cycle and on the pressure pulsations propagating in the pipelines. It is important to highlight that not only the power consumption and the overall flow rate are important design criteria but also the valve motion and moments on the piston, which influence the life-cycle of the machines considerably.

A method to numerically investigate the interaction between the source of noise and the connected system is to implement a hybrid model in which the compressor (time-domain model) directly acts on the pipelines (frequency-domain model). An example of such method in the literature is found in the work by Tramschek et al. [8] who developed a hybrid model of a single-cylinder chamber communicating with an acoustic pipelines. Moreover, Singh et al. [9] developed a multi-cylinder model in order to evaluate the

interaction among cylinders connected by pipelines. In both cases the acoustic pipelines are modelled by using lumped parameters (i.e. acoustic impedances) that strongly approximate the pipeline geometries (in particular the plena). Thus, the introduction of corrective terms like damping is needed to match the experimental data. In order to consider the effects of real complex geometry of compressor plena on pressure pulsations, a more detailed approach was developed by Novak et al. [10] who defined and used an acoustic FEM impedance function of compressor plena within the numerical model. However, the approach was limited to single inlet-single outlet plena (i.e. compressor with a single cylinder). Also in this case, heuristic parameters are introduced in the model in order to match the experimental data.

This suggests using a more detailed and generally applicable modelling of the compressor boundary elements, with particular attention to the compressor suction and discharge plena, in order to achieve a better matching with experimental data.

In this work is devised and defined a numerical model for the analysis of the reciprocating compressor that takes into account the reciprocal interaction between the machine and the piping system. Moreover, the piping system model allows the introduction of complex geometries with any number of inlets/outlets, by using acoustic FEM simulations procedures.

The hybrid model presented aims at predicting the machine-pipeline interaction and the influence of the pipeline acoustic response on compressor performance. The prompt to investigate this phenomenon came from both the oil&gas and the refrigeration-systems industries collaborating with the Department of Industrial Engineering of Florence University (D.I.E.F). To meet the industrial partners' requests, a fast and flexible numerical model able to support the design phase of the reciprocating compressors was developed. According to the aim, a 0D-1D code has been implemented in MATLAB®, for the simulation of both the reciprocating compressor performance and the pressure wave propagation in the pipelines.

The numerical model is made up by two main sub-models: one is the thermodynamic model of the compressor and the other is the acoustic model of the piping system. The compressor simulation is based on a quasi-stationary approach. The

thermodynamic parameters of the processed gas (i.e. pressure, temperature, density etc.) are analytically computed in subsequent time-steps. During the simulation, gas flow inside the cylinder is regulated by self-acting valves, whose dynamics is computed in parallel to the thermodynamic cycle. The other sub-model is that focused on compressor pipeline (e.g. compressor plena, ducts, orifices, etc.). This sub-model follows the mono-dimensional acoustic approach of the transfer matrix method. This approach allows one to calculate the pressure wave propagation through the elements of a defined geometry with a mono-dimensional approach. A system of linear equations describes the pipeline geometry. The reciprocal interaction of the compressor and pipelines is achieved through the sub-models coupling.

The transfer matrix describing a complex geometry can be obtained from its 3D-numerical acoustic characterization or from experimental measurements. In this work, the acoustic characterization of the compressor plena based on 3D numerical simulations is defined and described. The characterization aims at introducing in the acoustic model also these geometrically complex elements and to extend the hybrid model application to any kind of compressors. Once the transfer matrix of these elements is defined and implemented, the hybrid model allows one to simulate the behavior of pipeline-compressor system featuring complex geometries with little computational resources. This approach is perfectly suited for the preliminary design phases. The modelling of 3D elements with hybrid approach for a multi-port geometry is very innovative and can overcome the limitation of both mono-dimensional time-domain modelling and impedance transfer matrix functions, which cannot simulate elements with complex geometries with good accuracy.

This Thesis consists of four chapters, and describes how the hybrid model was developed to carry out an accurate analysis on a reciprocating compressor during the design phase, by making use of the 3D acoustic characterization.

Chapter 1 is an overview on reciprocating compressors and the connected suction and discharge pipelines. The structure, functioning and basic performance analysis of the machine are described. Moreover, a description of the physical phenomena involving the

pipelines is provided, and the main related issues are described. Particular attention is also paid to the compressor-pipelines interaction.

In Chapter 2 the numerical hybrid model structure is introduced, by presenting the way the interaction between the time-domain and frequency-domain sub-models is implemented. Subsequently, the sub-models of the compressor and the pipelines are described. Particular attention is paid to the acoustic theory, with the theoretical treatment of the basic principles on which the pipelines frequency-domain sub-model is based. Furthermore, the acoustic theory basic principles necessary to carry out an acoustic characterization of a multi-port geometry are described in details. Finally, the hybrid model methodology assessment is presented, by showing a comparison of a test case simulation performed with both the hybrid approach and a commercial 1D code (AMESim® by LMS).

In Chapter 3 the compressor test case is presented, and its technical data are given. All the activities, numerical and experimental, that lead to the compressor numerical validation and characterization are described extensively. The experimental setup for the acquisition of dynamic pressures on the compressor is presented, and the experimental measurement of the valve reeds stiffness is shown. This part of the experimental activity allows collecting fundamental data for the numerical model. In the second part of the chapter, the numerical activity for the compressor plena characterization is presented. The compressor plena are presented and the sensitivity test results on the main aspects of the acoustic FEM characterization are shown.

In Chapter 4 the results of numerical and experimental activities are presented. The comparison between numerical and experimental data is shown and examined. Two configurations of the numerical hybrid model are tested with different boundary conditions for the compressor and the sensitivity of the numerical model to such variations is assessed by comparing the results with experimental data. The advantages in using the hybrid model with the acoustic 3D characterization are highlighted together with the limits of the theoretical assumption done to build the numerical model.

1 The reciprocating compressor

The reciprocating compressor is an operative machine acted by a driver unit, dedicated to the compression of gas. The practice of applying mechanical work for pressure increasing of air has been realized in early times. In fact, operated bellows were used in metal foundries till the Middle Ages. In 1641 Otto von Guericke developed an air pump to create vacuum. On the 8th of May 1654, in Magdeburg, he performed the experiment shown in Figure 1.1. In this demonstration 16 horses could not pull apart the two halves of an evacuated sphere (known from then on as "*Magdeburg hemispheres*"). This experiment, so elementary and innovative at the same time, can be considered as the forerunner of today's piston compressors.

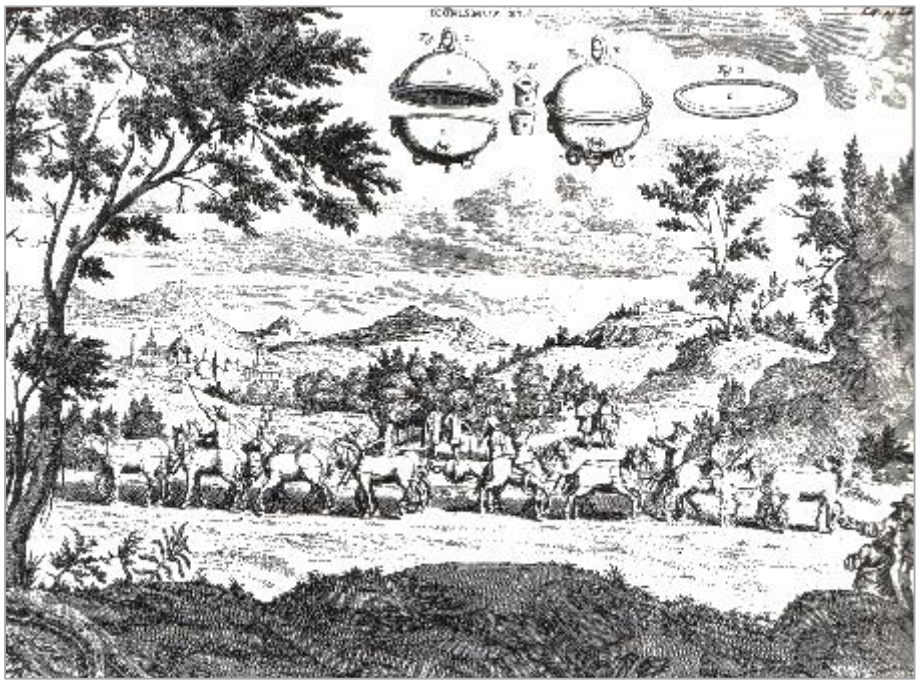

Figure 1.1 Engraving taken from 'Experimental Nova' (1672) by Otto von Guericke showing the evacuated sphere experiment, carried out at Magdeburg.

The development of reciprocating compressors has been supported by the born of the steam engine. The conceptual analogies of the two machines (the former transfers work to the fluid, the latter receives the work from the fluid) allows to couple them in the working conditions (Figure 1.2).

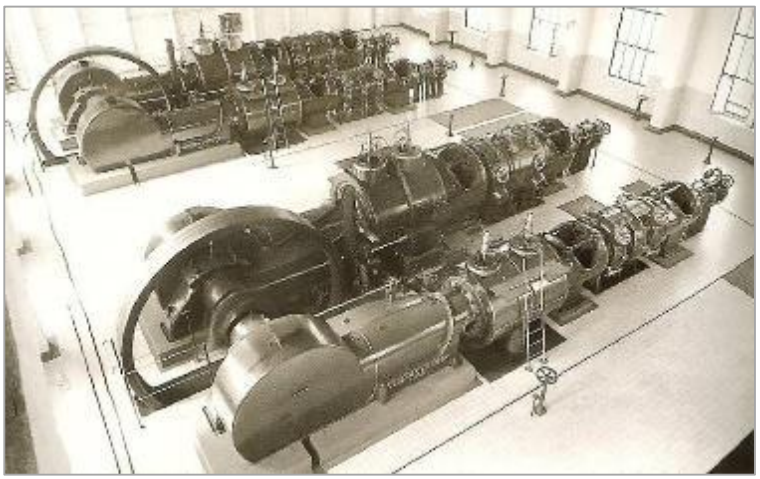

Figure 1.2 A reciprocating compressor acted by a steam engine.

The very efficient compression method and flexibility of working conditions make the reciprocating compressors suitable for the wide range of applications. Nowadays reciprocating compressors are widely employed. Because of their very efficient method of compressing almost any gas mixture in wide range of pressure, they are a fundamental component both for industrial plants and civil applications. They are involved in a high number of processes which differs both for typology and machinery size required: gas transportation and storage, oil&gas industry applications, refrigeration plants (both industrial and civil), and high pressure application such as the LDPE (*Low Density PoliEtilene*) production. It follows that they are the most diffused type of compressor. In fact, worldwide installed reciprocating compressor horsepower is approximately three times that of centrifugal compressors [11].

Reciprocating compressors are widely used when high pressure ratios and low volumetric flow rate are required. In Figure 1.3 the specific field of application of the main typologies of compressors (reciprocating, centrifugal, and screw compressors) are shown. It is important to notice that reciprocating compressors are widely used when high pressure ratios and low volumetric flow rates are required.

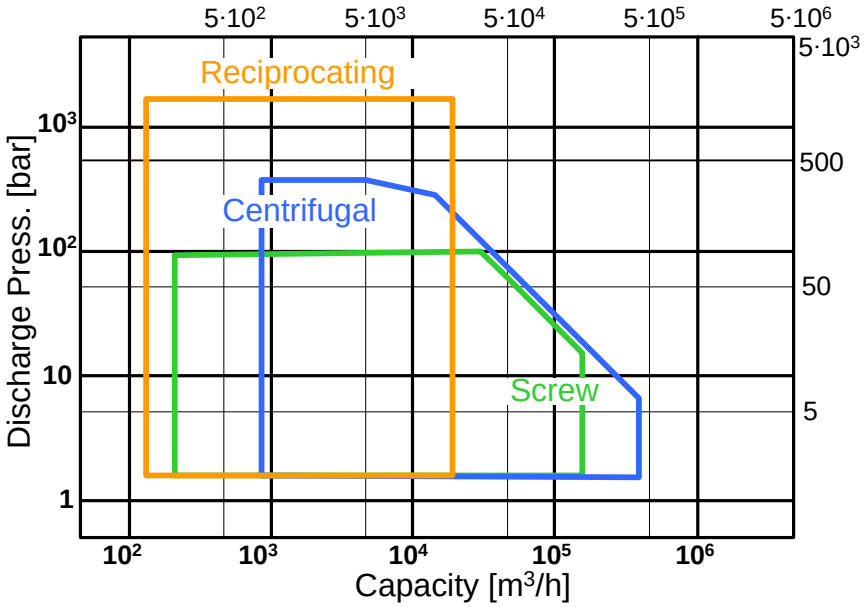

Figure 1.3 Application fields of compressors in function of pressure and volumetric flow.

The main advantages following by the use of reciprocating compressors can be summarized as follows:

- High compression efficiency respect to centrifugal compressors for the same operating conditions (flow rate and pressure ratio). This is more marked for pressure ratios higher than 2;
- High pressure ratios reached with a few stages of compression;
- Low operating condition sensitive respect to gas properties change , in particular for molecular weight variations;
- Effective compression also with low molecular weight gases;
- Good adaptability to flow rate variations.

On the other hand the reciprocating compressors show the following disadvantages respect to centrifugal compressors:

- High installation plot area for a given flow rate*;*
- Higher installation and maintenance costs (approximatively three and half times greater than those for centrifugal compressors);
- Pressure pulsations generation that need to be controlled in order to avoid structural vibrations, structural breaks and high operating conditions noise;

- Necessity of auxiliary plenum systems above the surge point in order to minimize pulsation phenomena;
- Contamination of processed gas with lube oil, necessary for crank thrust lubrication.

It follows that an effective modelling tool is necessary to make preliminary evaluations about the thermodynamic performances of the compressor and the pressure pulsation in the pipelines, in order to avoid and limit undesired effects and reduce the above disadvantages.

1.1 Structure and working principles

The *reciprocating compressor* is an operative machine dedicated to the compression of gas. The machine is acted by a driver unit. The main parts of a reciprocating compressor are the cylinder, the driven piston and the self-acting valves. As shown in Figure 1.4, inside the cylinder is connected by a rod to the crank-angle mechanism. The two cylinder chambers are divided by the self-acting valves from the suction and discharge plena. The self-acting valves are opened or closed by the pressure difference between the cylinder and the *plena* (volume cavity external to the cylinder and connecting the compressor chamber and the pipelines).

Commonly the piston movement compresses the gas inside the two cylinder ends, namely head-end (forward movement) and crank-end (backward movement). This configuration is called double-acting arrangement. In some particular working condition the piston compresses gas in one only cylinder end, while in the other end the gas flows by the suction valves only. This configuration is called *single-acting arrangement*.

The mass flow between the cylinder and the pipelines is regulated by the valves opening. The valves get open by the effect of the upstream/downstream pressure rate and under gas pressure forces. In the rest position and for pressure rate opposing to the flow conventional direction (i.e. from suction to the cylinder and from the cylinder to discharge), they are closed by the force of dedicated springs, whose loads are opposed to the gas flow direction (Figure 1.5).

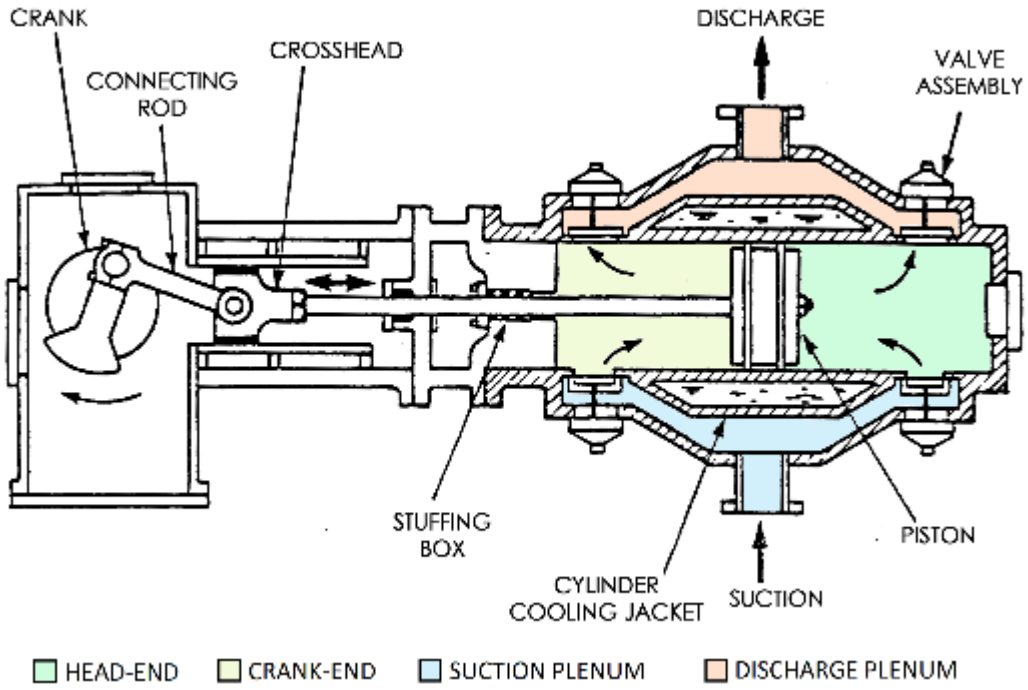

Figure 1.4 Schematic representation of a reciprocating compressor section.

(a)

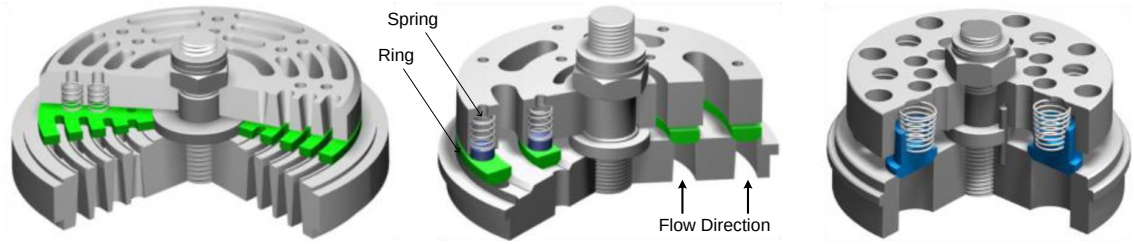

(b)

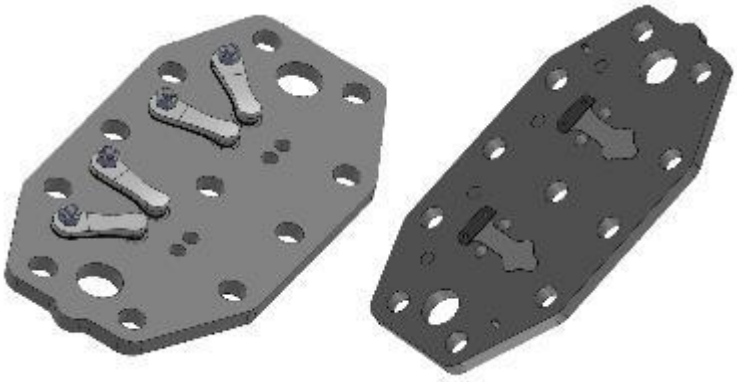

Figure 1.5 Reciprocating compressor self-acting valves. (a) ring valves (b) reed valves, discharge (left) and suction (right).

1.2 Thermodynamic cycle

The reciprocating compressor is a machine that transfers the power received from the drive engine to the handled gas by increasing its pressure from the suction value to the discharge one. It follows the importance of making a performance prediction in terms of adsorbed power, volumetric efficiency, maximum discharge temperature, real mass flow rate etc. This need imposes a rigorous analysis of the thermodynamic cycle.

The thermodynamic cycle of the reciprocating compressor (Figure 1.6) can be evaluated on different level of detail, considering various effects acting on the cycle (e.g. expansion of trapped gas, valve losses, etc.). For each level of detail considered, the thermodynamic cycle can be divided in four different phases. Starting from the TDC piston position, the thermodynamic cycle is composed by the following phases:

- *Expansion* - the valves are closed and the gas trapped in the dead volume at the end of the discharge phase is expanded until the suction pressure is reached;
- *Suction* - the suction valves open because the in-cylinder pressure is lower than the suction pressure, and the gas flows inside the cylinder until the suction pressure is reached;
- *Compression* - the valves are closed and the gas inside the cylinder is compressed until the discharge pressure is reached;
- *Discharge* - the discharge valves open because the in-cylinder pressure is higher than the discharge plenum pressure, and the gas flows outside the cylinder until the discharge pressure is reached.

In the following paragraphs the two different levels of cycle description (i.e. ideal and theoretical) will be described and compared in order to estimate the influence of each effect introduced in the physical model.

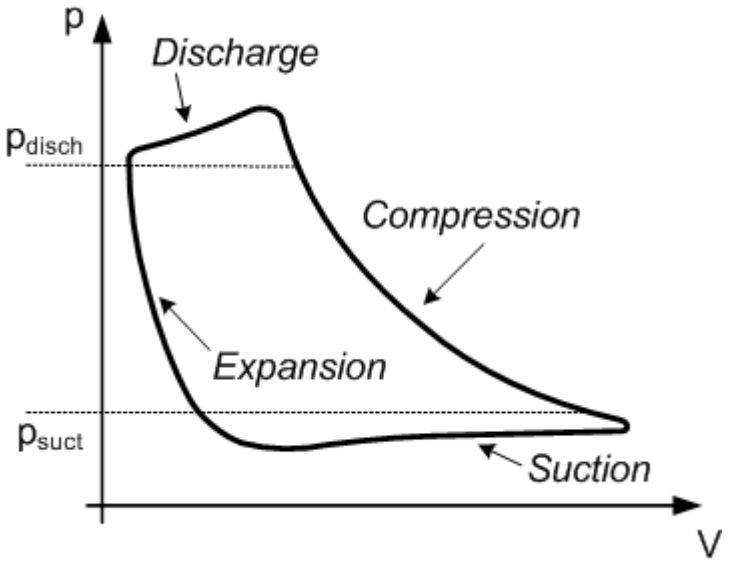

Figure 1.6 Phases of the reciprocating compressor thermodynamic cycle.

1.2.1 Ideal cycle

The ideal cycle analysis is the first and easier way to approach a reciprocating compressor performance evaluation. Figure 1.7 represents the Clapeyron diagram of the thermodynamic cycle. In this diagram, the trend of the in-cylinder pressure in function of the piston displacement is shown. All the cycle phases described above are described through ideal transformations of the gas.

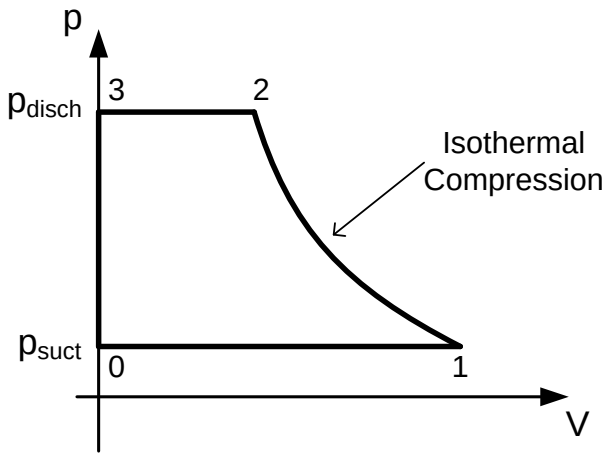

Figure 1.7 Clapeyron diagram of the ideal thermodynamic cycle.

More in details the cycle is composed by the following phases:

- *Suction* (0-1) - the piston moves from the TDC to the BDC, the cylinder is filled with the gas at the suction conditions (pressure and temperature) and the in-cylinder pressure is equal to the suction ambient pressure for the whole phase (*isobaric*);
- *Compression* (1-2) - the gas in the cylinder is compressed from the suction to the discharge pressure. The gas temperature is constant during the whole phase (*isothermal*);
- *Discharge* (2-3) - the compressed gas flows from the cylinder to the discharge ambient, the in-cylinder pressure is equal to the discharge ambient pressure for the whole phase (*isobaric*);
- *Expansion* (3-0) - the ideal expansion is an instantaneous transformation, the in-cylinder pressure drops from the discharge to the suction pressure instantaneously because of the gas was fully discharged and the in cylinder volume at the piston TDC is null[1].

Summarizing the ideal cycle and its four phases, it is composed by two isobaric transformations occurring at the gas inlet/outlet phases, one isothermal transformation corresponding to the gas compression, and an isochoric transformation corresponding to the instantaneous pressure reduction into the cylinder due to the complete discharge of all the compressed gas. The closed area of the cycle represents the work absorbed by the gas compression. The work absorbed in the ideal cycle is the one strictly necessary to compress the gas in one reciprocating compressor cycle, without considering the resistance effects correlated to the valves.

1.2.2 Theoretical cycle

First of all it is important to underline that the real gas compression cycle does not correspond to the theoretical cycle. The differences due to the influence of particular phenomena occurring in the real machine (e.g. presence of lubricant oil, components wearing, etc.) introduce weak discrepancies between the two cycles. However the

[1] In case of clearance between the piston at the TDP and the cylinder head, the residual gas undergoes to an isothermal expansion process.

theoretical cycle can be considered a good approximation of the real one, whereby it takes into account the main aspects of the real physical processes.

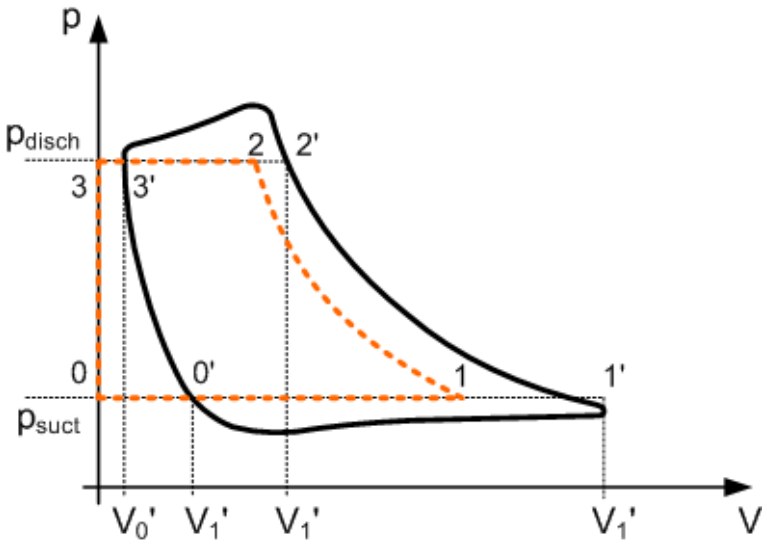

Figure 1.8 Clapeyron diagram of the theoretical cycle compared with the ideal one.

Differently from the ideal cycle, the theoretical cycle takes into account the influence of the following phenomena:

- Valves pressure drops and preload;
- Valves sticking;
- Compression phase deviates from the ideal isothermal transformation;
- Expansion phase due to the trapped gas in the cylinder dead volume;
- Gas heat exchange during the whole thermodynamic cycle;
- Gas leakages from the cylinder due to the non-ideal piston sealing;
- Cylinder pockets.

In Figure 1.8 the theoretical cycle is shown and compared to the ideal one. It is easy to notice that the thermodynamic cycle is composed by the same four phases. However these are modified as described below:

- *Suction* (0'-1') - the suction phase needs an in-cylinder pressure lower than the suction pressure because of the valves pressure losses and preload opposing respectively to the gas flowing inside the cylinder and the valve

opening. Consequently this phase takes place at a pressure lower than the corresponding ideal one;

- *Compression* (1'-2') – the compression phase does not follow an isothermal transformation, due to the heat exchange and non-isentropic effects in the compression process, these differences increase the compression work. However this phase can be well described by a polytropic law;
- *Discharge* (2'-3') - similarly to the suction phase, the discharge phase needs an in-cylinder pressure higher than the discharge pressure because of the valves influence;
- *Expansion* (3'-0') - because of the presence of trapped gas inside the cylinder at the end of the discharge phase, the expansion does not follow an isochoric transformation (instantaneous pressure drop). This difference is due to the re-expansion of the trapped gas from the suction to the discharge pressure. It follows a reduction of the net part of the suction stroke dedicated to the intake, and consequently a decrease of the working fluid capacity of the real machine. A polytropic law describes well this transformation.

1.2.3 Influence of valves on the thermodynamic cycle

The main differences between the theoretical cycle and the ideal one derives from the valve influence, particularly from two main effects due to the springs preload and the gas flow pressure drop due to the gas flowing through the valve. These two effects occur simultaneously, but for a better clarification they will be examined separately.

In Figure 1.9 a scheme of the valve working principle is shown. It can be noticed that self-acting valves are equipped with antagonist springs that assures the closure of the valve moving element. Because of the spring preload this element opposes to the opening. Once the valve is open, the mass flow force acts on the moving element counteracting the spring force until the pressure drop across the valve is enough to allow the gas flow passage.

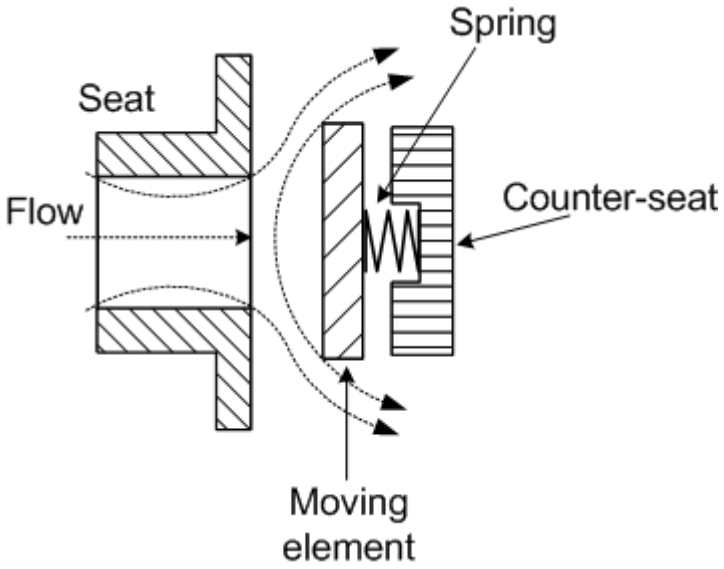

Figure 1.9 Schematic representation of a self-acting valve working principle.

The opposition due to the preload delays the opening of the valve. During the suction phase an in-cylinder pressure lower than the suction pressure is necessary to open the valve (Figure 1.10). Similarly, during the discharge phase an in-cylinder pressure higher than the discharge pressure is necessary. As a consequence of the influence of the springs' opposition, the result is an effective compression ratio that is higher than the nominal one (the rate of discharge and suction pressures). The compressor capacity decreases. The overpressure at the end of the discharge phase establishes a sucked capacity reduction for the re-expansion, starting at a higher pressure and completing at a higher volume. The decrease in intake pressure determines a proportional decrease in gas density, thus the mass flow rate reduction. The preload increases the work absorbed for gas compression at each cycle, even if the work is partially reduced by a reduction in handled gas quantity.

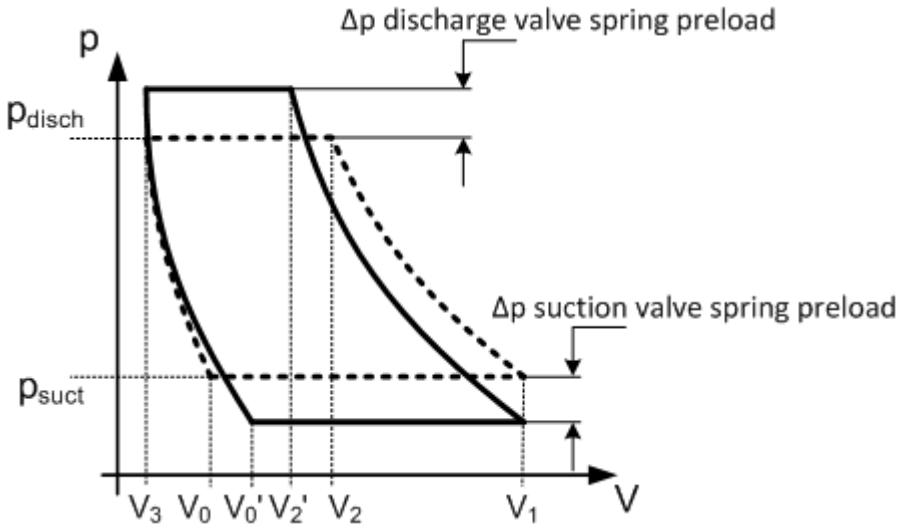

Figure 1.10 Influence of springs preload on the theoretical cycle.

The work absorbed is increased also by the pressure drop due to the gas flowing through the valve. The pressure drop is proportional to the square of gas flow instantaneous velocity. The opposition of the valves to the gas flow establishes further pressure drops that reduce the cylinder inner pressure during the suction phase and to increase the cylinder inner pressure during the discharge phase. It results in a further increase of compression ratio. Consequently, the gas discharge temperature and power spent for the compression are both increased. The effect of the valves losses can be taken into account by introducing a corrective factor ($\psi_v < 1$) that reduces the nominal gas flow.

Due to these influence of the valves on the thermodynamic cycle, it follows the importance to define the valve performance indicators in order to evaluation the valve pressure drop and the valve absorbed power [12].

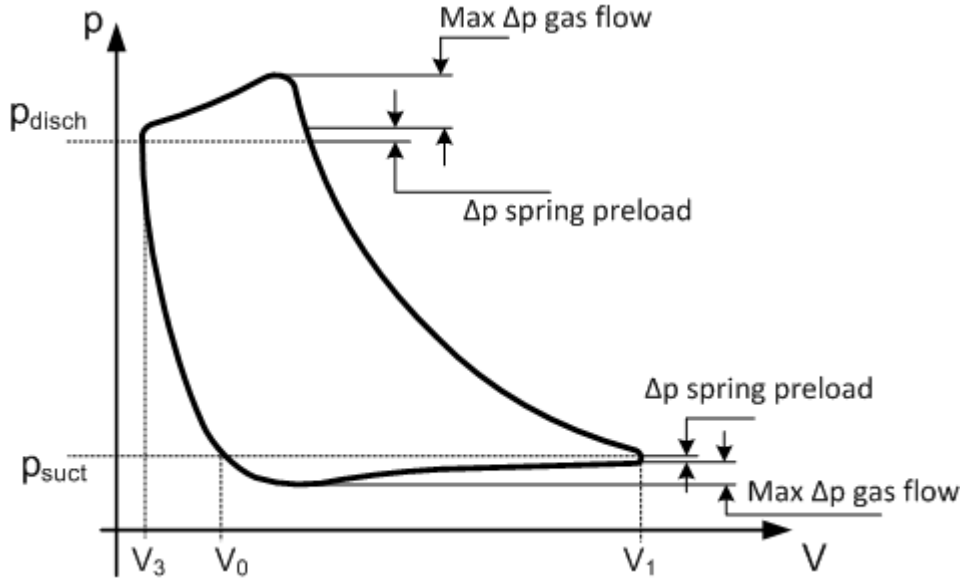

Figure 1.11 Influence of springs preload and pressure drop across the valves on the theoretical cycle.

The valve pressure drop due to the gas flowing through the valve can be evaluated as follow:

$$\Delta p_v = \rho \xi \frac{v_f^2}{2} \quad \textbf{[1.1]}$$

Where ξ is the loss coefficient of the valve (depending on its fluid dynamics features and its geometrical size), ρ is the gas flow density at the valve passage thermodynamic conditions and v_f is the gas flow velocity through the valve.

This formula allows calculating, in first approximation, both the maximum valve pressure drop and the average pressure drop depending only on the values of the valve gas velocities (maximum or average). The valve absorbed power, corresponding to the energy dissipated by the gas passage through the valve during suction and discharge phases, can be evaluated using the following formulas:

$$p_{suct} = \bar{v}_{suct}{}^2 C \xi_{suct} \lambda (3 - 2\lambda) \quad \textbf{[1.2]}$$

$$p_{disch} = \bar{v}_{disch}{}^2 C \xi_{disch} \frac{\lambda}{r^{\frac{1}{\gamma}}} \left(3 - 2 \frac{\lambda}{r^{\frac{1}{\gamma}}} \right) \quad \textbf{[1.3]}$$

Where p_{suct} and p_{disch} are respectively the suction and discharge valve absorbed power, $\bar{v}_{suct}$ and $\bar{v}_{disch}$ are the gas flow average velocities through the valves, C is the

volumetric capacity of gas passing through the valve; r is the compression ratio ($^{p_{suct}}/_{p_{disch}}$), γ is the specific heats ratio and λ is a parameter called filling coefficient.

1.2.4 Loss sources

Hereafter there are depicted the other sources of loss affecting the reciprocating compressor thermodynamic cycle.

The first is the gas heating at the suction side. The work spent for the compression establishes an increase in temperature of the compressed gas. A part of the received heat is transferred by the gas to the cylinder, both to its mechanical components and cooling medium (if provided). Therefore the gas sucked at the intake side at cycle by cycle increases its temperature while is approaching the cylinder, that keeps an intermediate temperature between suction and discharge temperatures. It follows that at the end of the suction phase, the cylinder is effectively filled with a gas warmer than that coming from the suction line. The gas density is lower than the suction nominal density, and consequently the capacity is reduced. This effect can be taken into account by introducing a corrective factor ($\psi_H < 1$) in order to reduce the nominal sucked gas capacity.

Another significant influence is represented by the deviation from isothermal compression during the compression stage. The phenomenon of gas heating during the compression, as a consequence of friction between gas molecules and mechanical parts, implies that that the isothermal curve is replaced by a polytropic compression curve. Generally the compression polytrophic curve can be considered adiabatic (Figure 1.12) with sufficient approximation, according to the following law:

$$pV^{\gamma} = const. \qquad \textbf{[1.4]}$$

Where p is the in-cylinder gas pressure, and V is the volume of the gas inside the cylinder. Otherwise, the heat exchange effects can be considered in the polytropic compression by changing the value of the polytropic law exponent.

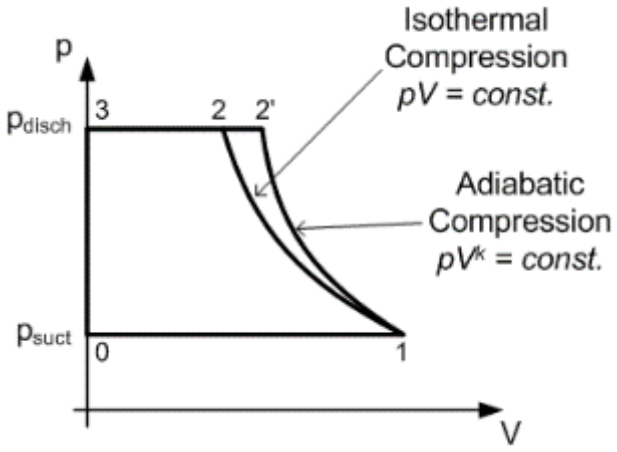

Figure 1.12 Isothermal and adiabatic compression comparison in the ideal cycle.

The presence of the cylinder clearance affects the amount of total volume where the gas is compressed. When the piston arrives at the TDC at the end of the discharge phase, the cylinder inner volume left at the gas disposal is not null. It is the result of the following contributions:

- Piston TDC clearance, necessary to avoid mechanical impacts;
- Inner volumes own of the valves;
- Volumes between valves and cylinder bore;
- Volume between the outer profile of the piston and the cylinder bore.

Therefore a certain amount of residual gas still remains to fill all the volume at its disposal at the discharge pressure. During the expansion phase the piston reverts the motion direction resulting in both a re-expansion of residual gas entrapped into the cylinder and a temperature reduction (contrarily to what happens during the polytropic compression).

Also this re-expansion curve can be considered adiabatic in first approximation, or even using a polytropic law with an exponent lower that the one used for the compression. The re-expansion is completed when the cylinder inner pressure is reduced to the value of the suction pressure, allowing the opening of the suction valve. It follows that the piston stroke dedicated to the gas suction is reduced.

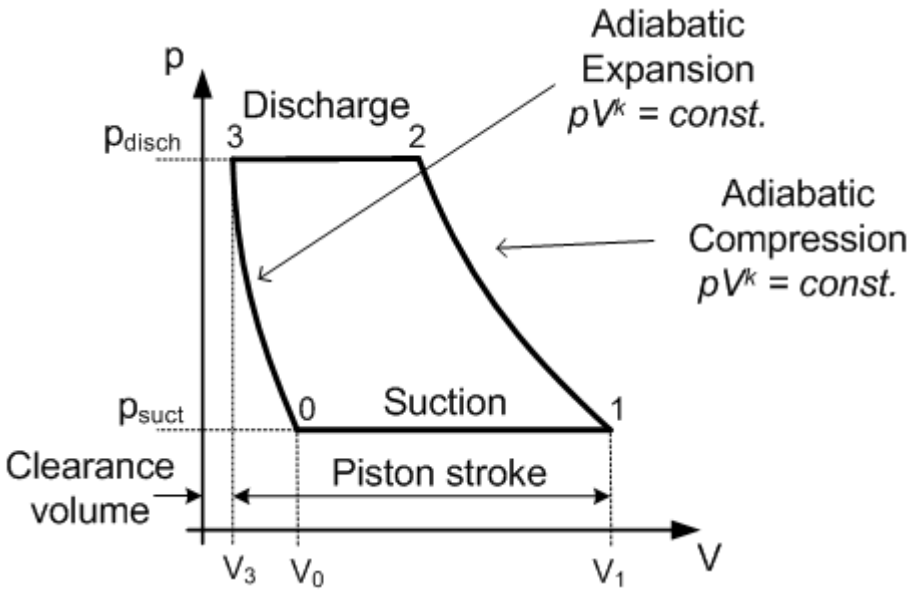

Figure 1.13

In the *pV* cycle, the volume difference V_1-V_3' corresponds to the cylinder displacement V_c (i.e. the volume swept by the piston). The effect of the clearance volume V_3' on the reduction of the handled capacity is higher as higher are both the clearance itself and the compression ratio, as highlighted in Figure 1.14.

The main analytical parameters that fix the effect of the clearance volume on the capacity are the following:

- *Filling coefficient* - it is indicative of how much of the cylinder volume is effectively used in order to get the cylinder capacity:

$$\lambda = \frac{V_1 - V_{0'}}{V_1 - V_{3'}} \qquad \textbf{[1.4]}$$

- *Clearance volume ratio* - it is indicative of how much of the cylinder volume is corresponding to the gas residual volume inside the cylinder at the end of the discharge phase:

$$\sigma = \frac{V_{3'}}{V_1 - V_{3'}} \qquad \textbf{[1.5]}$$

These parameters are connected together by the following relation that establishes the filling coefficient as function of the clearance volume:

$$\lambda = 1 - \sigma \left[\left(\frac{p_{disch}}{p_{suct}} \right)^{1/\gamma} - 1 \right] \qquad \textbf{[1.6]}$$

The parameter λ is the filling coefficient and gives indication about the capacity that can be got from the particular selected cylinder, once the clearance volume σ is known as a function of the compression ratio, This coefficient can be used to compare cylinders involved in the same application, assuming that all the other sources of losses are not taken into account in the comparison.

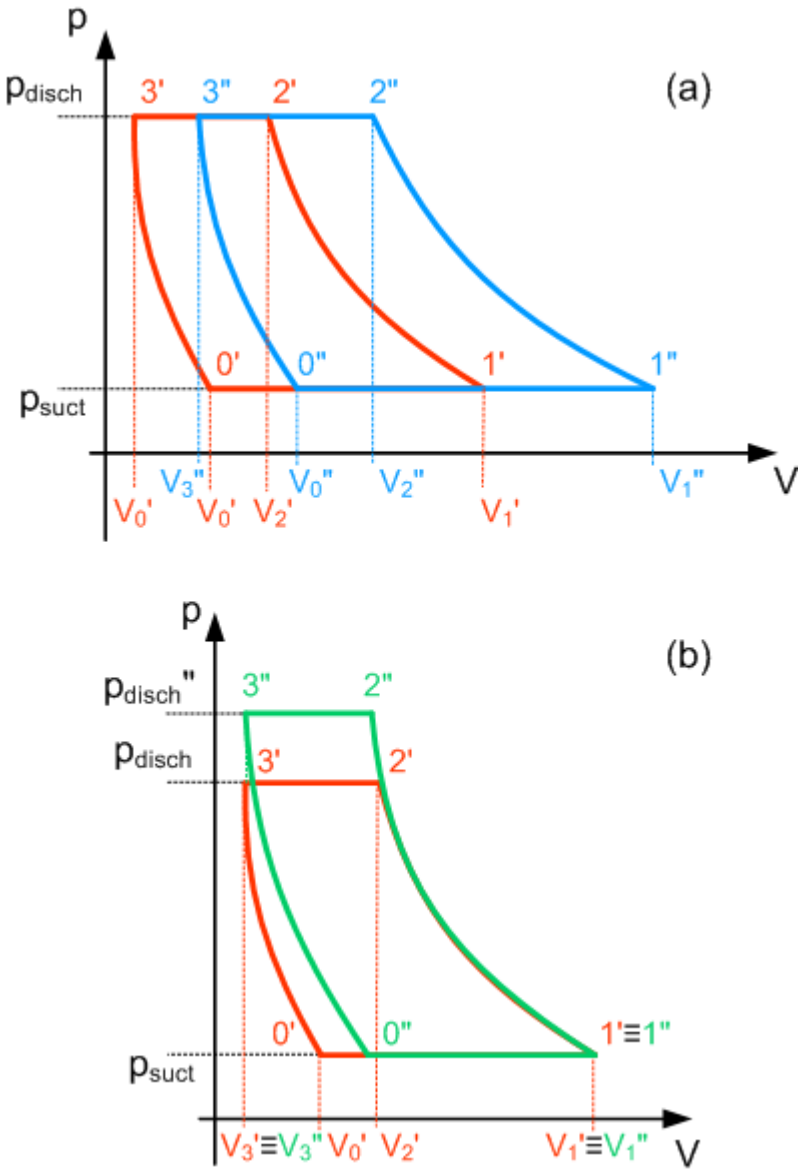

Figure 1.14 (a) Effects of higher clearance volume on the capacity (b) Effects of an increase of pressure ratio on the capacity

Another effect that influences the thermodynamic cycle is the gas leakages. This phenomenon occurs when the seals (mechanical, with or without dedicated gaskets) cannot assure perfect gas tight. More in details the gas leakage can be addressed to the valves (imperfect sealing between the valve moving elements and the valve seats and to an imperfect sealing and between valve seats and cylinder seats) and to the piston rings (considering a double-acting cylinder, when on one side of the piston the pressure reaches its maximum value, on the other side it approaches its minimum, so the pressure difference equals the design pressure ratio and the rings sealing can bring to gas flowing from one side to another).

The amount of the gas leakage is strictly connected to the following parameters:

- *Gas molecular weight* - lower molecular weights bring to greater leakages;
- *Compression ratio* - greater leakages occur with greater r;
- *Rotational speed* - greater leakages occur with lower speeds;
- *Cylinders arrangement* - greater leakages occur for dry lube cylinders and lower occur for the lubricated ones;
- *Operating hours after the last maintenance* - greater leakages occur when the wear rate of the employed components is at the maximum level, close to the next scheduled routine maintenance of the cylinders.

This effect can be taken into account by introducing a corrective factor ($\psi_L < 1$) that reduces the nominal sucked gas capacity.

1.3 Performance indicators

The cycle area enclosed among the two suction and discharge isobar transformations and the compression and expansion curves represents the work spent in a thermodynamic cycle to compress the gas. Therefore, taking into account the compressor rotational speed, that area allows calculating the power used for the gas compression.

In order to optimize the general performance of the compression system, each compression stage should have compression rations within a restricted range.

Basic rules to achieve the optimization of performances are the following:

- *Avoid low compression ratios* - compression ratios lower than 1.5 result in a rather low compression efficiency due to the very high power dissipated at the cylinder valves, compared to the adiabatic power necessary for the gas compression;
- *Avoid high compression ratios* - compression ratios higher than 4 will result both in a rather low volumetric efficiency (low efficiency of the cylinder in terms of capacity) and an excessive discharge gas temperature.

The *volumetric efficiency* is defined as follow:

$$\eta = \frac{V_{suct}}{V_{cyl}} = \frac{C_{suct}}{C_{cyl}} \quad \textbf{[1.7]}$$

Where V_{suct} is the volume of the gas that is sucked by the compressor, C_{suct} is the average volumetric capacity (during intake phase) of sucked gas, and C_{cyl} is the volumetric capacity corresponding to the volume of the cylinder, calculated as a function of geometrical and operational parameters (like bore diameter, rod diameter, stroke, rotational speed).

The *volumetric capacity* is defined as follow:

$$C_{cyl=}\Omega_{cyl} \cdot \bar{v}_p \quad \textbf{[1.8]}$$

Where Ω_{cyl} is the useful area of the cylinder and $\bar{v}_p$ is the average piston speed.

The volumetric efficiency can be expressed as a product of the filling coefficient λ and of the capacity total loss factor ψ, which takes into account the previously described phenomena that bring to losses (gas heating, effects of the valves, gas leakages).

$$\begin{gathered} \eta = \psi\lambda \\ \psi = \psi_v\psi_H\psi_L \end{gathered} \quad \textbf{[1.9]}$$

Then, from the previous formula, the sucked gas capacity can be expressed as follows:

$$C_{suct} = \eta C_{cyl} = (\psi\lambda)(\Omega_{cyl} V_p) \quad \textbf{[1.10]}$$

Because of the importance of evaluating the gas discharge adiabatic temperature, the following formula can be used:

$$T_{disch} = T_{suct} r^{\frac{\gamma-1}{\gamma}} \quad \textbf{[1.12]}$$

Where T_{disch} is the discharge adiabatic temperature, T_{suct} is the suction temperature and γ is the specific heats ratio.

This temperature must be restricted within a certain limit in order not to negatively affect the efficiency and the life of all cylinder components (e.g. piston seals, valves and packing).

The design of compressor with a too high compressor ratio leads to a low volumetric efficiency or to an excessive discharge gas temperature; it should be taken into account the possibility to divide the compression ratio in several compression stages, having all the same compression ratio. First of all it is fundamental minimizing the total power spent for the gas compression, consequently distributing and balancing it between all the stages. Nevertheless, it is important to consider that the multistage arrangement will involve a more complex and more expensive compressor.

1.4 Piping systems and auxiliaries

The reciprocating compressor in industrial application is necessarily composed of a lot of extra components that assure the proper functioning of the full plant. Due to the piston alternate motion, a reciprocating compressor generates a pulsating flow propagating through the suction and discharge lines. In a simplified analysis, the mass flow propagating along the pipelines can be considered as sequence of some periodic pulses of flow that can be assimilated to portions of sinusoid (marked area in Figure 1.15). For a double-acting reciprocating compressor, the pulsating flow doubles its frequency (marked area in Figure 1.16).

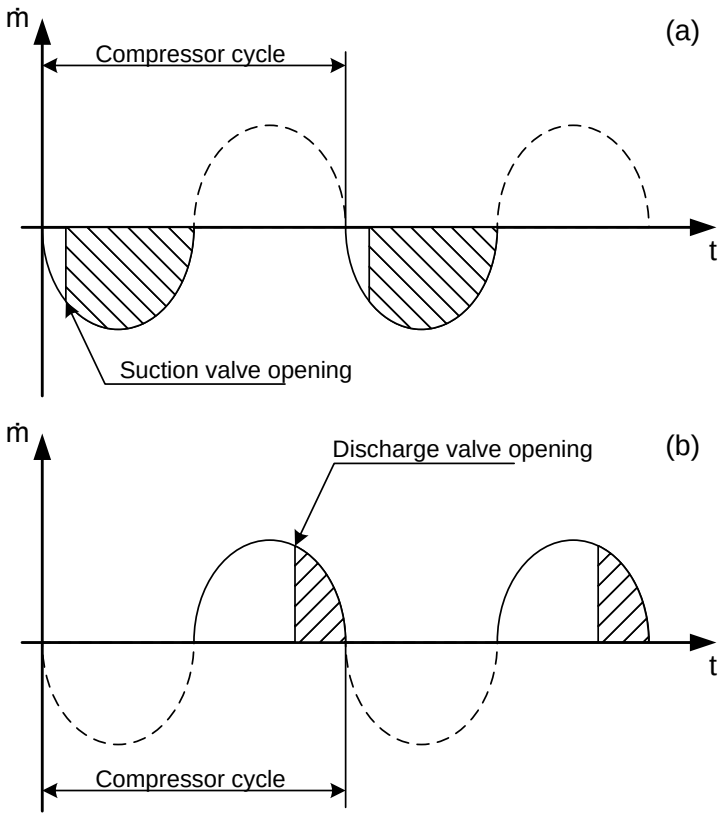

Figure 1.15 Single-acting compressor pulsating flow along the suction (a) and discharge (b) pipelines.

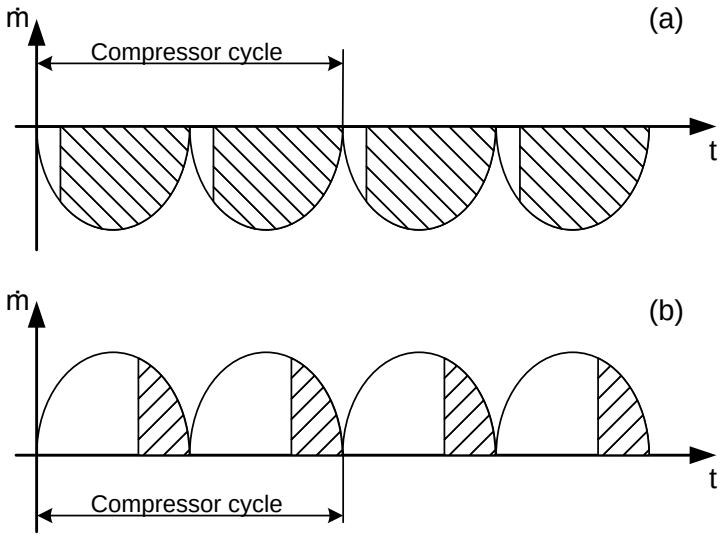

Figure 1.16 Double-acting compressor pulsating flow along the suction (a) and discharge (b) pipelines.

The pulsating flow creates a pulsating pressure field in the fluid domain of the pipelines. The generated pressure waves are composed by a fundamental wave, having

the same frequency of the reciprocating compressor cycle, and by a sum of other harmonic waves. These have a frequency equal to a multiple of the base frequency and decreasing amplitude. The fundamental wave is produced by the piston motion and the harmonic waves are originated by the flow passage through the valves. Along the ducts the pressure waves propagating at the sound speed, interact with the line singularities like duct cross-section variations, regulating valves, vessels etc. This interaction causes the occurrence of reflected waves. The interaction between incident and reflected waves generates the pulsating pressure field. In presence of acoustic resonances, a series of phenomena affecting the pipelines and the compressor can arise [13].

The main issues generated by the pressure pulsations are:

- *Cylinder Natural dynamic overeating/underfeeding* - it occurs when the suction stroke is near to an over pressure peak. For positive peaks, so the gas goes inside the cylinder at a density higher than the nominal one. Otherwise, for negative peaks, the gas has a density lower than the nominal one;
- *Self-acting valves malfunctioning* - it occurs if the acoustic frequency of the pressure waves is the same frequency the natural resonance of the valves mechanical system;
- *Shaking forces on the pipelines components* - forces generated by the pressure pulsations at section discontinuities (e.g. orifices, duct cross section changes, vessel bottoms, etc.) or flow direction deviations. These forces generate structural vibrations;
- *Mechanical vibrations* - occurs when the forces generated by both the machine and the pressure waves are not well neutralized by structural constrains;
- *Noise* - it affects the ambient working conditions;
- *Structural damages* - an undesired consequence of the abovementioned phenomena.

1.4.1 Reciprocating compressor plant

In Figure 1.17 a simplified scheme of a typical reciprocating compressor plant is shown. It is composed by:

1) *Interception valve*;
2) *Gas filter* - dust or abrasive particulate filtering;
3) *Condenser* - gas flow vapour or oil particles reduction;
4) *Vessel* - pressure pulsation amplitudes reduction. In some cases the vessel can be matched with a cooler, which reduces the inlet gas temperature. As a consequence, the gas density is increased and the compressor absorbed power is reduced. The cooler is designed to reduce pressure pulsation amplitudes too;
5) *Plenum* - cavity inside the cylinder basement. The plenum reduces the amplitude of pressure pulsations propagating upstream the compressor;
6) *Reciprocating compressor*
7) *Plenum* - reduction of the amplitude of pressure pulsations propagating downstream the compressor;
8) *Cooler/Vessel*
9) *Condenser*
10) *One-way valve* - compressed gas backflow avoidance in case of machine stop;
11) *Interception valve*.

In case of a non-optimal pipelines design, the pulsation generated by a reciprocating compressor can be particularly high leading to intense wearing, and then an increase of downtime and maintenance costs.

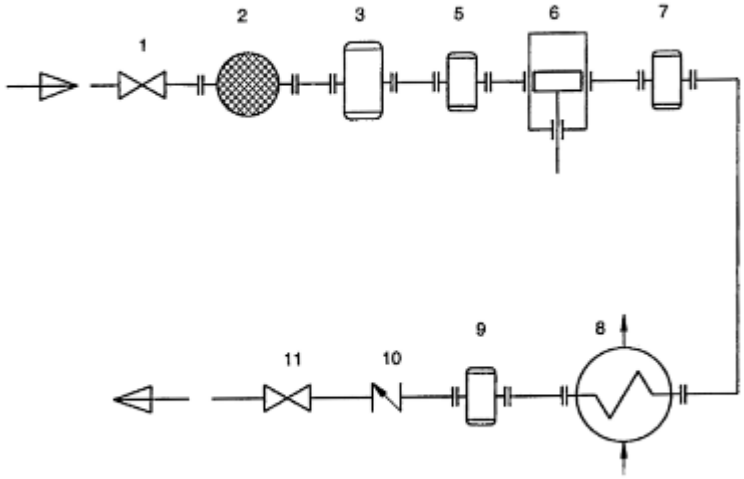

Figure 1.17 Typical reciprocating compressor plant.

1.4.2 Acoustic filters design

In order to reduce the amplitude of pulsating pressures generated by a reciprocating compressor, it is important to provide the pipe line with the proper acoustic filters. The design of the acoustic filters is strongly related whit the entire reciprocating compressor design [6] as illustrated by the scheme of Figure 1.18.

The elements commonly used in order to alter the flow pulsation are: surge volumes, pressure drop elements like orifice and restrictions, and acoustic filters. To reduce pulsation in high flow environment, using only surge volume, it would require an unrealistic large sure volume, for this reason acoustic filter represents a better solution.

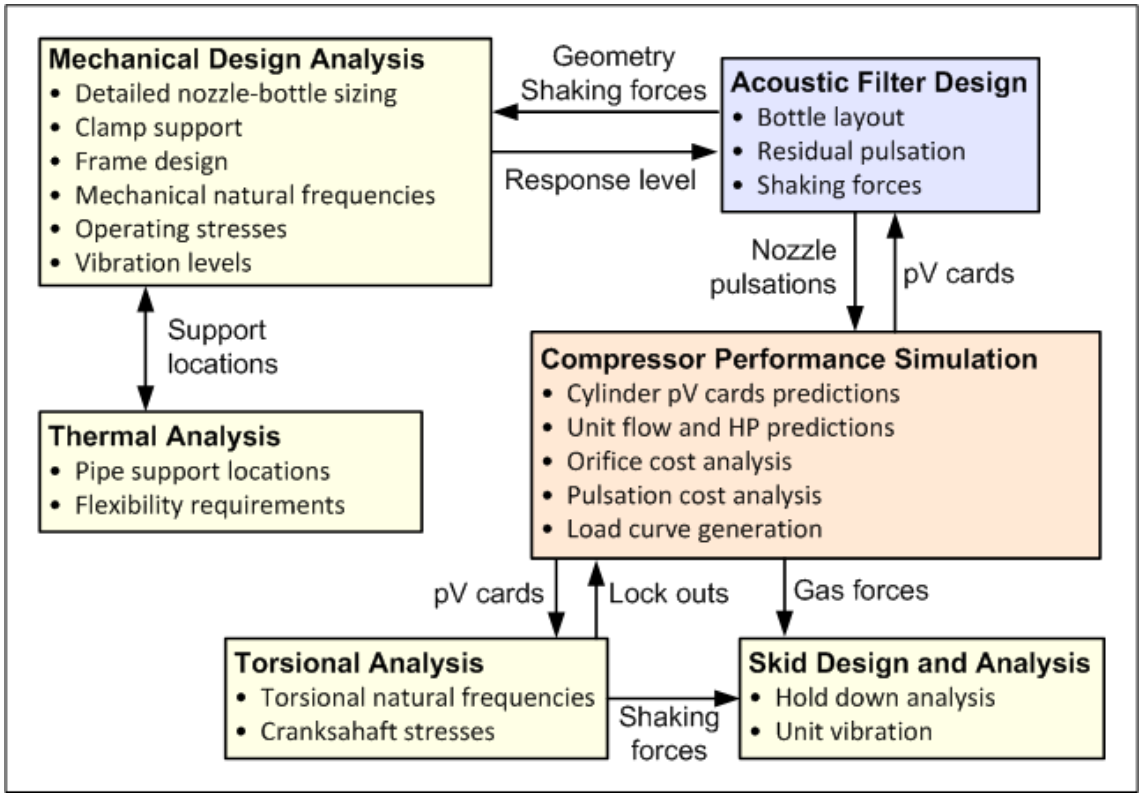

Figure 1.18 Synergic design of compressor and pipelines.

1.5 Compressor-pipelines interaction

In a reciprocating compressor equipped with self-acting valves, the valve movement during the suction and discharge phases is a function of the pressure difference across the valve. Since the mass flow of gas through positive displacement compressors is intermittent, a fluctuation of pressure occurs in the finite volume plenum chambers and connected piping. This fluctuation couples with the valve action, each one having a significant effect on the other and on compressor performance [8].

Considering a multi-cylinders configuration, gas oscillations are complicated because of the cylinders interaction. Suction/discharge piping of a cylinder influences unsteady flows in the suction/discharge piping of other cylinders [9].

This happens also in a double-acting cylinder. In this case, the reciprocal interaction between the two cylinder chambers must be considered. Each chamber, both communicating through the suction and discharge compressor plena, generate an oscillating pressure field in the plenum that can influence the thermodynamic cycle of the

other cylinder chamber. It follows that gas pulsations can affect compressor capacity and the machine absorbed work, and can lead to valve malfunctioning, structural pipeline vibrations and radiated noise.

Moreover, the compressor-pipelines interaction influences the mass flow profiles generated by the compressor cylinders. In fact, the reciprocal interaction among the cylinders, modifies the mass flow profiles entering the pipelines. Considering a double-acting cylinder, the complex geometry of the plena acts on the composition of the total mass flow profile entering the pipelines. It follows that the mass flow profiles (suction and discharge) of the cylinder are different from the simple superposition of the mass flows generated by each cylinder chamber. This may lead to strong differences on the pulsation analysis and on the pipelines design.

2 Hybrid numerical model

In the reciprocating compressor field, strong attention is paid to the study of pressure wave propagation in the discharge and suction pipelines. Oscillating pressure waves may lead to mechanical vibrations and failures and affect the machine performance. For this reason, an accurate analysis of the acoustic response of suction and discharge pipelines in a reciprocating compressor plant is of great interest. It follows that it is fundamental to estimate the pressure wave dynamics in suction and discharge pipelines of the reciprocating compressors plants. In order to carry out an accurate design of both the compressor and pipelines, it is important to evaluate their reciprocal interaction since the preliminary phases of the work. It follows that a reliable, fast and flexible tool is necessary to test a large number of compressor and pipelines configurations in order to reach the optimum design of the pipelines and carry out an accurate analysis of the compressor performance.

The hybrid numerical model was developed to consider the compressor-pipelines interaction. The hybrid model is composed by the compressor and the pipelines sub-models. The compressor sub-model performs in the time-domain, while the pipelines sub-model performs in the frequency-domain. The hybrid model couples these sub-models using the FFT algorithm and its inverse. The algorithm at the basis of the hybrid approach links the time-domain and frequency-domain systems, and builds the compressor and pipelines sub-models reciprocal interaction. The whole procedure is iterative and is repeated until the convergence condition of the compressor thermodynamic cycle is reached. The complexity of this kind of approach allows taking the advantages of both the approaches for the compressor-pipelines system analysis. Tramschek et al. [8] developed a hybrid model of a single-cylinder chamber communicating with an acoustic

pipelines. Moreover, Singh et al. [9] developed a multi-cylinder model in order to evaluate the interaction among cylinders connected by pipelines. In both cases the acoustic pipelines were modelled by lumped parameters (i.e. acoustic impedances) that strongly approximated the pipelines geometries (in particular the plena geometries) and the introduction of corrective terms like damping is needed to match the experimental data. In order to consider the effects of real complex geometry of compressor plena on pressure pulsations, a more detailed approach was developed by Novak et al. [10] who defined and used an acoustic FEM impedance function of compressor plena within the numerical model. However, the approach is limited to single inlet-single outlet plena (i.e. compressor with a single cylinder). Also in this case, heuristic parameters was introduced in the model in order to match the experimental data.

In this work a hybrid numerical model in MATLAB® was developed to take into account the compressor-pipelines reciprocal interaction in order to estimate the reciprocating compressor performance and carry out an acoustic pulsation analysis in the pipelines of the full system considering also geometrically complex elements. In this work the 0D quasi-steady numerical sub-model of the reciprocating compressor named Re.Co.A. (Reciprocating Compressor Analysis) and the acoustic 1D sub-model based on the four-pole method were improved. The former defining a new algorithm for the thermodynamic cycle computation that takes into account the real gas properties computation and solves the energy and mass balance equation in the whole cycle (instead of using average gas properties and polytropic equations for the compression and expansion phases). The latter introducing in the pipelines the transfer matrix of geometrically complex elements (i.e. suction and discharge plena) derived through a characterization procedure based on 3D acoustic FEM simulations. Above all, the coupling of these sub-models is obtained using the hybrid model algorithm based on FFT and IFFT.

The hybrid model joins the advantages of the quasi-steady time-domain model with the advantages of the acoustic transfer matrix method, resulting both in a fast simulation tool for reciprocating compressor performance evaluation and pipelines pulsation analysis. More in details, the time-domain compressor cycle computation allows evaluating the variation of the whole thermodynamic parameters (e.g. in-cylinder

pressure, density, temperature, internal energy) and mass flow considering the valve dynamic in the whole 360 degrees of the cycle. Regarding the pipelines, the frequency-domain has the advantages of being simple and ideally suited for synthesis of suction and discharge pipelines systems, carrying out a fast resolution of the system, reducing both the time necessary to build up a large number of test-configuration and the computational cost. By solving a linear system of equations, the acoustic domain of a piping system can be easily determined. Moreover, the acoustic approach allows to model easily geometrically complex elements like suction and discharge plena respect to a simplified (i.e. 1D) fluid-dynamic time-domain approach. This makes the acoustic approach the ideal tool for the analysis in the first design phases.

2.1 The time-frequency domains interaction

The time-frequency domain interaction of the hybrid model is achieved using the FFT and IFFT. In this work, the hybrid model couples the the Re.Co.A. (Reciprocating Compressors Analysis) and the acoustic transfer matrix sub-models. It is based on the reciprocal interaction between time-domain and frequency-domain approaches (Figure 2.1).

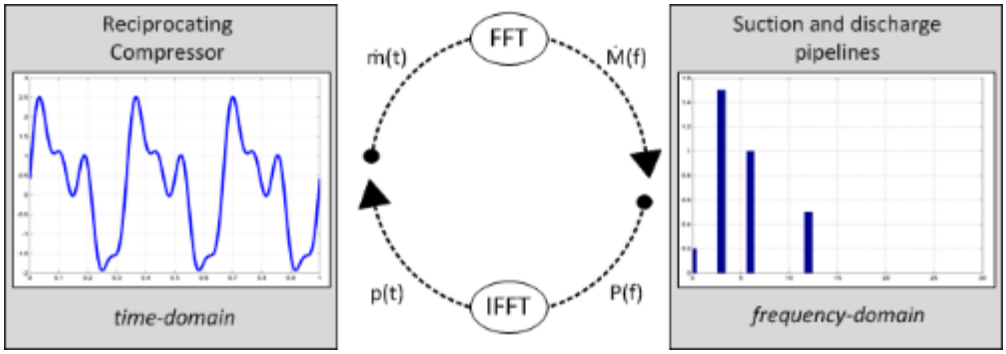

Figure 2.1 FFT-IFFT analysis: compressor (time domain) and pipelines (frequency domain) interaction. ṁ(t) is the time-domain mass flow profile in time-domain, and Ṁ(f) is the same profile in the frequency-domain. Similarly, p(t) and P(f) are the pressure profiles in the two domains.

The first step of the hybrid algorithm is the computation of the compressor thermodynamic cycle. Constant pressure profiles for both suction and discharge boundary conditions are imposed. Subsequently, the mass flow profiles of the thermodynamic cycle are transformed in the frequency domain by the FFT algorithm. The time-step of the

compressor sub-model defines the resolution of the processed signal (i.e. mass flow), and has a duration equal to a thermodynamic cycle (i.e. 360 CA degree).

Then the transformed mass flow profiles are the inputs of the pipeline sub-models. The pipeline sub-models compute the acoustic response in terms of pressure at the compressor interface. The suction and discharge pressure profiles, expressed in the frequency-domain, are transformed by the IFFT (Inverse Fast Fourier Transform) in the time-domain pressure profiles over a compressor cycle. These profiles are the new boundary conditions imposed to the compressor sub-model that computes the new thermodynamic cycle.

These steps are iterated until the convergence condition on the compressor thermodynamic cycle is reached.

It follows that the FFT and the IFFT are the fundamentals tools that allows one to work in both the physical domains. The reliability of the fast FFT in case of signals like the mass flow rate at the suction and discharge valves was fully assessed in previous works [14].

2.2 Re.Co.A. sub-model

The Re.Co.A. sub-model was developed in DIEF (Department of Industrial Engineering of Florence) for industrial research. Re.Co.A. is a 0D quasi-steady numerical model that solves the energy and mass continuity equations in the fluid volume inside the cylinder for subsequent time-steps (namely *i-th* time step).

The motion of the piston controls the thermodynamic cycle phases. The single CA degree is divided in function of the precision that is needed, and for each computational step the thermodynamic conditions inside the cylinder chamber and the mass flow profiles at the suction and discharge valves are calculated. The thermodynamic cycle depends on the pressure profiles imposed at the suction and discharge boundaries. These profiles, together with the in-cylinder thermodynamic conditions, influences the dynamics of compressor valves, then the magnitude and direction of the flow passing through the valves.

2.2.1 Cylinder chamber

The in-cylinder chamber is a lumped element where gas properties are uniform. In this domain, the equations are solved for each time-step of the simulation until the imposed convergence condition of the thermodynamic cycle is reached.

The thermodynamic cycle is regulated by the motion of the piston. Referring to Figure 2.2, the piston displacement is calculated using the cinematic equation of the crankshaft mechanism:

$$s = \sqrt{l^2 - (r \cdot \sin(\omega \cdot t))^2} + r \cdot \cos(\omega \cdot t) \qquad \textbf{[2.1]}$$

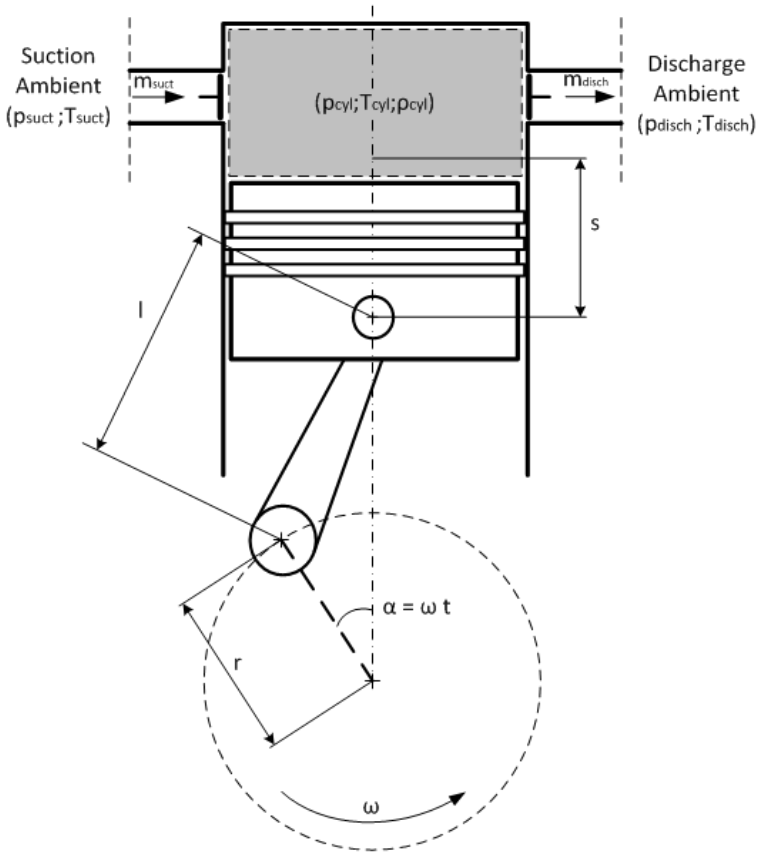

Figure 2.2 Re.Co.A. computational domain (grey area) and crank-shaft mechanism scheme.

The Re.Co.A. sub-model follows a two-step numerical computation. At a first time, a set of preliminary thermodynamic conditions inside the cylinder is calculated solving the mass continuity and energy equations for the new in-cylinder volume value. The in-

cylinder pressure and temperature are derived from the real gas properties tables starting from the previously computed gas values of density and specific internal energy.

Subsequently, depending on the preliminary in-cylinder pressure, the model determines whether perform the suction and discharge valves dynamics (suction and discharge phases of the thermodynamic cycle) and computes the mass flow of gas entering or outgoing the in-cylinder chamber. The in-cylinder mass of gas and specific internal energy are computed by solving the mass continuity and energy equations:

$$M^i = M^{i-1} + \sum_k \dot{m}_k^i \cdot dt \qquad \textbf{[2.2]}$$

$$u^i = \frac{u^{i-1} \cdot M^{i-1} - dV \cdot p^{i-1} + \sum_k \dot{m}_k^i \cdot h_k^i + \dot{Q}^i \cdot dt}{M^{i-1}} \qquad \textbf{[2.3]}$$

These new values are the effective thermodynamic conditions inside the cylinder.

It follows that, during the compressor and expansion thermodynamic phases, both the suction and discharge valves are closed and the above equations are solved with null mass flow values ($\dot{m}_k^i = 0$). Finally, the in-cylinder pressure and temperature effective values are derived from the real gas properties tables using the above density and specific internal energy values.

In Figure 2.3 the Re.Co.A. computational logic flow-chart is shown.

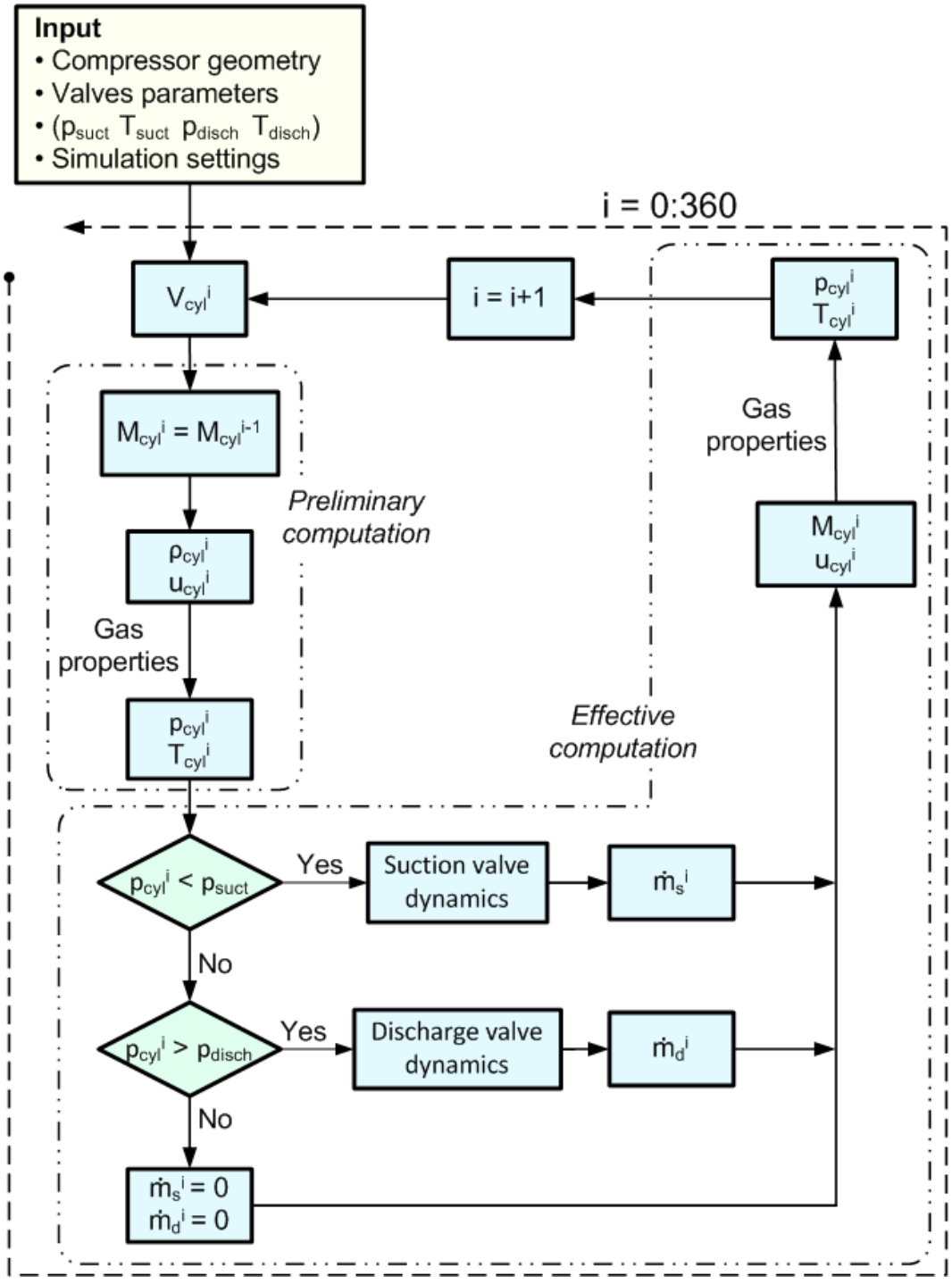

Figure 2.3 Re.Co.A. computational logic flow-chart.

2.2.2 Valve dynamics

The valve dynamics [15] [15] is implemented in the reciprocating compressor sub-model and is calculated at each time step. The valve dynamics computational logic flow chart is shown in Figure 2.5.

The discharge valve dynamics calculation starts when the pressure inside the cylinder is higher than the pressure of the discharge ambient. On the other hand, the suction valve dynamics calculation starts when the cylinder pressure is lower than the suction ambient. The valve dynamic, represented by a mass-spring-damper model, is mathematically described by the second order differential equation:

$$m_r\ddot{x} + b\dot{x} + k_r x = F(t) \quad \textbf{[2.4]}$$

The movable mass is represented by the reeds mass, the spring stiffness by the stiffness of the reed valve and the damper by the overall damping of the system. The solution of the differential equation is obtained by applying the Euler method [16] in order to compute the valve lift and the valve velocity. During their motion, the reed valves move up to the maximum allowable height. When the valve displacement is higher than the maximum allowable value, the reeds rebound on the valve seats. The same behavior is simulated when a displacement lower than the minimum allowable value is reached. In order to model this condition the rebound coefficient is introduced.

The driving force $F(t)$ is represented by the pressure that acts on the reeds surface (Figure 2.4). If the valve at the previous time-step of computation is closed, the pressure acting on the reeds is equal to the difference between the ambient pressure and the in-cylinder pressure, acting respectively on a surface equal to the hole on the valve plate and on the reed surface:

$$F(t) = \pm\left(p_{cyl} \cdot S_{hole} - p_{ext} \cdot S_r\right) - F_p \quad \textbf{[2.5]}$$

When the valve opens, the driving force of the system is the product of the stagnation pressure on the reeds surface acting on a portion of reed surface equal to the valve plate hole:

$$F(t) = \frac{1}{2} C_D \cdot S_{hole} \cdot \rho_f \cdot \left(v_f - v_r\right)^2 \quad \textbf{[2.6]}$$

The geometrical section of the valve is the minimum value between the cylinder which height is equal to the valve displacement, and the diameter equal to the diameter of the valve plate hole, and the surface of the valve plate hole.

$$A_v = \min(S_{hole}, \frac{\pi d_{hole}^2}{4}) \quad \textbf{[2.7]}$$

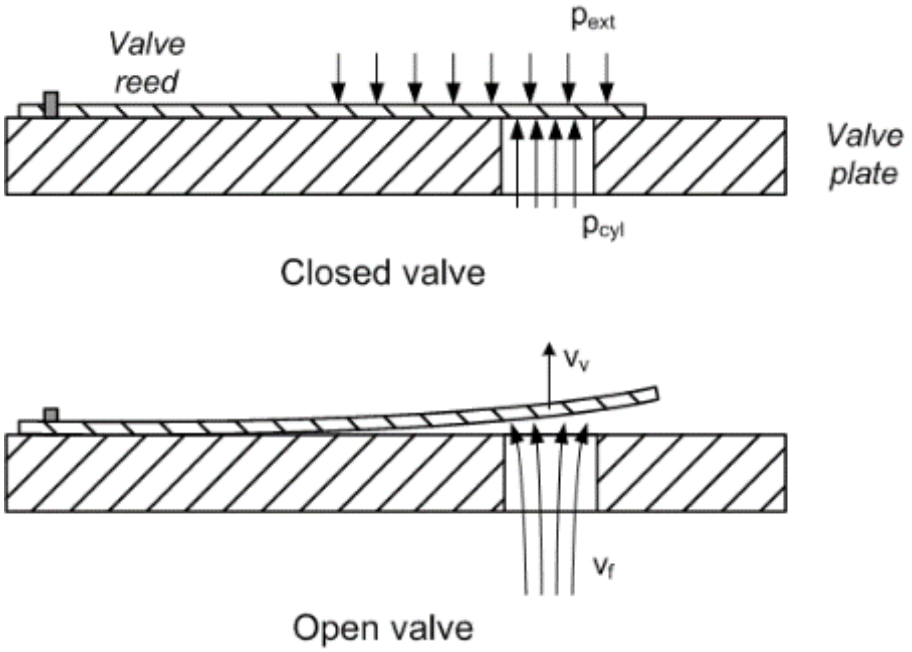

Figure 2.4 Forces acting on the valve reed in the closed and open conditions.

Once the valve displacement value is computed, the valve dynamics routine compares it with its maximum and minimum allowable values. If the computed displacement is out of its boundary values, the rebound of the valve reed on the seat is simulated using a rebound coefficient (i.e. c_r).

Once the valve is opened, the mass flow is computed using the nozzle isentropic flow formulation. The mass flow function evaluates the pressure conditions across the valve and defines whether the flow is choked or not in function of the pressures rate critical value (Figure 2.6):

$$\left(\frac{p_2}{p_{01}}\right)_{crit} = \left(\frac{2}{\gamma+1}\right)^{\frac{\gamma}{\gamma-1}} \quad \textbf{[2.8]}$$

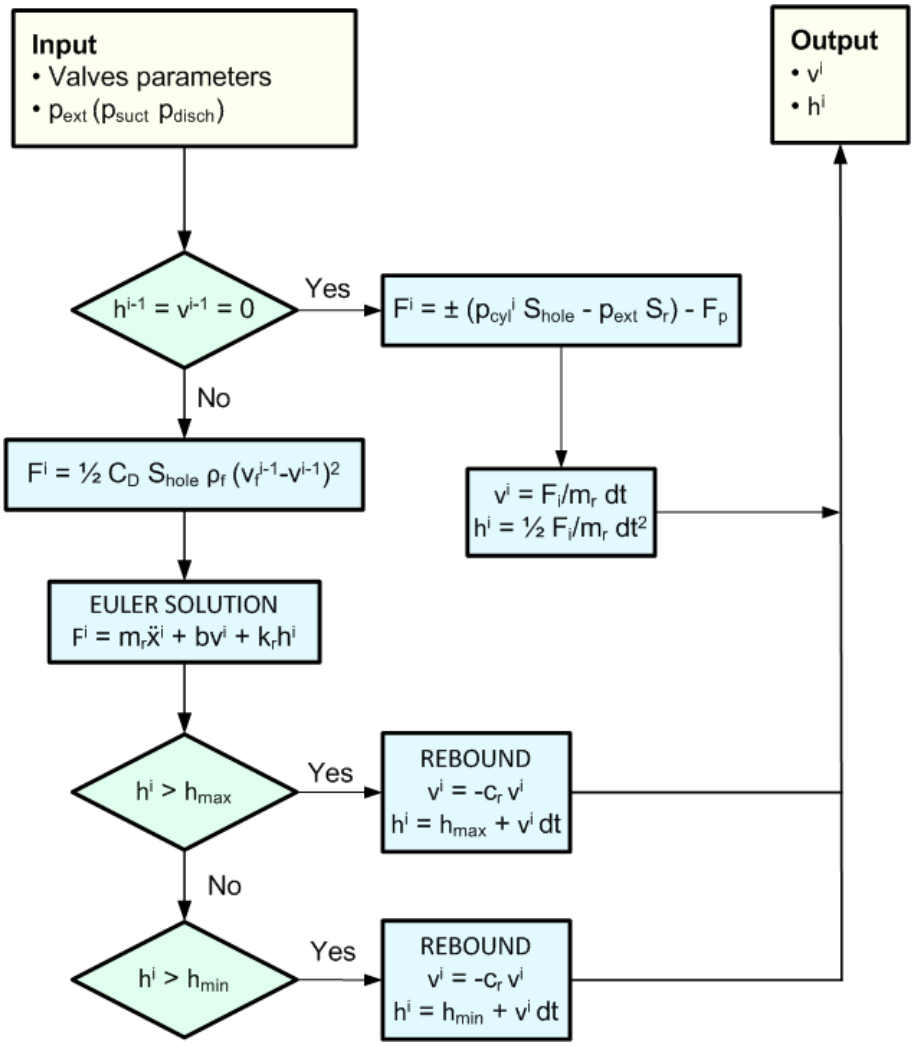

Figure 2.5 Valve dynamics computational logic flow chart.

If the pressure rate across the valve (downstream pressure on upstream total pressure) is higher than the critical rate value, the mass flow is computed using the isentropic mass flow formulation:

$$\dot{m} = K_s \cdot A_v \cdot \sqrt{\left[\frac{2\gamma}{\gamma-1}\right]\left\{\rho_1 \cdot p_{01}\left[\left(\frac{p_2}{p_{01}}\right)^{2/\gamma} - \left(\frac{p_2}{p_{01}}\right)^{1+1/\gamma}\right]\right\}} \quad \textbf{[2.9]}$$

Otherwise the choked mass flow formulation is used.

$$\dot{m} = K_s \cdot A_v \cdot \frac{p_{01}}{T_{01}R} \cdot \gamma^{1/2} \cdot \left(\frac{2}{\gamma+1}\right)^{\frac{\gamma+1}{2(\gamma-1)}} \quad \textbf{[2.10]}$$

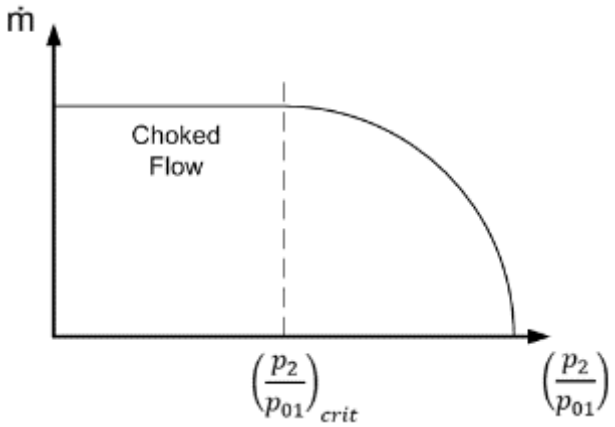

Figure 2.6 Mass flow as a function of the pressure rate across the valve.

The non-isentropic behavior of the mass flow is taken into account using the flow coefficient (i.e. K_s).

The mass flow routine (Figure 2.7) computes the mass flow value and the specific enthalpy of the mass flow, fundamental data for solving the in-cylinder chamber energy balance equation.

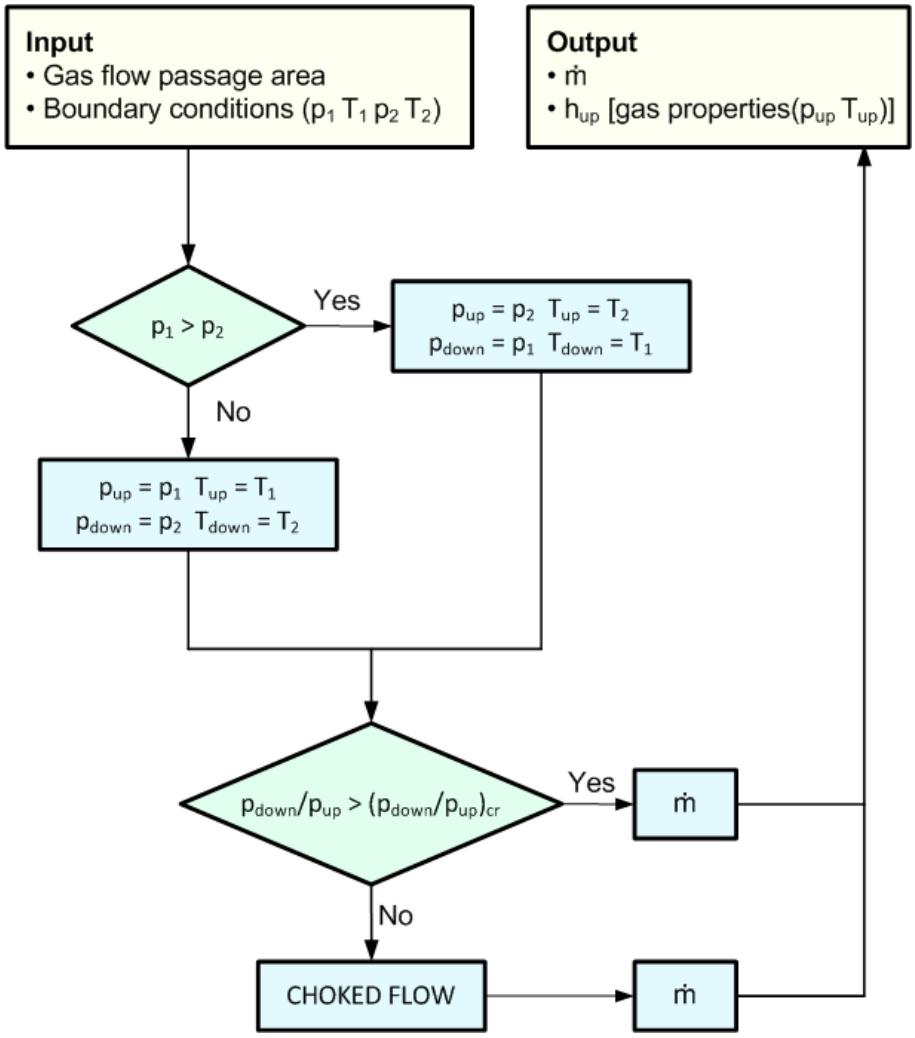

Figure 2.7 Mass flow computational logic flow chart.

2.2.3 Heat exchange

As previously reported, the in-cylinder energy balance takes into account the heat exchange between the gas and the cylinder walls. It's well known that heating and cooling of the gas are unavoidable events that influence compression and expansion in reciprocating compressors. This results in the heat transfer from and to the gas which also occurs in an unsteady manner. Such a transfer has both advantages as well as disadvantages [17]. Among these, regenerative heat transfer as it is known, is the major contributor to the detrimental effects of suction gas heating and the consequent loss of volumetric efficiency.

Most studies in the literature in heat transfer inside cylinders are focused on internal combustion engines, but recently their application was extended also to the reciprocating compressors. The well know formulation for the heat transfer computation is reported below:

$$\dot{Q}_{heat}(t) = h_{heat}(t) \cdot S_{heat}(t) \cdot (T_{cyl} - T_{gas}(t)) \quad \textbf{[2.11]}$$

In this work, the refrigerant to cylinder wall heat transfer coefficient (h_{heat}) is computed using the equation of [18]:

$$h_{heat}(t) = 0.7 \cdot \left[\frac{\lambda(t)}{D}\right]\left[\frac{\rho(t)\bar{u}_p D}{\mu(t)}\right]^{0.7} \quad \textbf{[2.12]}$$

where $\lambda(t)$ is the thermal conductivity of the gas, $\mu(t)$ is the dynamic viscosity of the gas, D is the piston diameter and $\bar{u}_p$ is the average piston speed. All the gas properties are computed with the thermodynamic conditions at each time step of the compressor sub-model.

The heat exchange area is the surface of the in-cylinder chamber volume at each time step:

$$S_{heat}(t) = 2 \cdot \frac{\pi D^2}{4} + \pi D \cdot (\sqrt{l^2 - (r \cdot \sin(\omega \cdot t))^2} + r \cdot \cos(\omega \cdot t)) \quad \textbf{[2.13]}$$

2.3 Acoustic sub-model

The acoustic sub-model is a frequency-domain computational environment based on the electro-acoustic analogy. More in details, the pipelines of the reciprocating compressor are modelled in the frequency-domain using the transfer matrix method [19]. This method allows one to correlate the upstream and downstream state variables (pressure and acoustic velocity) of an acoustic element using a simple matrix formulation.

2.3.1 Fundamentals of acoustics

The acoustic modelling is based on the plane wave propagation theory [20]. In acoustic theory the perturbation of a fluid in a duct can be considered as acoustic plane wave if it is uniform on the duct cross section and propagates in the direction of the duct

axis. Considering x as the axial coordinate, the equations at the basis of the acoustic theory are:

- Mass continuity

$$\rho_0 \frac{\delta u}{\delta x} + \frac{\delta \rho}{\delta t} = 0 \quad \textbf{[2.14]}$$

- Dynamic equilibrium

$$\rho_0 \frac{\delta u}{\delta t} + \frac{\delta p}{\delta x} = 0 \quad \textbf{[2.15]}$$

- Energy equation (*isoentropic*)

$$\left(\frac{\delta p}{\delta \rho}\right)_s = \frac{y(P_0 + P)}{\rho_0 + \rho} \cong \frac{yP_0}{\rho_0} = a_0^2 \quad \textbf{[2.16]}$$

From the energy equation it follows that $\rho_0 = \frac{P_0}{a_0}$, , where a_0 is the sound velocity. Combining the above equations, the acoustic pressure wave propagation is described by the following equation:

$$\left[\frac{\delta^2}{\delta t^2} - a_0^2 \frac{\delta^2}{\delta x^2}\right] p = 0 \quad \textbf{[2.17]}$$

The above equation solution is the composition of two waves (namely forward and backward) propagating in opposite directions with a velocity equal to the sound speed in the fluid (i.e. a_0.). The two waves amplitude are C_1 and C_2 respectively. The following equations describe the solution we had referred to:

$$p(x,t) = C_1 f(x - a_0 t) + C_2 g(x + a_0 t) \quad \textbf{[2.18]}$$

$$p(x,t) = [C_1 e^{-jk_0 x} + C_2 e^{jk_0 x}] e^{jwt} \quad \textbf{[2.19]}$$

In the same way it is possible to obtain the mass flow ($v = \rho u S$) relation:

$$v(x,t) = \frac{1}{Y}[C_1 e^{-jk_0 x} - C_2 e^{jk_0 x}] e^{jwt} \quad \textbf{[2.20]}$$

Where $Y = \frac{a0}{S}$ is the characteristic impedance of the duct and $k_0 = {}^{w}/_{a_0}$ is the wave number or propagation number, for plane wave.

The subscript "0" indicates the non-viscous stationary medium condition. In case of viscous medium the acoustic wave propagation undergoes a progressive reduction in amplitude. In this case, the standing wave solution is expressed as follows:

$$p(x,t) = [C_1 e^{-\alpha x - jkx} + C_2 e^{\alpha x + jkx}] e^{jwt} \quad \textbf{[2.21]}$$

$$v(z,t) = \frac{1}{y}[C_1 e^{-\alpha x - jkx} - C_2 e^{\alpha z + jkx}] e^{jwt} \quad \textbf{[2.22]}$$

Where $y = y_0 \left[1 - \frac{\alpha}{k_0} + j\frac{\alpha}{k_0}\right]$ is the acoustic impedance of the viscous medium, $k = k_0 + \alpha$ is the wave number of the wave propagating in the viscous medium and $\alpha = \frac{1}{r_0 a_0}\left(\frac{u\mu}{2\rho_0}\right)^{\frac{1}{2}}$ is the attenuation constant (r_0 duct radius and μ fluid viscosity).

Substituting $p(x,t)$ and $v(x,t)$ in the dynamic equilibrium equation, it is obtained that the constant values C_1, C_2, C_3 and C_4 are linked by the following relations:

$$C_1 = Y_0 C_3 \; ; C_2 = Y_0 C_4 \quad \textbf{[2.23]}$$

Then, defining the two parameters $A = C_1 = Y_0 C_3$ and $B = C_2 = Y_0 C_4$ (forward and backward wave respectively) the acoustic state variables in function of the axial coordinate z of a straight duct can be expressed as follows:

$$p(x) = Ae^{-jk_0 x} + Be^{+jk_0 x} \quad \textbf{[2.24]}$$

$$v(x) = \frac{Ae^{-jk_0 x} - Be^{+jk_0 x}}{Y_0} \quad \textbf{[2.25]}$$

It is important to notice that A and B are to be determined by the boundary conditions imposed by the elements that precede and follow the particular element under investigation.

The above theory allows modelling complex systems, like acoustic filters. An acoustic filter consists in an element or in a series of elements inserted between a source of acoustic signals and a receiver. In the theory of acoustic filter the medium is considered as stationary and the wave propagation as one-dimensional. The variables characterizing an acoustic wave are the acoustic pressure *p(x,t)* and the mass particle velocity *v(x,t)*. A fundamental parameter is the characteristic impedance:

$$Y = \frac{acoustic\ pressure\ of\ the\ forward\ wave}{acoustc\ mass\ velocity\ of\ the\ forward\ wave}$$

Y is the impedance relative to the medium and the flow section related to the forward wave. In the same manner, it is possible to express the acoustic impedance $Z(x)$, which represents the equivalent impedance of the whole subsystem downstream of the axial coordinate x point:

$$Z(x) = \frac{p(x)}{v(x)} = Y_0 \frac{Ae^{-jk_0x} + Be^{+jk_0x}}{Ae^{-jk_0x} - Be^{+jk_0x}} \quad \textbf{[2.26]}$$

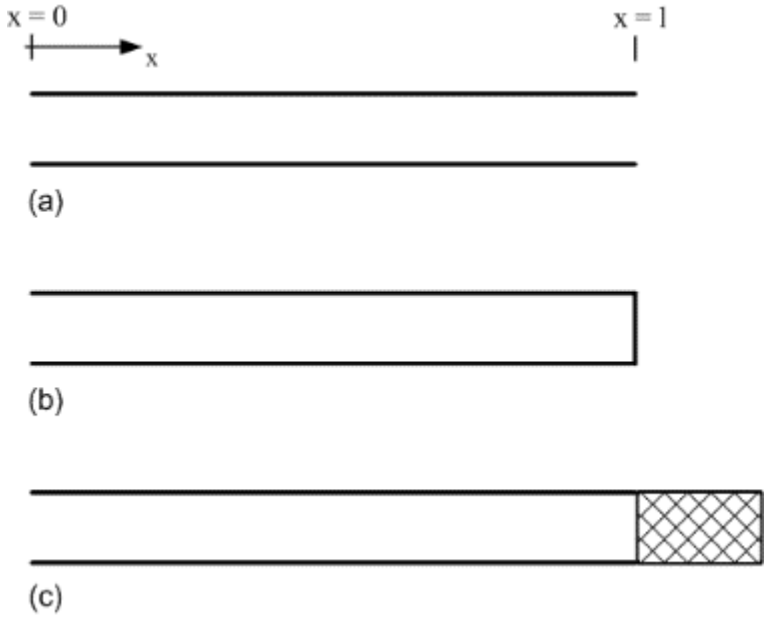

Figure 2.8 Acoustic boundary conditions: (a) open duct (b) duct with rigid closed end (c) duct with anechoic termination.

For a duct of length l, with open end (Figure 2.8(a)), the acoustic impedance is defined as follows:

$$Z(0) = Y_0 \frac{A + B}{A - B} \quad \textbf{[2.27]}$$

$$Z(l) = \frac{Z(0)cosk_0l - jsink_0l}{-jZ(0)/Y_0 sink_0l} \quad \textbf{[2.28]}$$

For a duct with an infinite rigid end (Figure 2.8(b)) *v(l)=0*, the acoustic impedance is:

$$Z(l)_{rigid} \to \infty \quad \textbf{[2.29]}$$

$$Z(0)_{rigid} = -jY_0 cosk_0 l \quad \textbf{[2.30]}$$

Another fundamental parameter in acoustic theory is the reflection coefficient *R:*

$$R = |R|e^{j\omega\theta} \quad \textbf{[2.31]}$$

It is the ratio between the reflected wave pressure and the incident wave pressure. Generally it is possible to define the acoustic impedance Z in function of the reflection coefficient *R* and of the characteristic impedance *Y,* as shown in the equation below:

$$Z = Y_0 \frac{1+R}{1-R} \quad \textbf{[2.32]}$$

In case of rigid termination $R = 1$ and in case of an anechoic termination $R = 0$ (Figure 2.8(c)). From these considerations it follows that $Z_{anec} = Y_0$.

2.3.2 Transfer matrix method

From the equations written above, it follows that the acoustic physical domain is described by a system of linear equations. For a generic acoustic element, these equations can be reported in matrix form in order to link the upstream and downstream acoustic state variables:

$$\begin{bmatrix} p_u \\ v_u \end{bmatrix} = \begin{bmatrix} T_{11} & T_{12} \\ T_{21} & T_{22} \end{bmatrix} \begin{bmatrix} p_d \\ v_d \end{bmatrix} \quad \textbf{[2.33]}$$

The matrix coefficients depend on the geometrical parameters of the element, the thermodynamic conditions of the fluid and the investigated frequency.

By following this approach, a pipeline system can be modelled as a composition of adjacent simple elements. This results in a single transfer matrix that is the product of the single matrix.

$$\begin{bmatrix} p_n \\ v_n \end{bmatrix} = T_n \cdot T_{n-1} \cdot \ldots \cdot T_n \cdot T_0 \begin{bmatrix} p_0 \\ v_0 \end{bmatrix} \quad \textbf{[2.34]}$$

2.3.3 Lumped elements

The transfer matrix acoustic formulations of the main elements composing the acoustic pipelines models are described in details and widely used in the literature of

interest. Among these formulations, the ones used in this work to model the pipelines are the following:

- *Duct* – Circular cross-section duct of length l. The upstream and downstream state variables are correlated by using the linear acoustic theory.

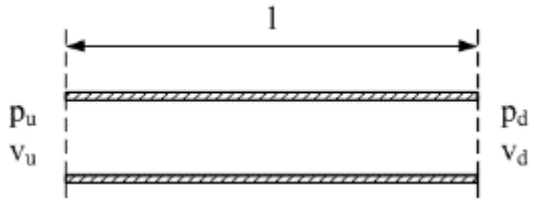

Figure 2.9 Duct scheme of the transfer matrix model.

$$\begin{bmatrix} p_u \\ v_u \end{bmatrix} = \begin{bmatrix} \dfrac{e^{-ikl}+e^{ikl}}{2} & Y_0\dfrac{e^{-ikl}-e^{ikl}}{2} \\ \dfrac{1}{Y_0}\dfrac{e^{-ikl}-e^{ikl}}{2} & \dfrac{e^{-ikl}+e^{ikl}}{2} \end{bmatrix} \begin{bmatrix} p_d \\ v_d \end{bmatrix} \quad \textbf{[2.35]}$$

- *Volume* – The transfer matrix of a cavity of volume V is derived by using the electroacoustic analogy. The volume is modeled as a lumped compliance.

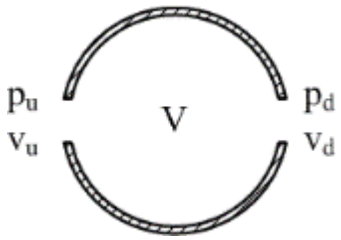

Figure 2.10 Volume cavity scheme of the transfer matrix model.

$$\begin{bmatrix} p_u \\ v_u \end{bmatrix} = \begin{bmatrix} 1 & 0 \\ i\dfrac{2\pi f V}{a^2} & 1 \end{bmatrix} \begin{bmatrix} p_d \\ v_d \end{bmatrix} \quad \textbf{[2.36]}$$

- *Ambient* – the ambient transfer matrix of an ambient termination is modelled as a lumped impedance. Besides the impedance of the termination, the

boundary condition of null pressure oscillation $p_d = 0$ must be considered. In fact, the ambient forces the pressure oscillations to the constant ambient pressure p_0.

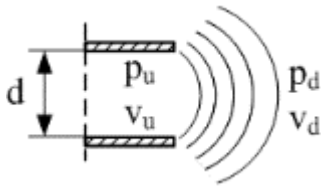

Figure 2.11 ambient termination scheme of the transfer matrix model.

$$\begin{bmatrix} p_u \\ v_u \end{bmatrix} = \begin{bmatrix} 1 & Y_0\left(\frac{k^2 d^2}{16} + i\,0.6\frac{kd}{2}\right) \\ 0 & 1 \end{bmatrix} \begin{bmatrix} p_d \\ v_d \end{bmatrix} \quad \textbf{[2.37]}$$

▪ *T-junction* – The acoustic T-junction element is based on the pressure and particle velocity oscillations equilibrium. Depending on the configuration modelled, the particle velocity oscillation equilibrium has different forms.

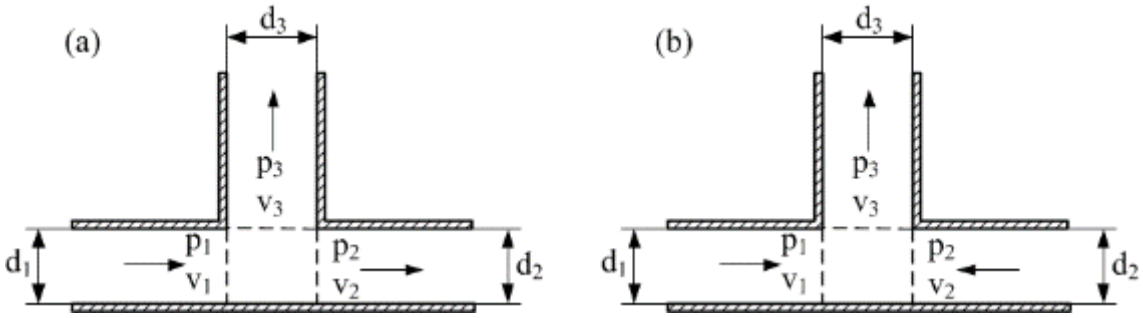

Figure 2.12 T-junction scheme of the transfer matrix model. (a) inlet 1, outlets 2 and 3 (b) inlets 1 and 2, outlet 3.

If the generated pressure excitation comes from one direction only of the T-junction (Figure 2.12a), the equilibrium equations are the following:

$$\begin{aligned} p_1 &= p_2 = p_3 \\ d_1^2 v_1 &= d_2^2 v_2 + d_3^2 v_3 \end{aligned} \quad \textbf{[2.38]}$$

Otherwise, if the pressure excitation of the T-junction come from two different directions (Figure 2.12b), the equilibrium conditions are expressed as follows:

$$\begin{gathered} p_1 = p_2 = p_3 \\ d_1^2 v_1 + d_2^2 v_2 = d_3^2 v_3 \end{gathered} \quad \textbf{[2.39]}$$

2.3.4 Transfer matrix for multiple boundaries

The conventional transfer matrix method [20] [21] is usually used to compute the transfer matrix of simple geometries. The same approach can be applied to geometries with multiple inputs [22]. In this work, an alternative method is used to compute the transfer matrix of complex geometries. The method is based on the scattering parameters computation. Bilal et al. [22] developed a method for calculating the transfer matrix of a for a single inlet-single outlet fluid domain by using acoustic BEM simulations. The procedure is based on the pressure response functions. However, the approach cannot be directly extended to the case of multiple inlets-multiple outlets, like for the plena of a multi-cylinder compressor. In this work a method based on the boundary waves decomposition is described and tested. The purpose of this method is obtaining a multiple inlets-multiple outlets transfer matrix.

In case of a geometry with n-boundaries (Figure 2.13), the backward waves B_i can be expressed as a function of the forward waves A_i for each boundary of the geometry:

$$\begin{gathered} B_1 = A_1 r_1 + A_2 t_{21} + \cdots + A_i t_{i1} + \cdots + A_n t_{n1} \\ B_2 = A_1 t_{12} + A_2 r_2 + \cdots + A_i t_{i2} + \cdots + A_n t_{n2} \\ \vdots \\ B_i = A_1 t_{1i} + A_2 t_{2i} + \cdots + A_i r_i + \cdots + A_n t_{ni} \\ \vdots \\ B_n = A_1 t_{1n} + A_2 t_{2n} + \cdots + A_i t_{in} + \cdots + A_n r_n \end{gathered} \quad \textbf{[2.40]}$$

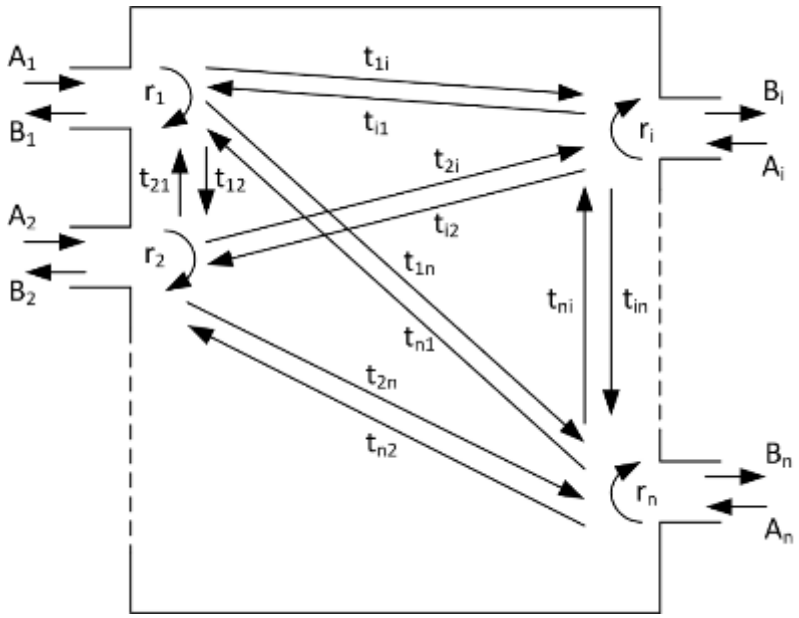

Figure 2.13 Schematic representation of a multiple boundaries geometry.

Imposing an incident pressure wave on one boundary, and the non-reflective (anechoic) conditions to all the other boundaries, the reflection and transmission coefficients are obtained. From these boundary conditions it follows that A_i is the only non-zero incident pressure wave:

$$r_i = \frac{B_i}{A_i} \quad \textbf{[2.41]}$$

$$t_{ij} = \frac{B_j}{A_i} \quad \textbf{[2.42]}$$

Each pressure wave is linked to the boundary acoustic state variables (i.e. acoustic pressure p_i and particle velocity u_i):

$$A_i = \frac{p_i + v_i Y_i}{2} \quad \textbf{[2.43]}$$

$$B_i = \frac{p_i - v_i Y_i}{2} \quad \textbf{[2.44]}$$

where $Y = \rho a_0$ is the characteristic impedance. By replacing the above conditions in the equations system, the following matrix correlation among the boundaries state variables.

$$\begin{bmatrix} 1-r_1 & -Y_1(1+r_1) & -t_{21} & -Y_2t_{21} & \dots & -t_{i1} & -Y_it_{i1} & \dots & -t_{n1} & -Y_nt_{n1} \\ -t_{12} & -Y_1t_{12} & 1-r_2 & -Y_2(1+r_2) & \dots & -t_{i2} & -Y_it_{i2} & \dots & -t_{n2} & -Y_nt_{n2} \\ \dots & & & & \dots & & & & & \dots \\ -t_{1i} & -Y_1t_{1i} & -t_{2i} & -Y_2t_{2i} & \dots & 1-r_i & -Y_i(1+r_i) & \dots & -t_{ni} & -Y_nt_{ni} \\ \dots & & & & \dots & & & & & \dots \\ -t_{1n} & -Y_1t_{1n} & -t_{2n} & -Y_2t_{2n} & \dots & -t_{in} & -Y_it_{in} & \dots & 1-r_n & -Y_n(1+r_n) \end{bmatrix} \begin{Bmatrix} p_1 \\ v_1 \\ p_2 \\ v_2 \\ \dots \\ p_i \\ v_i \\ \dots \\ p_n \\ v_n \end{Bmatrix} = 0 \quad \textbf{[2.45]}$$

Thanks to this method, the acoustic characterization of an n-boundaries geometry can be obtained combining the results of n numerical simulations with the imposed incident wave and non-reflective boundary conditions. As shown, a $nx2n$ transfer matrix correlates the $2n$ acoustic state variables.

2.3.5 FEM acoustics

Nowadays the acoustic FEM computation is successfully applied to the acoustic filters performance analysis in the ICE field [23]. The theory of the method is known and well explained by [24]. The steady-state acoustic pressure $p(x,y,z)$ in an enclosed volume is governed by the 3D Helmholtz equation:

$$\nabla^2 p(x,y,z) + k^2 p(x,y,z) = -j\rho_0 \omega q(x,y,z) \quad \textbf{[2.46]}$$

where q represents the external source distribution, $k = \omega/a_0 = 2\pi f/a_0$ is the acoustic wavenumber and c is the speed of sound. In order to solve this differential equation, the definition of boundary conditions in each position on the closed boundary surface is needed. The BCs could be of three different types:

- imposed pressure: $p(x,y,z) = \bar{\bar{p}}$
- imposed normal velocity: $v_n = \frac{j}{\rho_0 \omega}\frac{\delta p}{\delta n} = \bar{\bar{v_n}}$
- imposed normal impedance: $p = \bar{Z} v_n$

The FEM is based on the transformation of the fluid domain into an equivalent weighted residual formulation, in order to determine the state variables (i.e. pressure and velocity) in some determined discrete positions of the domain. With this approach, the fluid domain has to be mapped by means of elements whose length is provided by the maximum frequency of analysis. A good level of accuracy is obtained with an element

length at least 10 times lower than the acoustic wavelength. In the weighted residual concept, the Helmholtz equation is defined in an equivalent integral formulation. The weak form is:

$$\int_V (\nabla\tilde{p}\nabla \mathrm{p})\mathrm{dV} - \omega^2 \int_V \left(\frac{1}{c^2}\tilde{p}\mathrm{p}\right)\mathrm{dV} = \int_V (\mathrm{j}\rho_0\,\omega\tilde{p}q)\mathrm{dV} - \int_\Omega (\mathrm{j}\rho_0\,\omega\tilde{p}\bar{v}\bar{n})\mathrm{d}\Omega \quad \textbf{[2.47]}$$

which is satisfied for any weighting function $\tilde{p}$. The acoustic pressure can be computed in each node of the fluid domain resolving the algebraic system obtained from the above equation:

$$([K_a] + j\omega[C_a] - \omega^2[M_a])\{p_i\} = \{F_{ai}\} \quad \textbf{[2.48]}$$

where the vector $\{p_i\}$ contains the unknown nodal pressure, $[K_a]$, $[C_a]$ and $[M_a]$ are the acoustic stiffness, damping and mass matrices respectively, whereas the vector $\{F_{ai}\}$ contains the contribution from the input pressure and velocity boundary conditions and the acoustic source vector.

It is important to notice from the above equations the acoustic behaviour of the investigated fluid domain is affected by the domain geometry, the boundary conditions and the fluid properties. More in details, the fluid density and sound speed have a critical role.

2.4 Hybrid model numerical comparison

In order to assess the hybrid methodology reliability, an analysis on a geometrically simplified test case was carried out. The hybrid approach was assessed by comparing the results of the simulation of a test case performed with both the hybrid numerical model and a commercial 1D code (AMESim® by LMS). The tested configuration (Figure 2.14) is a single cylinder chamber reciprocating compressor for refrigeration applications.

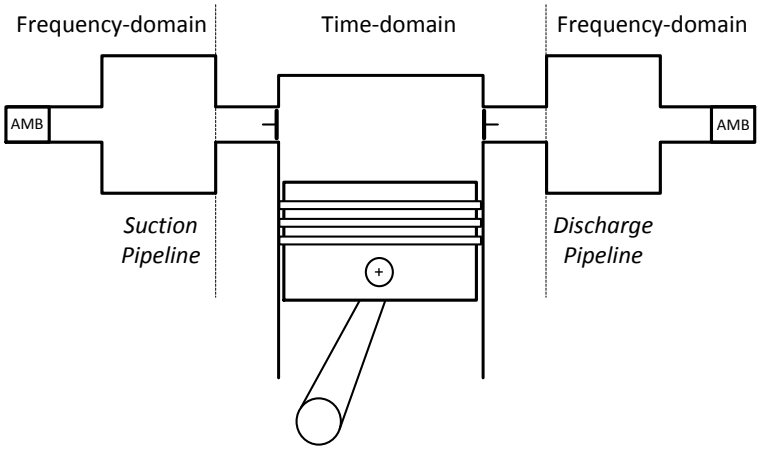

Figure 2.14 Scheme of the hybrid model tested configuration.

The suction and discharge pipelines are composed by a volume (representing the compressor plenum) and a duct which is connected to an ambient at constant thermodynamic conditions (i.e. pressure and temperature). In both the simulations, the viscous effects, the frictions of the flow and the heat exchange in both the pipelines and the cylinder are neglected. The main simulation data are reported in Table 2.1.

Compressor		
Rotating speed	[rpm]	1440
Fluid	-	CO_2
Bore	[mm]	61
Stroke	[mm]	52
Rod length	[mm]	98
Suction valve diameter	[mm]	15
Discharge valve diameter	[mm]	9.5
		whose

Suction		
Pressure	[bar]	2.06
Temperature	[°C]	21.6
Discharge		
Pressure	[bar]	18.98
Temperature	[°C]	118
Pipelines geometry		
volume	[dm^3]	0.3
Duct length	[m]	1.0
Duct diameter	[mm]	30

Table 2.1 Technical data of the numerical tested configuration.

It is important to underline that time-domain sub-model (i.e. the reciprocating compressor) of the hybrid model solves the same equations of the AMESim® model. Concerning the pipelines, the AMESim® model follows a 1D time-domain approach, conversely in the hybrid model the electroacoustic approach is followed. The equivalence of the pipelines components between the two models was previously verified through an acoustic characterization of the time-domain components. In Figure 2.15 the comparison

in terms of Transmission Loss between the time-domain 1D volume element and the corresponding acoustic volume is shown.

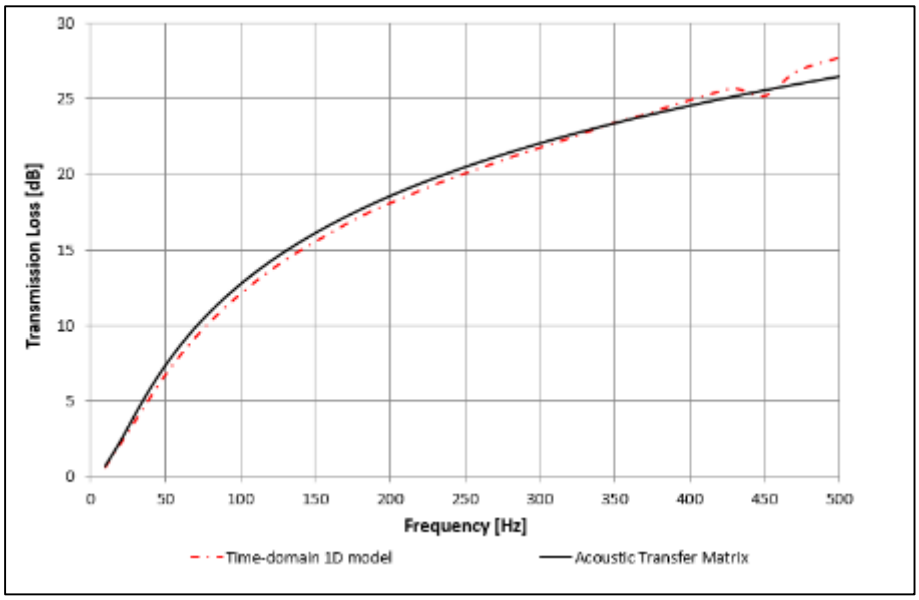

Figure 2.15 Transmission Loss comparison between the time-domain 1D volume and the corresponding acoustic volume.

Due to the equivalence of the two models' elements, the results comparison between the two models allows testing the hybrid model interaction between the two different computational domains (i.e. time-domain and frequency-domain). As shown in Figure 2.16 and Figure 2.17, the results of the hybrid model agree with the results of the time domain model on the whole thermodynamic cycle, both in terms of in-cylinder pressure and in-cylinder mass of gas. It implies that the compressor in the two models computes the thermodynamic cycle with the same boundary conditions (i.e. suction and discharge pressure profiles).

In Figure 2.18 and Figure 2.19, the results in terms of suction and discharge pressure profiles are shown. These pressure profiles directly depend on the compressor-pipelines coupling. The good agreement between the two models' pressure profiles highlights the coherence of the hybrid modelling respect to the full time-domain model. The equivalence between the two different modellings allows proceeding with further improvements of the hybrid model, by introducing in the pipelines the geometrically complex elements defined through the acoustic FEM characterization.

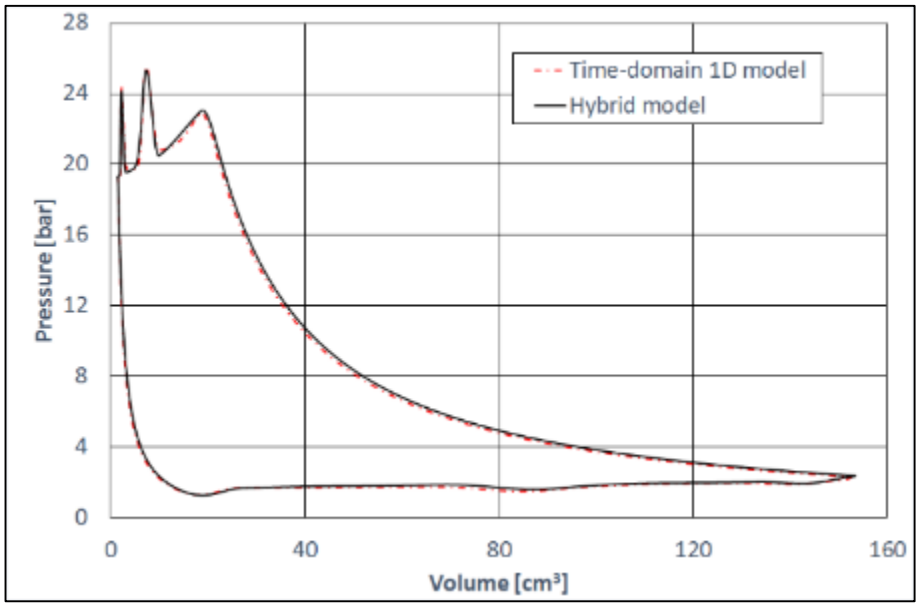

Figure 2.16 In-cylinder pressures, comparison between the hybrid model and the time-domain 1D model

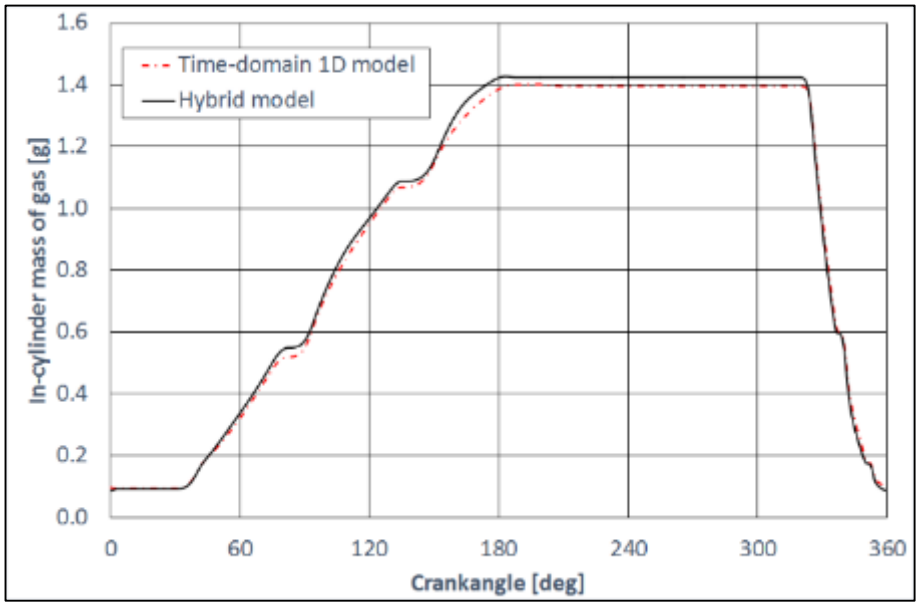

Figure 2.17 In-cylinder mass of gas, comparison between the hybrid model and the time-domain 1D model.

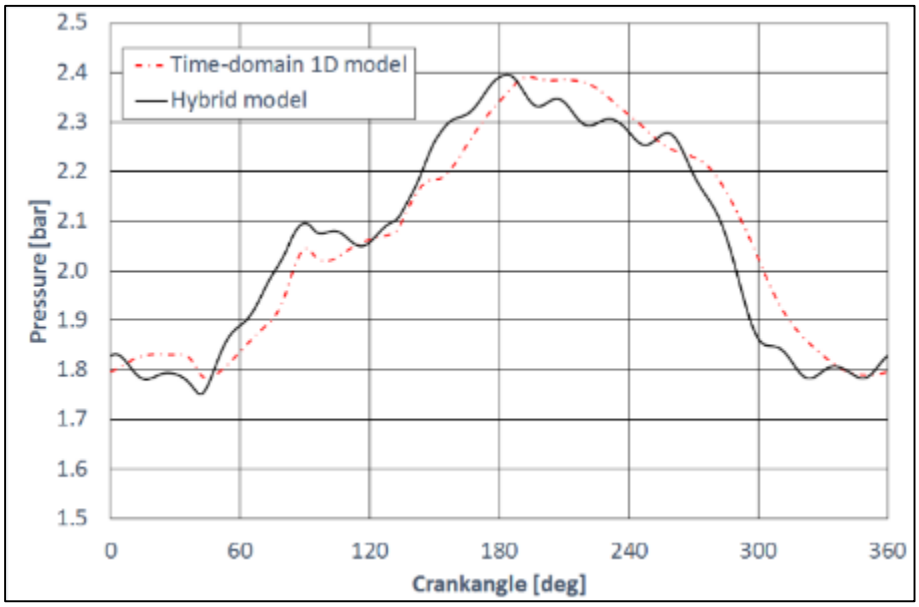

Figure 2.18 Suction pressure profiles, comparison between the hybrid model and the time-domain 1D model.

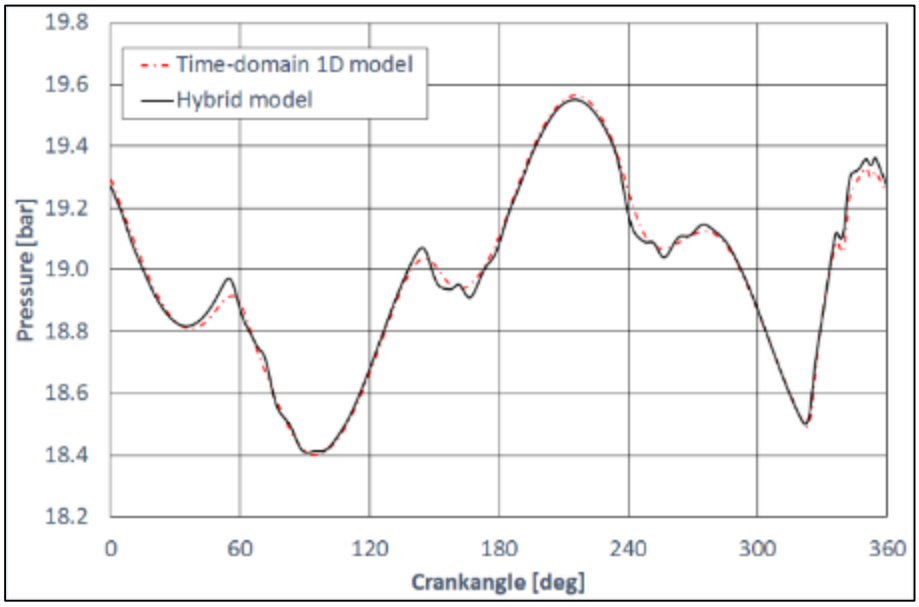

Figure 2.19 Discharge pressure profiles, comparison between the hybrid model and the time-domain 1D model.

3 Reciprocating compressor test case

In order to assess the predictability of a numerical model, a comparison with experimental data is needed. In this study, due to the aspects considered in the simulation, a detailed study of the test case is a fundamental part of the work that aims to realize accurate simulations using the hybrid model. In this chapter, the experimental activity on the real reciprocating compressor to measure the comparison experimental data will be presented. Moreover, the experimental and numerical activities carried out to obtain the necessary data for the model will be presented. More in details, the experimental valve stiffness characterization will be shown, and the numerical activity of the compressor plena acoustic 3D characterization will be described in depth.

3.1 Experimental activity

The predictability of a numerical model is assessed through a comparison with experimental data. It follows that an accurate and well conducted experimental activity is necessary

The tested case of this study is a CO_2 semi-hermetic reciprocating compressor for refrigerating applications (Figure 3.1). The machine is a single stage compressor with two cylinders. The specific compressor model is the CD700H series produced by Dorin©, an Italian factory specialized in design and manufacturing of reciprocating compressors for refrigeration.

Figure 3.1 A semi-hermetic CO2 reciprocating compressor for refrigeration produced by Dorin©.

The CD700H technical data are summarized in Table 3.1.

CD700H Compressor		
Rotating speed	[rpm]	1485
Fluid	-	CO_2
Bore	[mm]	34
Stroke	[mm]	27.5
Rod length	[mm]	109.5
Suction valve diameter	[mm]	7
Discharge valve diameter	[mm]	6
Number of cylinders	-	2
CA phase	[deg]	180

Table 3.1 CD700H semi-hermetic compressor technical data.

The layout of the compressor test circuit is shown in Figure 3.2. The circuit is a conventional and basic refrigeration circuit that is composed by:

- Reciprocating compressor [COMP];

- Condenser [COND];
- Thermal expansion valve [VALVE];
- Evaporator [EVA];
- Two storage tanks [ST].

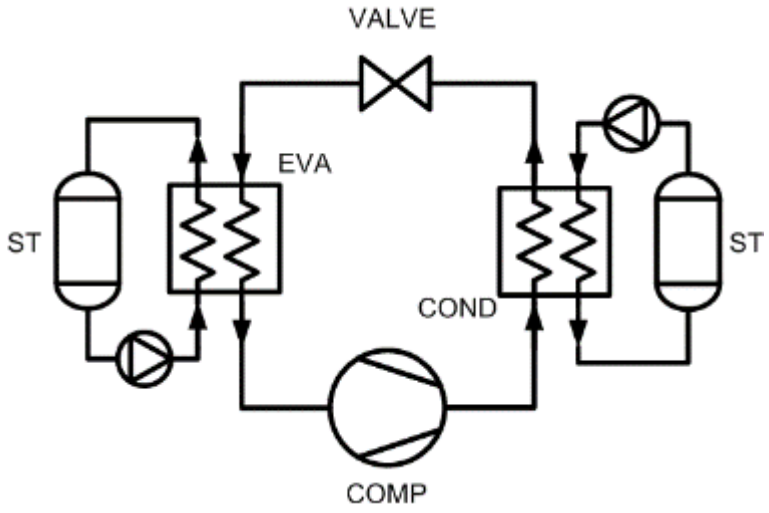

Figure 3.2 Reciprocating compressor test circuit.

The circuit is designed for testing the compressor during its real working conditions. The two storage tanks are introduced into the circuit in order to guarantee a heat sink for the cold fluid passing through the evaporator, and for the hot fluid passing through the condenser.

For the measurement of the indicating cycle a proper measurement apparatus has been designed in order to guarantee the correct timing of the in-cylinder pressure with the crank shaft rotation.

3.1.1 Experimental test setup

The experimental test setup is designed for the measurement of the following compressor working parameters:

- In-cylinder dynamic pressure (for both cylinders);
- Suction plenum dynamic pressure;
- Discharge plenum dynamic pressure;
- Crank shaft position (CA) ;

- Suction pipeline temperature;
- Discharge pipeline temperature.

Particular attention is paid to the crank shaft position measurement. The crank shaft position is fundamental to determine the piston displacement of each cylinder. Due to the compressor design, the CA could not be measured using an encoder housed on the crankshaft. Then a specific measurement chain based on a hall sensor was developed. The measurement chain is composed by:

- Circular ferromagnetic plate with 24-2 holes housed on the crankshaft (Figure 3.3). The plate is perpendicular to the crankshaft axis;
- Hall sensor (Figure 3.4) by Elen. The sensor is housed on the compressor bottom cover and pointing the plate's holes;
- AVL Crank Angle Calculator (CAC).

The hall sensor for the measurement of the crank shaft angular position is placed on the compressor bottom cover. Particular attention is paid to the sensor positioning since the compressor case contains high pressure gas and oil (for lubrication reasons). So a hall sensor for high pressure environment has been chosen. At the side end of the crank shaft a steel disc (24 less 2 holes on the external circumference) is housed coaxially with the shaft. The hall sensor is perpendicular to the disc and is placed at 0.65 mm of distance in correspondence of the markers, in order to allow the hall sensor reading the passage of the markers. The two missing holes helps in identifying the revolution start (and finish). The AVL CAC is used in order to reconstruct a virtual encoder signal using the information of the hall sensor. More in details, the signals of the hall sensor go to CAC in form of voltage peak. Each marker corresponds to a voltage peak. For the identification of the single revolution passage no peak voltage is transmitted to CAC (because of the missing markers). The CAC, starting from the signal information of the hall sensor, reconstructs a detailed virtual encoder signal with the desired resolution and provides as outputs an angle digital signal and a revolution digital signal. In Figure 3.5 the trends of the hall sensor voltage output (yellow signal) and CAC revolution digital signal (blue) are shown. The red line underlines the TDC angular position. The angular resolution is set to 0.5 degrees (and that means 720 outputs per revolution). For the reconstruction of the indicating cycles a proper software has been developed in LabView® environment.

The SW allows the visualization of the pressure-volume diagram of the compressor and the data storage. The acquisition of the pressure voltage signals starts at the passage of the revolution digital signal (hardware trigger); each pressure signal is sampled every 0.5 degrees.

Figure 3.3 Circular ferromagnetic plate with 24-2 holes housed on the crankshaft.

Figure 3.4 Elen hall sensor.

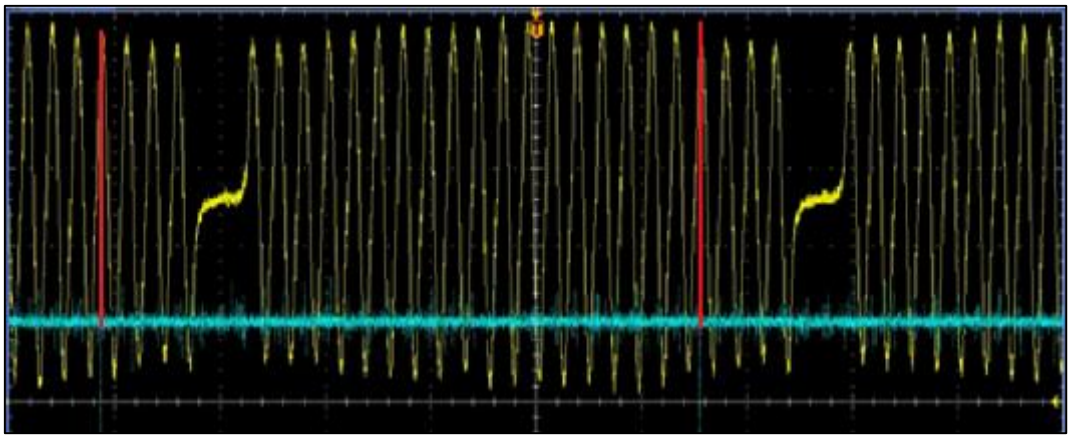

Figure 3.5 Hall sensor signal (yellow), CAC revolution signal (blue), crank revolution trigger (red).

In Figure 3.6 the experimental setup for the dynamic pressures measurement is shown. The dynamic pressure analog signals (voltage) and the digital signal of the crank angle calculator are the input signals for the electronic board.

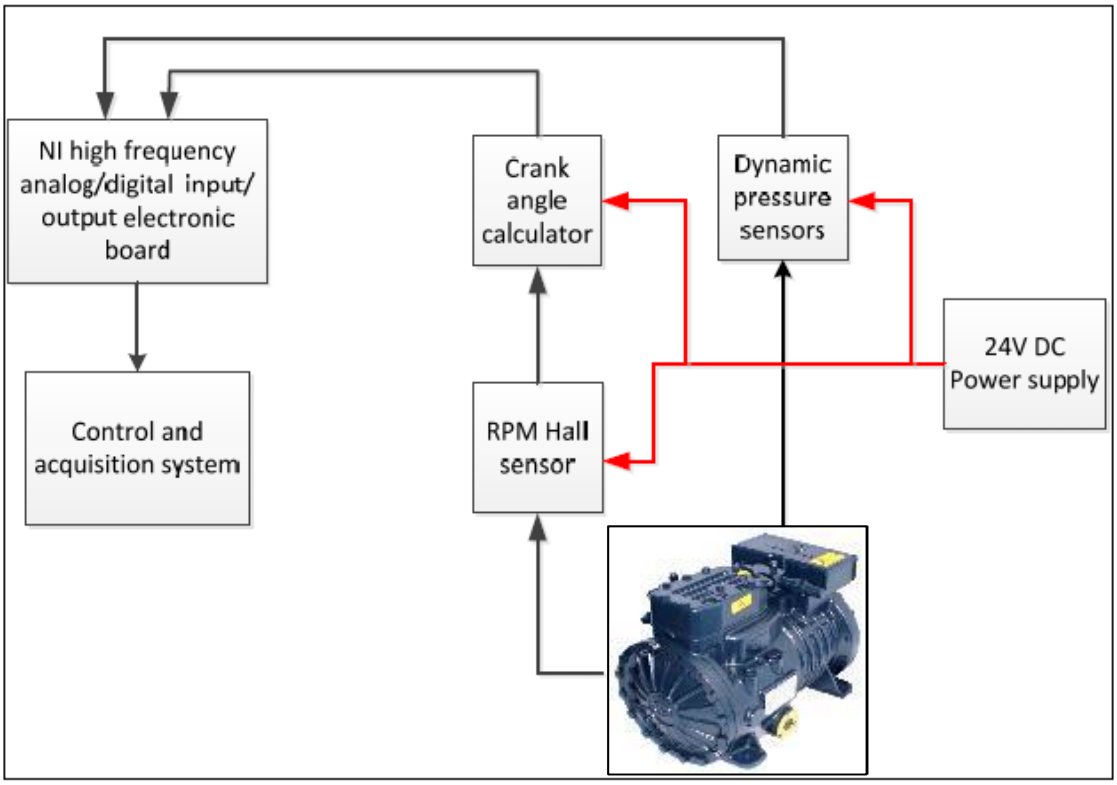

Figure 3.6 Experimental test rig measurement chain.

The dynamic pressures are acquired using High frequency pressure sensor, mod. Kulite XTL (Figure 3.7). In Figure 3.8 is shown the in-cylinder pressure sensor positioning.

Figure 3.7 Kulite XTL Dynamic pressure sensor.

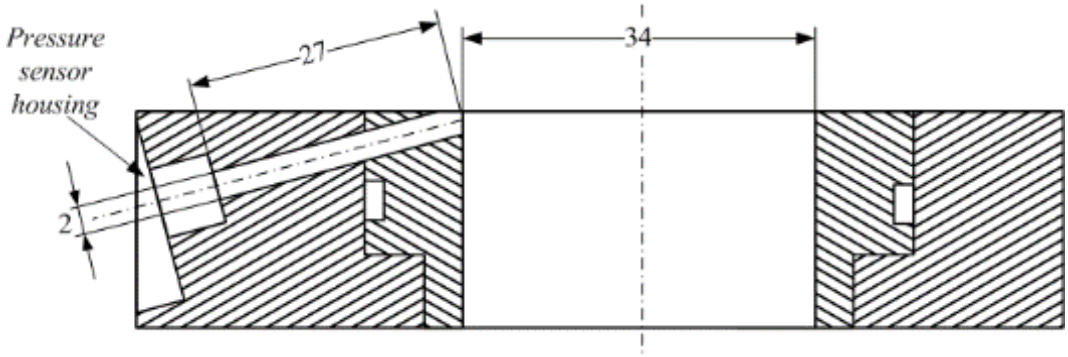

Figure 3.8 In-cylinder pressure sensor housing.

In Figure 3.9 are shown the pressure sensors housed on the compressor head cover for in-cylinder, suction and discharge pressures acquisition.

The whole experimental setup allows a rigorous monitoring of the pressure trends inside the cylinder. In fact, possible rotational speed variations of the crank shaft, during the compression-expansion phases, don't cause any mistakes on the Clapeyron diagram reconstruction.

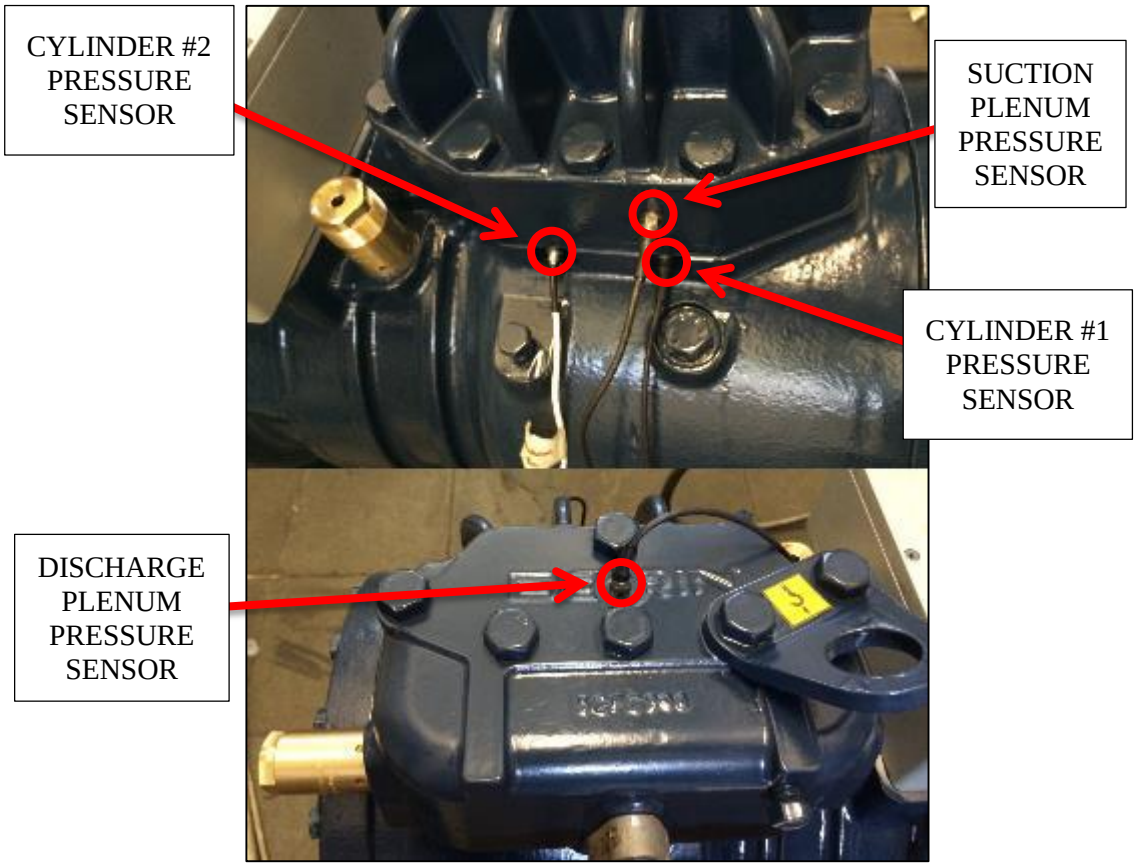

Figure 3.9 Pressure sensors housing on the compressor cylinder head cover.

3.1.2 Valves stiffness characterization

In order to satisfy the numerical model request about the complete characterization of the compressor valves, an experimental activity to measure the valve reeds stiffness was conducted. The experimental rig used was composed by:

- Drilling machine
- Precision balance
- Mechanical comparator
- Steel precision tip

In is shown the experimental setup for the valve reeds stiffness characterization.

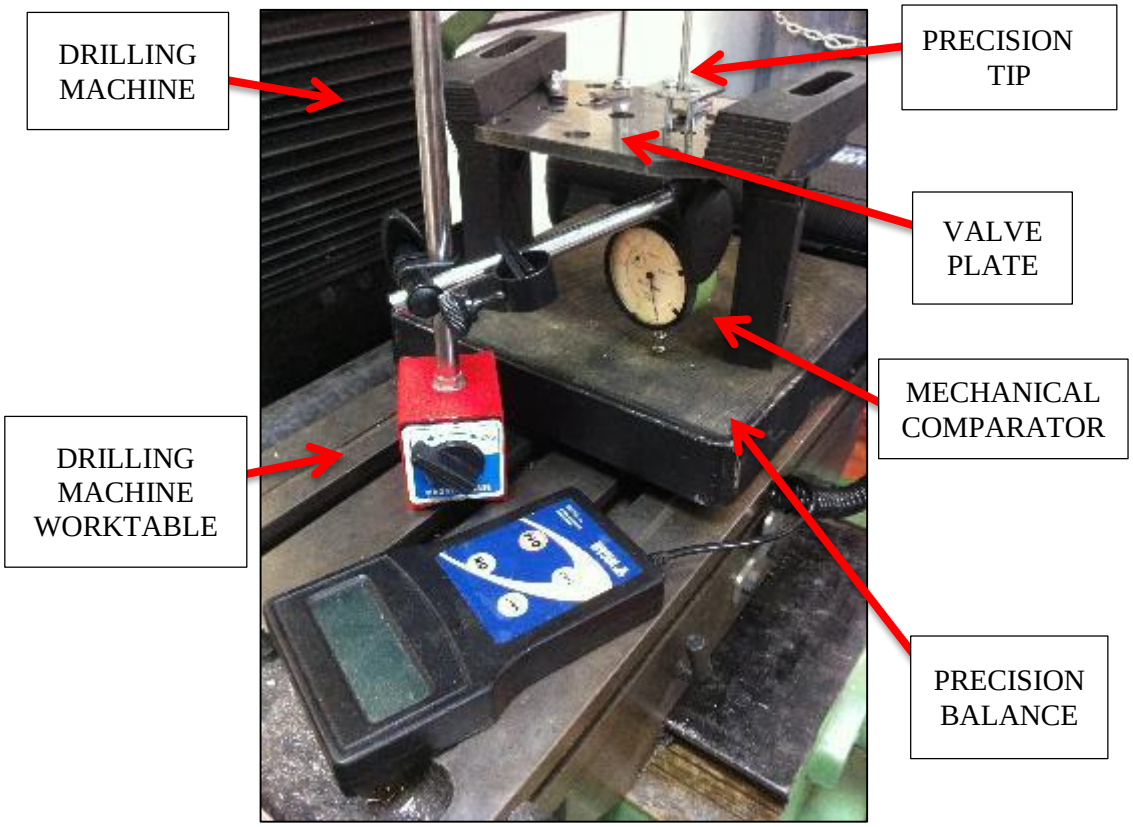

Figure 3.10 Experimental setup for the valve reeds stiffness characterization.

The compressor valve plate is placed on the precision balance and it is suspended on two steel columns. The sensitive tip of the mechanical comparator is placed in correspondence of the reed valve (Figure 3.11), pointing the center of the valve plate hole that is the gas flow passage between the cylinder and the discharge and suction plena. In this way the valve reed displacement can be measured with high precision.

The whole instrumentation described above is placed on the work table of the drilling machine. The depth adjustment system of the drilling machine is used to control the tip advance. Thus, the above described instruments allow the reed valve movement and, contemporary, the force employed to move the valve is measured with the digital balance.

Figure 3.11 Detail view of the mechanical comparator tip positioning on the valve reed.

In Figure 3.15 the measured suction and discharge valve reeds stiffness are shown. The reed stiffness is computed considering displacements up to the upper displacement limit imposed by the counter-seats. The polynomial functions that interpolate the experimental data will be introduced in the numerical model for the compute of the valve reeds stiffness as a function of the displacement. The stiffness curves show how fundamental the experimental characterization of the reed is in order to make a reliable numerical simulation of the reed dynamics in the compressor sub-model. By using the polynomial interpolating functions, the numerical model is able to simulate the valve dynamics with the effective stiffness values as a function of the reed displacement.

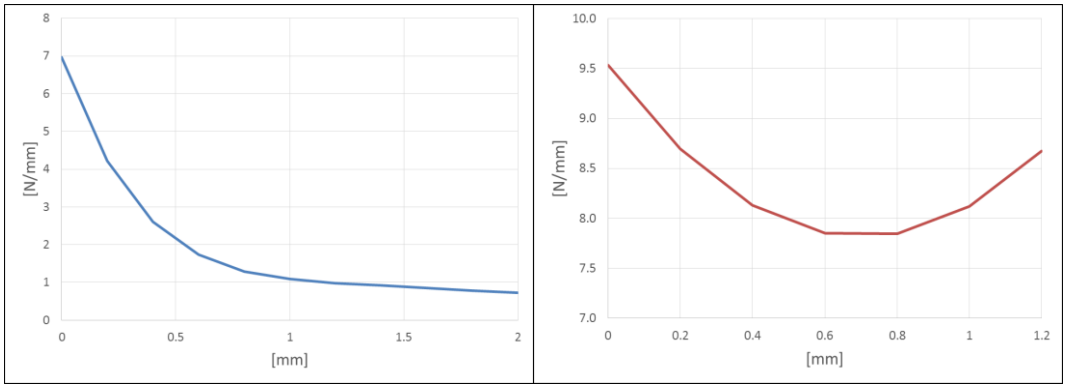

Figure 3.12 Suction (left) and discharge (right) reed stiffness, experimental data.

3.1.3 Test conditions

The test conditions for the compressor are regulated by acting on the lamination valve of the compressor test circuit. The thermodynamic boundary conditions are summarized in Table 3.2.

	Suction	**Discharge**
Pressure [bar]	36.7	120
Temperature [°C]	50	125

Table 3.2 Compressor thermodynamic boundary conditions.

Both temperature and static pressure are measured inside the suction and discharge plena. These information are fundamental in order to set up properly the boundary conditions of the numerical simulations.

3.2 Acoustic 3D characterization

In order to introduce in the acoustic sub-model of the compressor the suction and discharge plena, their acoustic FEM characterization are used. Due to the complexity of the compressor plena geometries, it is not possible to use acoustic lumped elements to achieve a reliable modelling of the plena. As shown in Figure 3.13 the compressor plena have a high number of boundaries (five for each plenum) and a consistent 3D growth that prevents using the acoustic lumped elements (e.g. ducts, volumes, discontinuities. etc.) whose analytically formulations are well known from literature [20].

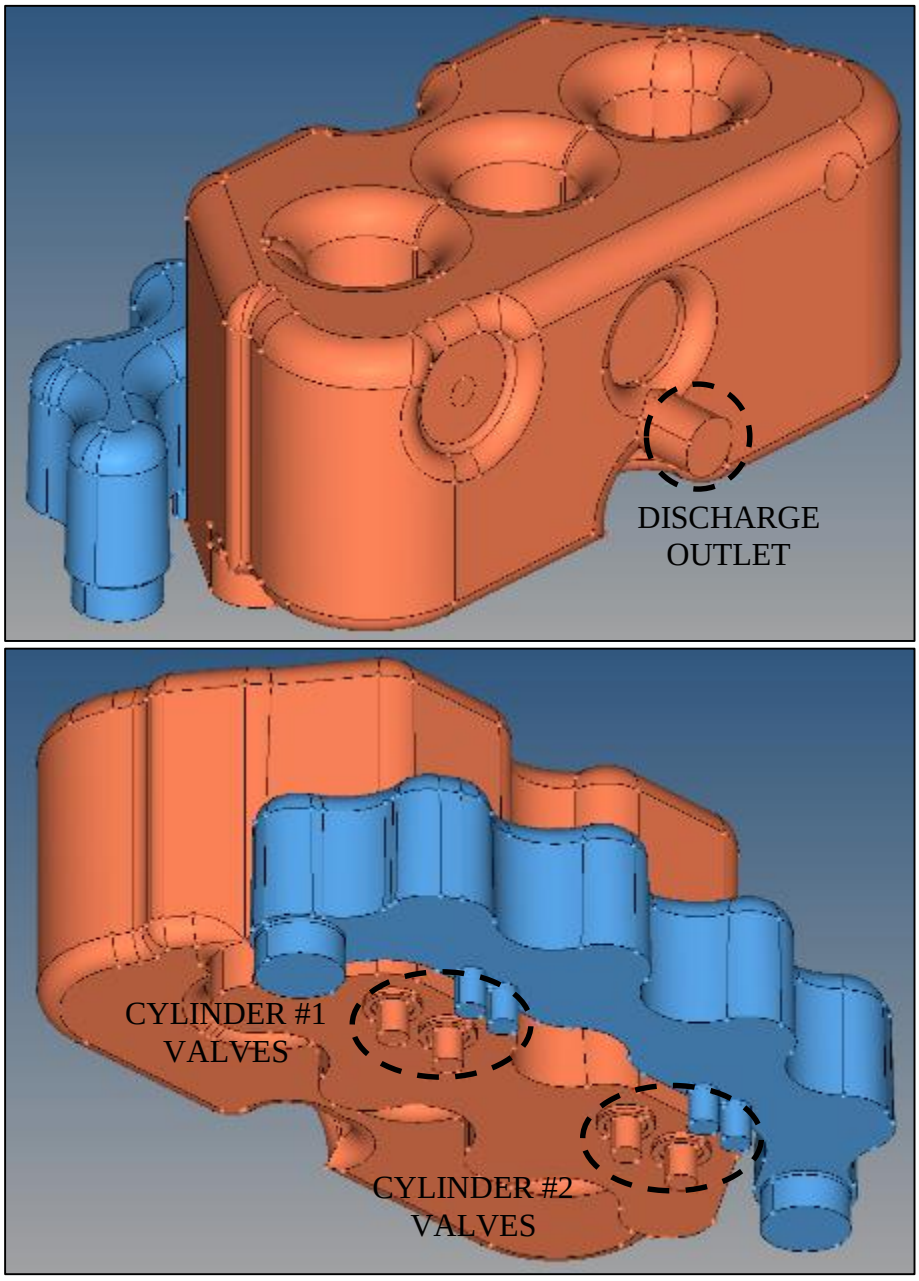

Figure 3.13 Compressor suction (blue) and discharge (orange) plena.

It follows that the use of more detailed instruments like the acoustic FEM is necessary. For this purpose, the acoustic characterization theoretically described in the previous chapter is used. The focus of such procedure is to define a lumped transfer matrix that describes the acoustic response of each plenum. The transfer matrix will subsequently be used in the compressor acoustic sub-model of the compressor.

3.2.1 Plenum transfer matrix

The acoustic characterization procedure requires a number of simulations equal to the total boundaries of the plenum. Each simulation allows computing the reflection and transmission coefficients corresponding to each boundary. The coefficient of all the boundaries are subsequently combined to obtain the transfer matrix of the plenum.

In this work the acoustic FEM simulations are performed by using the software VirtualLab Acoustic® by LMS. Both the suction and discharge plenum have five boundaries each one: four corresponds to the valves of the two compressor cylinders, and the fifth is the plenum connection to the pipelines.

The thermodynamic conditions of the acoustic characterization are shown in Table 3.3 and corresponds to the experimental test conditions.

	Suction	**Discharge**
Pressure [bar]	36.7	120
Temperature [°C]	50	125
Density [kg/m^3]	70.1	204.2
Sound Speed [m/s]	256.3	285.2
Characteristic impedance [kg/(m^{2}s)]	17963.23	58236.21

Table 3.3 Thermodynamic conditions for suction and discharge plena simulations.

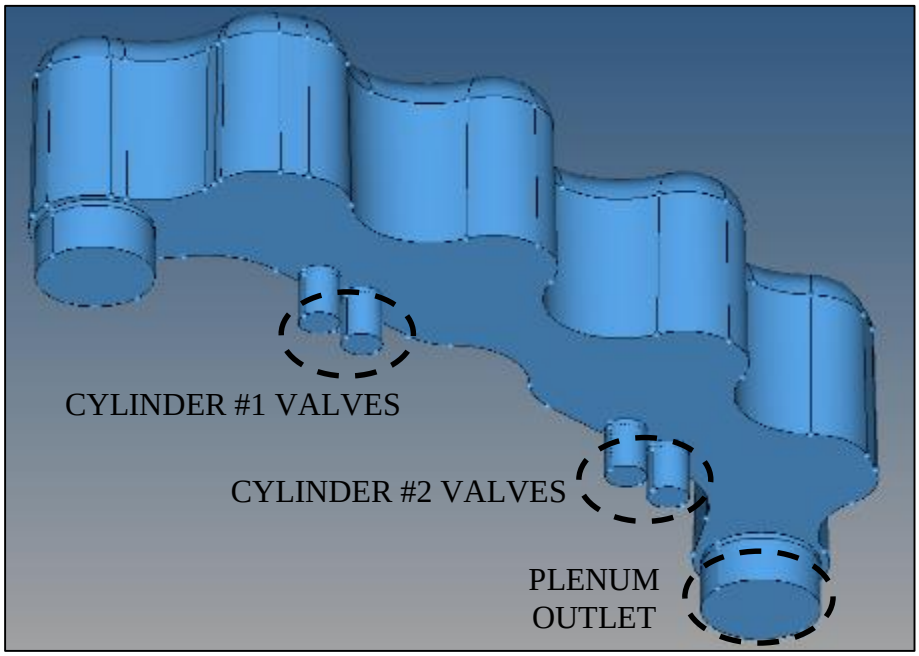

Figure 3.14 Compressor suction plenum.

Although the first five pulsation harmonics affect compressor the most, the harmonic analysis is performed from 1 Hz up to 2000 Hz with a step of 10 Hz. In the data processing phase, the simulations numerical results were interpolated in order to obtain an acoustic characterization with a step of 1 Hz.

The fluid domain was meshed with triangular shape of the cells, whose minimum size was set to 5 mm, a value 100 times lower than the minimum wavelength. A mesh sensitivity was performed and showed that a reduction of the element size led only to an increase of the calculation time without an improving of the accuracy. Due to the total number of the boundaries, five runs for each plenum were carried out in order to define the plena transfer matrix. The boundary conditions of each analysis are a fixed acoustic velocity on one boundary and the anechoic termination (the incident wave is null) on the others.

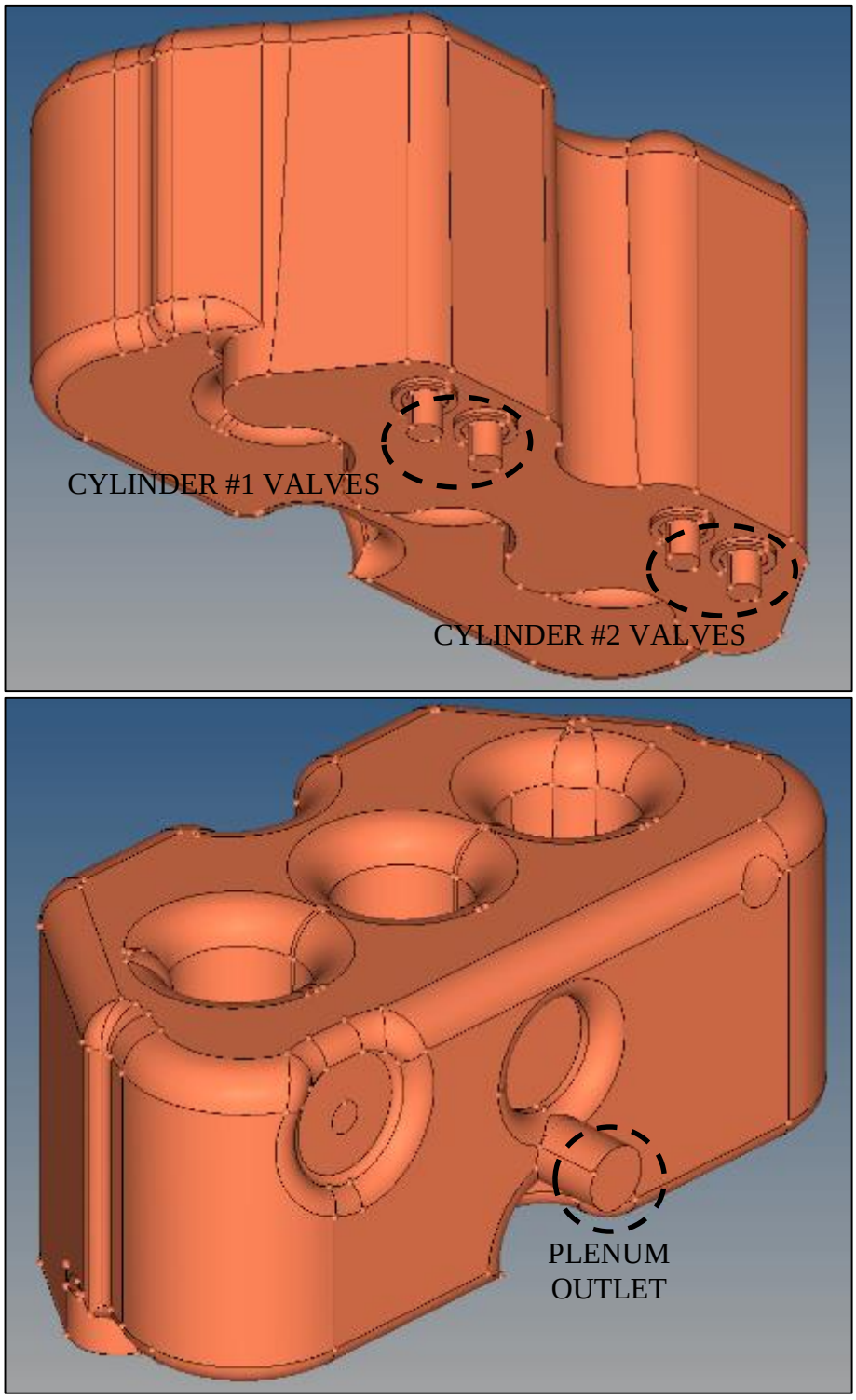

Figure 3.15 Compressor discharge plenum.

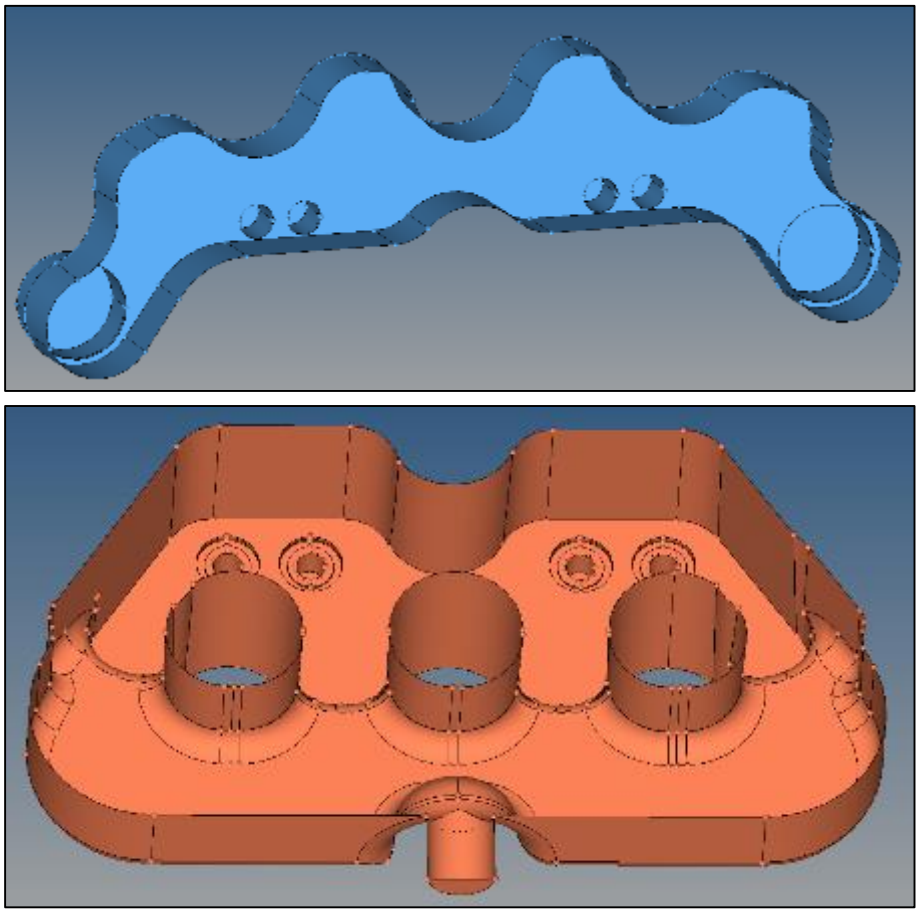

Figure 3.16 Suction (up) and discharge (down) plena sections.

Each simulation computes the state variables (i.e. acoustic pressure and velocity) in the whole fluid domain. The state variables at the boundaries allow computing the corresponding incident and reflected waves (defined by amplitude and phase) and subsequently the reflection and acoustic coefficients. It follows that for an effective acoustic coefficients computing at each plenum boundary, the plane wave condition is necessary. In order to ensure the plane wave conditions at the boundaries, ducts with a length equal to a multiple of the diameter are added. These ducts do not affect the acoustic propagation of the waves in the fluid domain because of the linearity of the acoustic equations solved that neglect the dissipative non-linear effects. The ducts allow working with planar waves at the boundaries without affecting the waves with dissipative effects. Otherwise, the ducts introduce a phase-shift of the waves that needs to be considered in the data processing to define properly the acoustic coefficients phase. The computed pressure p_{sim} and particle velocity u_{sim} are shifted to the physical section of the plenum using the following relations [20].

$$p = p_{sim}\cos(kL_d) - iu_{sim}Y_0\sin(kL_d) \quad \textbf{[3.1]}$$

$$u = u_{sim}\cos(kL_d) - i\,{}^{p_{sim}}/_{Y_0}\sin(kL_d) \quad \textbf{[3.2]}$$

where L_d is the length of the added duct. The values of p and u are combined to obtain the corresponding incident and reflected waves at the boundary, and subsequently the reflection and transmission coefficients. More details about the analytical procedure of the acoustic characterization are reported in the previous chapter.

By processing the simulations data, the transfer matrix are computed for each frequency from 1 Hz to 2000 Hz. As a final processing step, the transfer matrix are summarized with the wavenumber corresponding to each frequency for the simulations thermodynamic conditions. The definition of the wavenumber k is the following:

$$k = 2\pi f/c \quad \textbf{[3.3]}$$

This allows making the acoustic characterization independently from the thermodynamic conditions of the simulation. Once the transfer matrix is introduced in the acoustic sub-model of the compressor, the thermodynamic boundary conditions (i.e. suction and discharge temperature and static pressure) of the compressor can be changed and the previously defined matrix can be used even if they were computed for specific thermodynamic conditions.

3.2.2 Ducts length sensitivity

The acoustic characteristics of a fluid domain are strictly connected to its geometry. In this case the extension of fluid domain with additional ducts introduces additional resonances to the acoustic response of the plenum. However, because of the assumption of linearity in the acoustic equations describing the domain, the acoustic coefficients derived from the state variables processing for each simulation are not influenced by such additional resonances. In order to confirm these theoretical assumptions, a sensitivity analysis on the acoustic response of the fluid domain defined by the plenum was carried out.

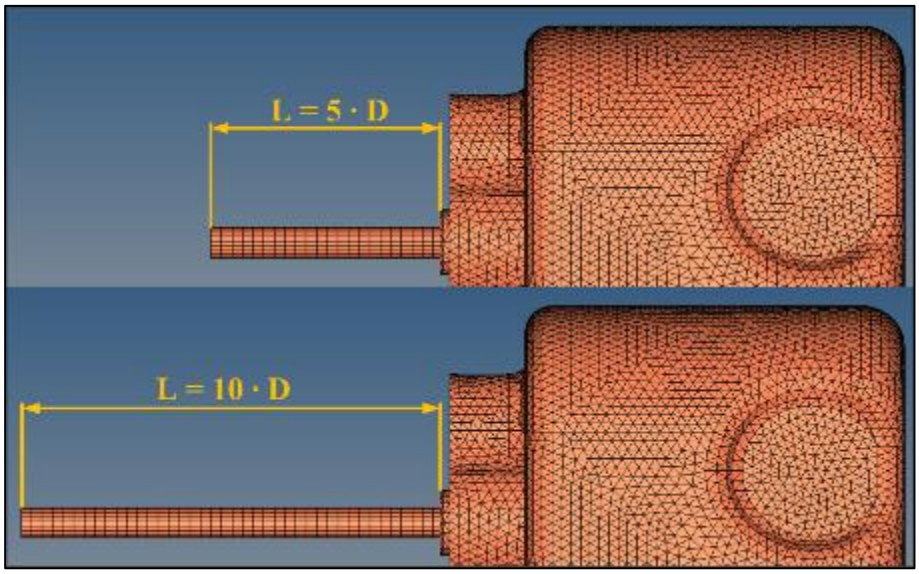

Figure 3.17 Discharge plenum inlet with different ducts extension. Mod 5 D (up) and Mod 10 D (down).

The suction plenum modified with ducts of different length (Figure 3.17) was simulated, by imposing the same boundary and thermodynamic conditions in both cases. In the first case the added duct length was of five times the diameter (namely "Mod 5 D"), while in the other case ten times (namely "Mod 10 D"). Both the pressures at the excited boundary (Figure 3.18) and the pressures at one of the outlet boundaries with anechoic termination condition (Figure 3.19) show the different acoustic response of the fluid domain. As a consequence of the different length of the added ducts, the resonant frequencies (identified by the peaks of the curves) are different in the two cases. More in details, a longer duct (Mod 10 D, solid line in the graphs) introduce resonances at lower frequencies. Otherwise shorter ducts (Mod 5 D, dotted line in the graphs) shifts resonances to higher frequencies.

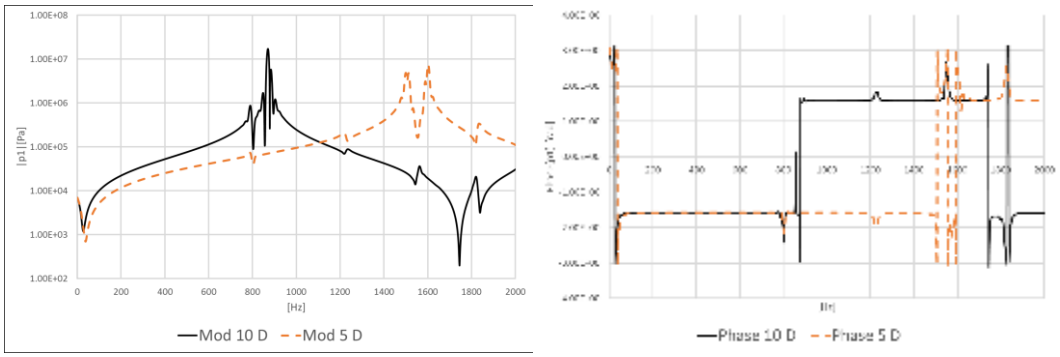

Figure 3.18 Inlet boundary (#1) pressure for the two tested configurations with different duct lengths, module (left) and phase (right).

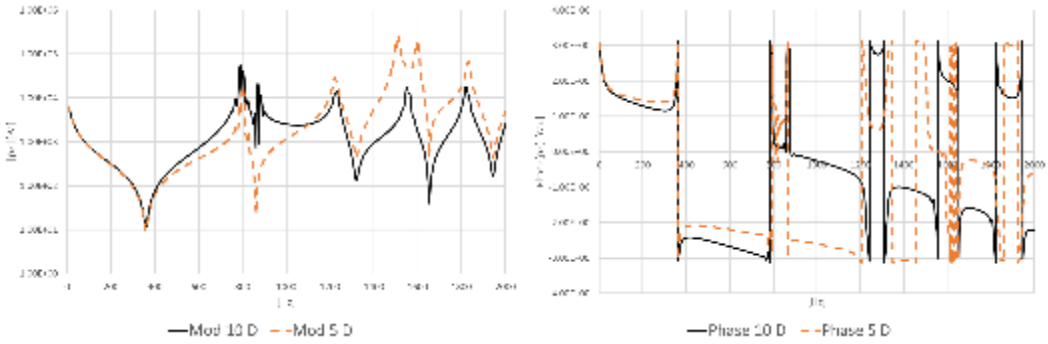

Figure 3.19 Outlet boundary (#2) pressure for the two tested configurations with different duct lengths, module (left) and phase (right).

However, the computed acoustic coefficients computation obtained by processing the simulations data confirmed that resonances do not vary the acoustic characteristic coefficients of the plenum. The state variables was shifted to the real inlet of the plenum, as described in the previous paragraph, in order to compute the plenum (without added ducts) acoustic coefficients.

In Figure 3.20 and Figure 3.21 the r_1 reflection coefficient at the inlet boundary and the t_{12} transmission coefficient (from inlet to outlet #2) are shown. The good agreement between the coefficients of the two tested configurations are not affected by the ducts and the resonances that they introduce. It follows that the acoustic properties of the characterized plenum are not influenced by the ducts added to the fluid domain.

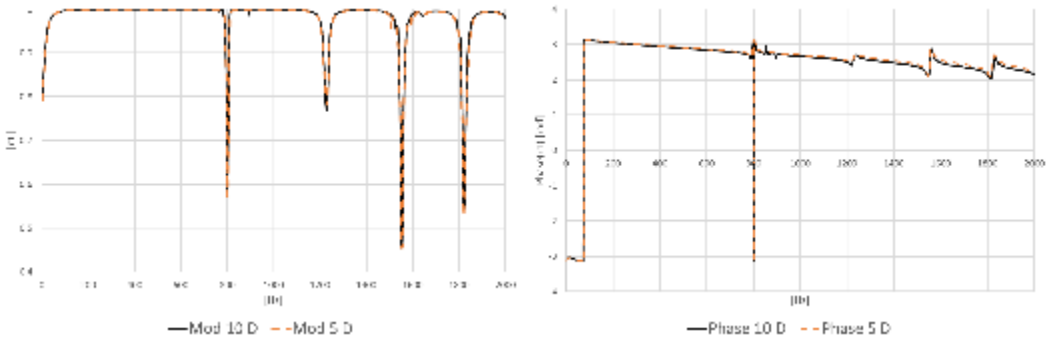

Figure 3.20 Reflection coefficient r_1 at the inlet boundary (#1) for the two tested configurations with different duct lengths, module (left) and phase (right).

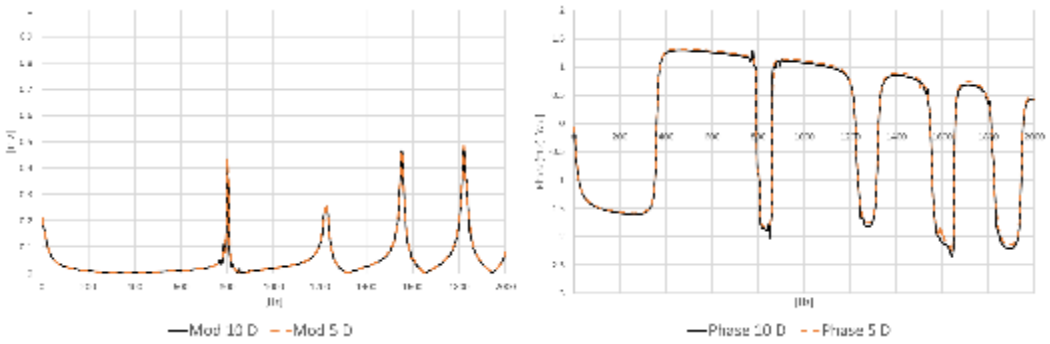

Figure 3.21 Transmission coefficient t_{12} (inlet #1-outlet #2) for the two tested configurations with different duct lengths, module (left) and phase (right).

4 Comparison of experimental and numerical data

In this chapter, the comparison between numerical and experimental data is shown. The reciprocating compressor and the experimental test circuit are simulated by using the hybrid model approach. In the analysis, two different hybrid numerical models of the compressor are tested. These models are different because of the acoustic modelling of the compressor plena. In one model, the plena are modelled with lumped acoustic volume elements (lumped elements). In the other one, the acoustic of the plena is modelled by using the 3D FEM transfer matrix. Moreover, both models are set to simulate two different configurations of pipelines external to the compressor plena: the ideal case of anechoic termination and the pipelines of the experimental test circuit. The results of each simulation are compared with experimental data in order to evaluate the numerical models reliability on the basis of both the thermodynamic cycle and the pressure wave profiles in the pipelines.

Finally, the results of the stand-alone Re.Co.A. model (i.e. constant boundary pressure profiles) are shown and compared with the results of the hybrid model with the 3D FEM matrix and the experimental test case pipelines. The differences between the hybrid model and the compressor with constant boundary pressures model are underlined by comparing the thermodynamic cycles and the mass flow profiles of the two models. A deep analysis of the work absorbed per cycle by the compressor of the two different models is also presented and compared with the experimental data.

4.1 Hybrid model

The compressor and its test circuit is simulated by using the hybrid model approach with the acoustic FEM characterized elements (i.e. the compressor plena) and the acoustic lumped elements. Both the models test two different configurations of the suction and discharge pipelines. The first configuration is the compressor and plena with anechoic terminations on the pipeline side of each plenum. In the other configuration, the elements on the pipelines are introduced in the acoustic sub-model of the hybrid model in order to consider the acoustic reflection effects. The main difference between the two configurations is that in the former there are no pressure wave reflected by the pipelines, and the pressure profiles simulated inside the plena are generated only by the two cylinders of the compressor during the suction and discharge phases. In the latter case, the numerical pressure profiles inside the plena are the superposition of the pressure waves generated by the compressor and the waves reflected by the pipelines.

4.1.1 Anechoic terminations configuration

The configuration simulated by the hybrid model is shown in Figure 4.1. In this case the hybrid model simulates the reciprocating compressor by imposing at the pipeline side of each plenum the anechoic termination condition. Such boundary condition does not introduce reflections of the pressure wave that leaves the plenum, so the only influence on the compressor thermodynamic cycle is due to the acoustic response of the plena and their interaction with the compressor.

In Figure 4.2 the thermodynamic cycles of the two compressor cylinders are compared with the experimental data. A good agreement between numerical and experimental data is observed for both the numerical simulations.

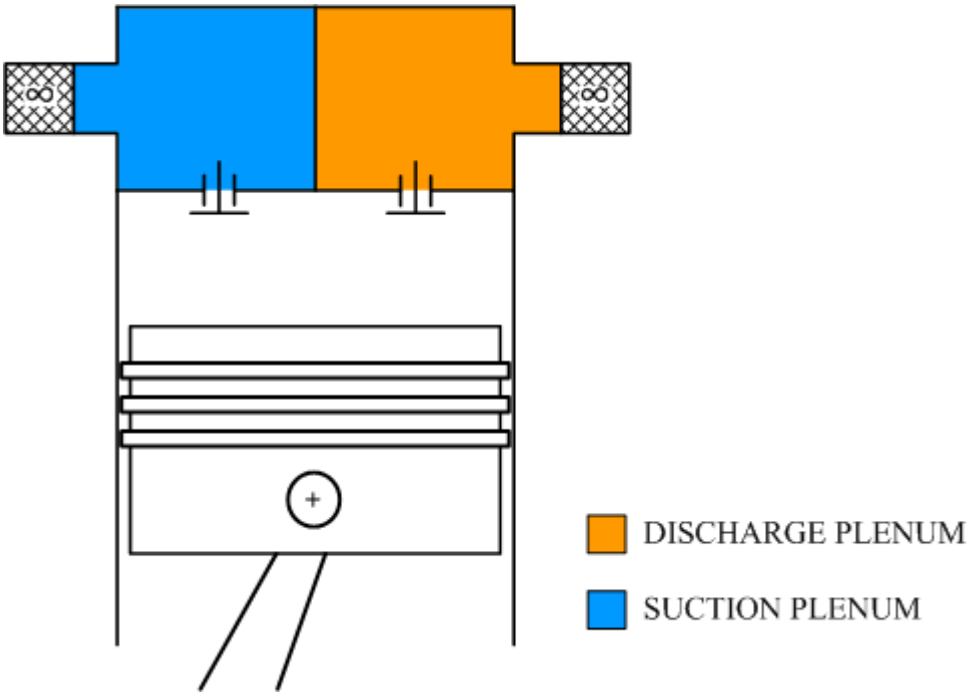

Figure 4.1 Scheme of the hybrid model configuration with anechoic terminations at the suction and discharge pipelines.

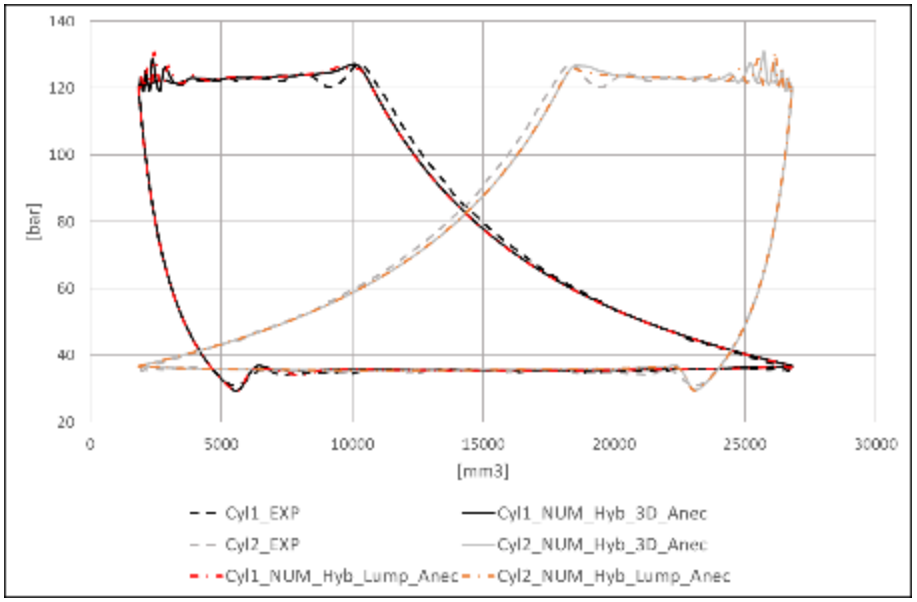

Figure 4.2 Compressor thermodynamic cycles of the two hybrid models with anechoic terminations. Comparison between numerical (NUM) and experimental (EXP) data.

The more detailed analysis of the suction phase (Figure 4.3) does not show great differences between the two models. In fact, the pressure profiles in the suction plenum of the two models are almost the same. This means that the acoustic response of the suction plenum modelled by using the acoustic FEM characterization is almost the same

of the hybrid model with the lumped acoustic elements. In fact, the pressure profiles inside the suction plenum (Figure 4.5) have almost the same trend. The small differences between the two pressure profiles are not so consistent that they can affect significantly the pressure inside the cylinder.

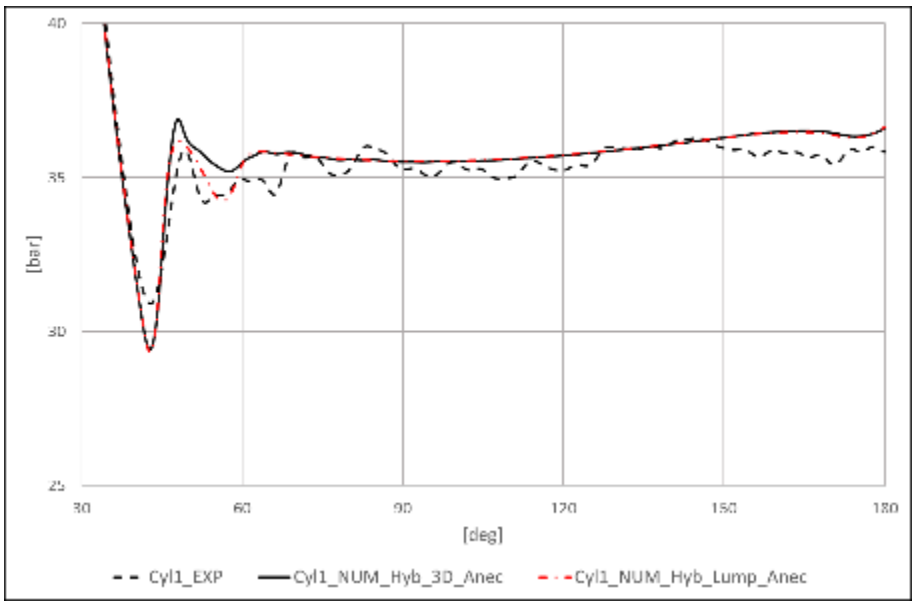

Figure 4.3 Suction phase pressures of the two hybrid models with anechoic terminations. Comparison between numerical (NUM) and experimental (EXP) data.

More marked differences between the two hybrid models are underlined by a further detailed analysis of the discharge phase (Figure 4.4). The small differences of the pressure profiles affects the valves dynamics and the mass flow during the discharge phase. More in details, in the hybrid model with lumped elements the valves open earlier than in the hybrid model with the acoustic FEM characterization, and this is due to a different acoustic response of the two different discharge plena models. This is shown in Figure 4.6, where the two discharge plena pressure profiles are shown. The small differences that affects weakly the in-cylinder pressure.

In Figure 4.5 and Figure 4.6 the plena pressure profiles of the numerical model are compared with experimental data, both in the time and in the frequency domain. Suction and discharge numerical profiles of both the simulations do not agree well with experimental data. Such differences are due to the influence on the measured pressures of the reflections introduced by the pipelines components external to the plena. In fact, the anechoic termination is not able to reproduce such reflection phenomena.

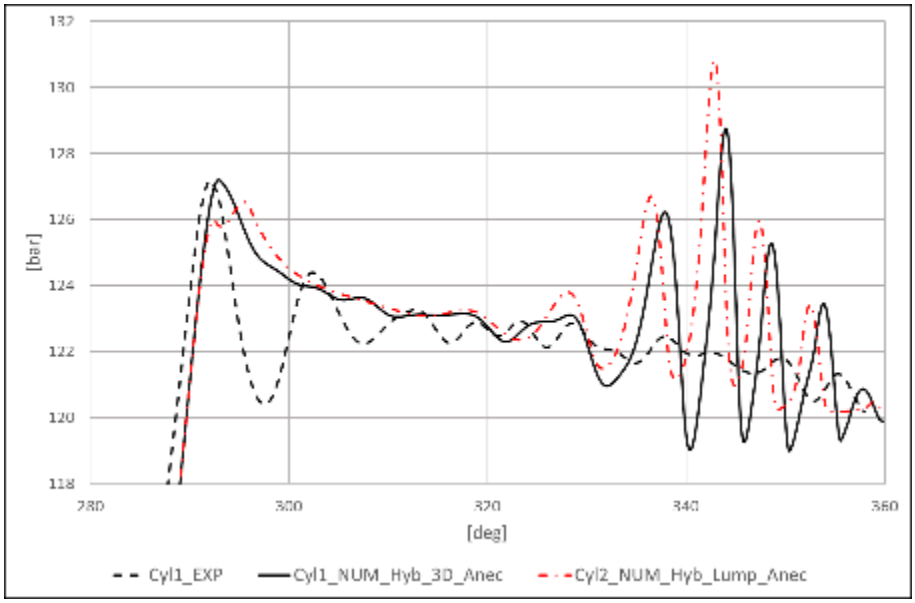

Figure 4.4 Discharge phase pressures of the two hybrid models with anechoic terminations. Comparison between numerical (NUM) and experimental (EXP) data.

It is to be noticed that the suction pressure profile is more affected by the pipeline reflection than the discharge pressure profile. In this case the fundamental oscillatory part of the pressure profile is well simulated because the acoustic response of the plenum affects the real (i.e. measured) pressure profile the most. However, the high frequency pressure oscillation in the pressure profiles are weakly reproduced by the hybrid model with the acoustic FEM characterization, while the lumped elements model computes a smooth pressure profile.

In order to carry out a complete analysis of the plena pressure wave profiles, the FFT of the experimental data and numerical results are also reported in Figure 4.5 and Figure 4.6. The comparison underlines that the numerical results are not in good agreement with the experimental data.

All these considerations suggest increasing the model complexity, modelling in the acoustic sub-model of the hybrid models also the pipelines components external to the compressor plena.

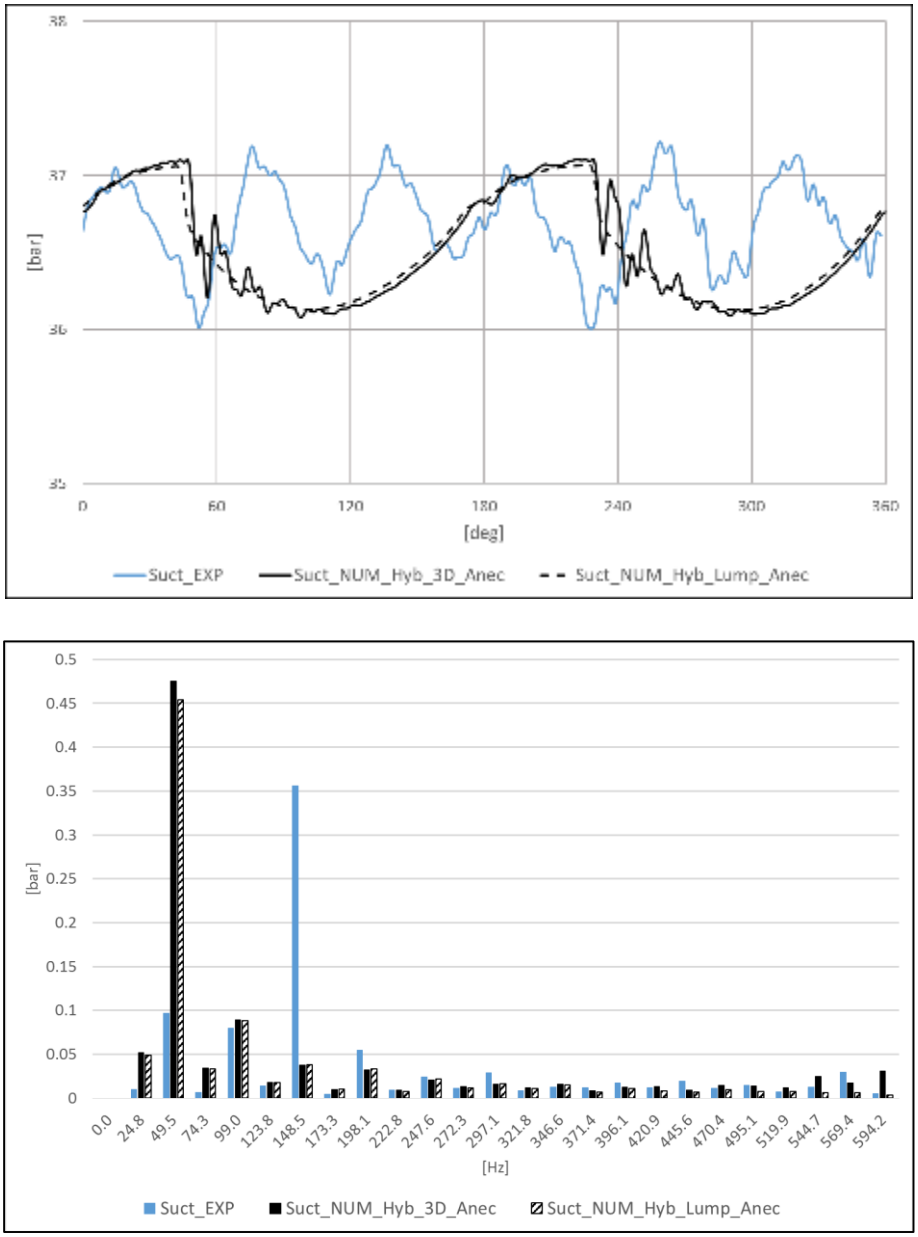

Figure 4.5 Suction plenum pressure profile of the two hybrid models with anechoic terminations. Comparison between numerical (NUM) and experimental (EXP) data. Results are expressed on the crank angle (up) and by the FFT (down).

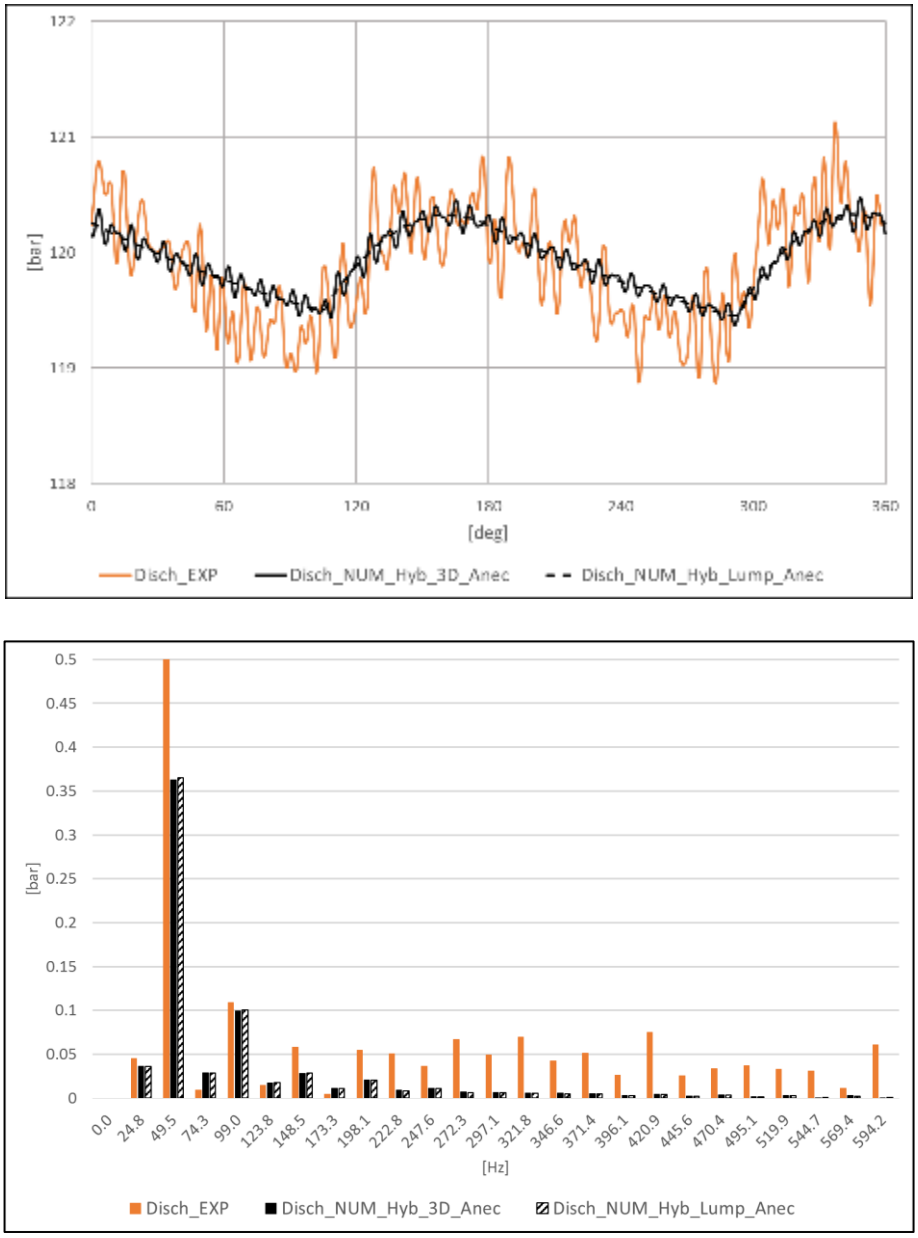

Figure 4.6 Discharge plenum pressure profile of the two hybrid models with anechoic terminations. Comparison between numerical (NUM) and experimental (EXP) data. Results are expressed on the crank angle (up) and by the FFT (down).

4.1.2 Pipelines configuration

In this configuration, the pipelines components external to the compressor plena are modelled in the acoustic sub-model of the two hybrid models. Differently from the ideal configuration with anechoic terminations, the additional elements external to the plena make the model more similar to the real test case. More in details, the pipelines boundary elements allow considering the influence on the plena pressure profiles of the pressure

waves reflected by the pipeline outside the plena. The modelled configuration is shown in Figure 4.7.

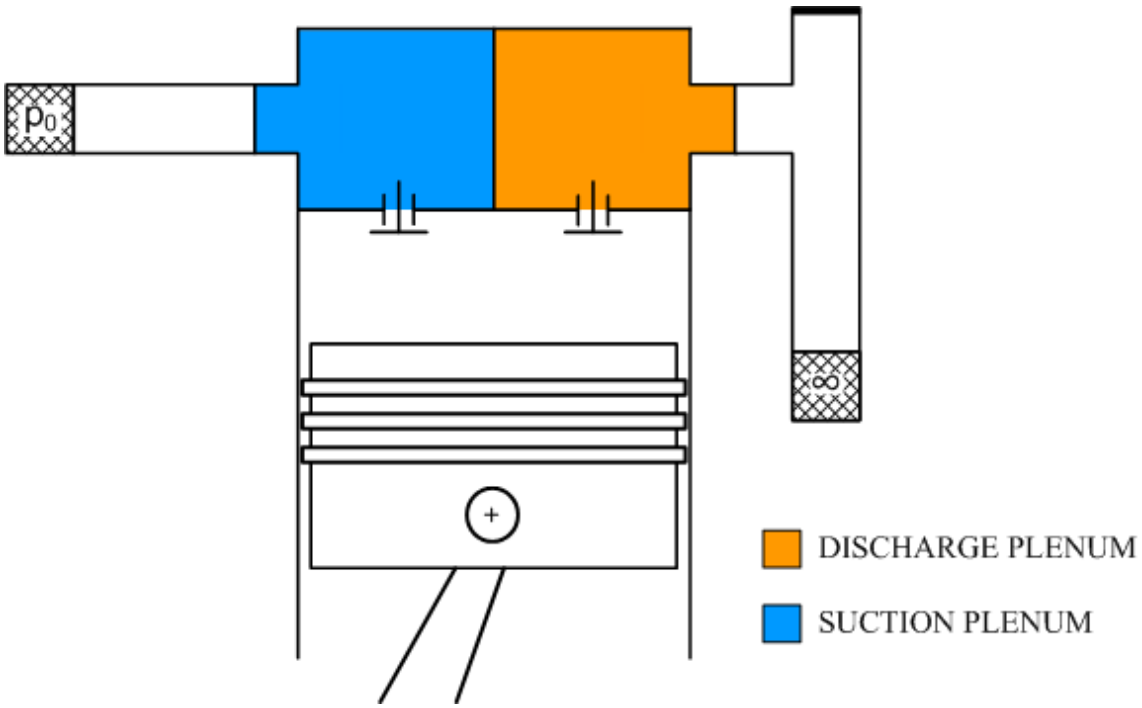

Figure 4.7 Scheme of the hybrid model configuration with the experimental test circuit pipelines.

As shown in Figure 4.7, the pipelines elements are the following:

- *Suction* – duct with ambient termination. The suction plenum communicates through a duct with the compressor basement chamber where the electric motor is (Figure 4.8). This chamber is well modelled by an ambient termination, due to its geometrical dimensions and the constant pressure conditions.
- *Discharge* – T-junction with a rigid ended duct and a duct with anechoic termination. This geometrical configuration represents exactly the discharge pipeline of the experimental test case circuit.

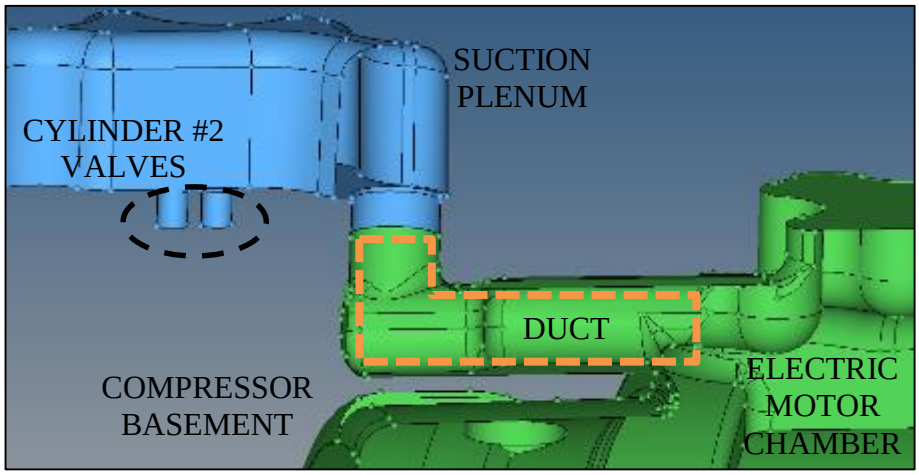

Figure 4.8 Section of the suction plenum (blue) that communicates through a duct with the electric motor chamber inside the compressor basement (green).

The thermodynamic cycles of the two simulations are shown in Figure 4.9. The pipelines configuration leads to a good global agreement between numerical and experimental data for both the hybrid models. This means that the part of pressure waves reflected by the pipelines element do not affect strongly the compressor thermodynamic cycle. However, small differences can be noted respect to the compressor model configuration with anechoic terminations.

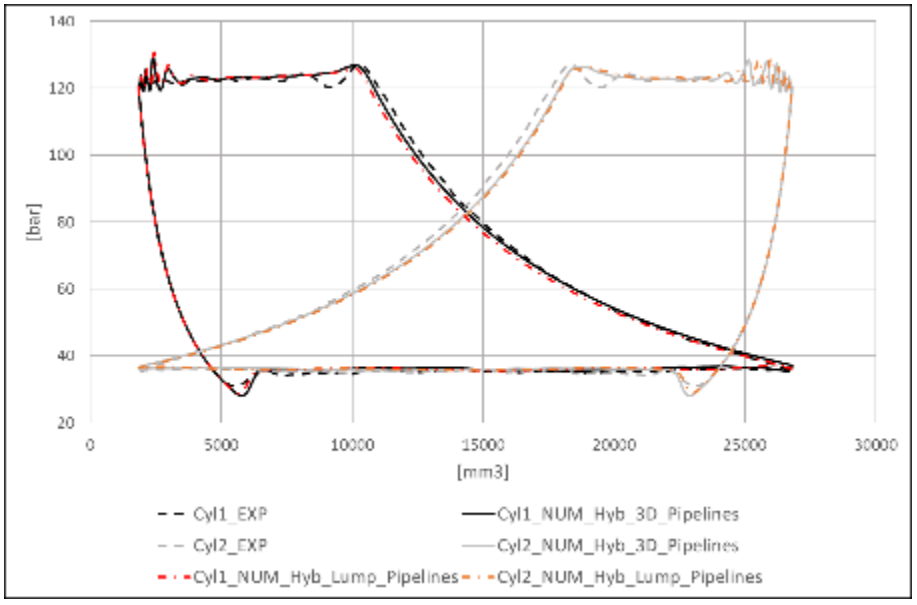

Figure 4.9 Compressor thermodynamic cycles of the hybrid models with pipelines. Comparison between numerical (NUM) and experimental (EXP) data.

A more detailed analysis of the in-cylinder pressure highlights the differences between the two hybrid models. In Figure 4.10 it is possible to notice how the in cylinder pressure of the hybrid model with the acoustic FEM characterization follows the trend of experimental data. Conversely, the hybrid model with lumped elements does not follow the same oscillatory trend of the experimental in-cylinder pressure. As shown in Figure 4.12, the two models compute different pressure trends inside the plenum. The comparison with experimental data highlights the reliability of the hybrid model with acoustic FEM characterization. With respect to the acoustic lumped elements, the higher complexity of the acoustic FEM model allows simulating well the acoustic response of the plenum, leading to a good agreement with the experimental data.

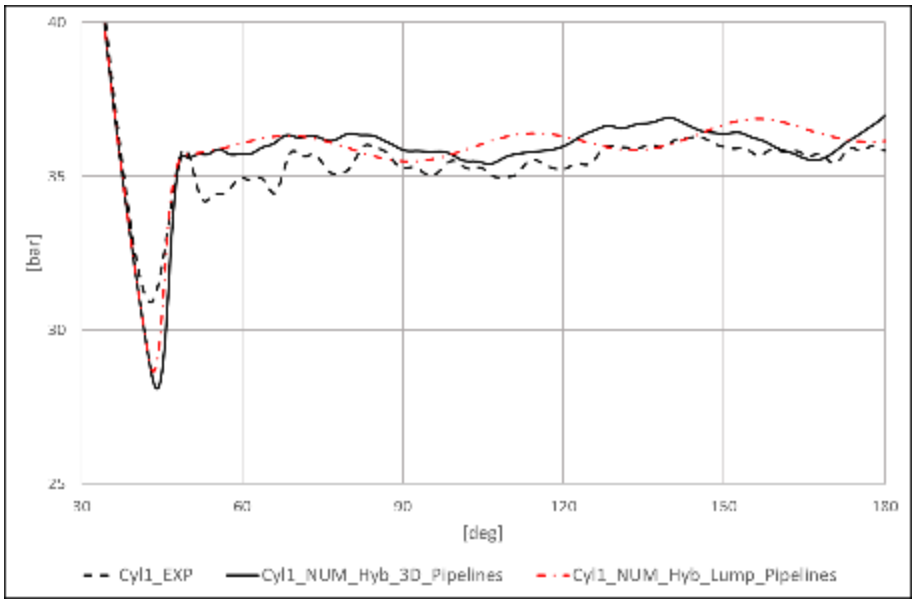

Figure 4.10 Suction phase pressures of the two hybrid models with pipelines. Comparison between numerical (NUM) and experimental (EXP) data.

A deep analysis of the in-cylinder pressure discharge phase (Figure 4.11) underlines the differences between the results of the two hybrid models. Also in this case, the acoustic FEM detailed modelling of the discharge plena lead to a better agreement with the experimental data respect to the acoustic lumped elements modelling. Respect to the anechoic termination configuration, the hybrid model with lumped elements shows a better agreement with the experimental data in the discharge phase, but the acoustic response of the plenum is still not modelled as well as by the acoustic FEM

characterization, as shown in Figure 4.11. This is confirmed also by the comparison with the experimental pressure profile inside the discharge plenum (Figure 4.13).

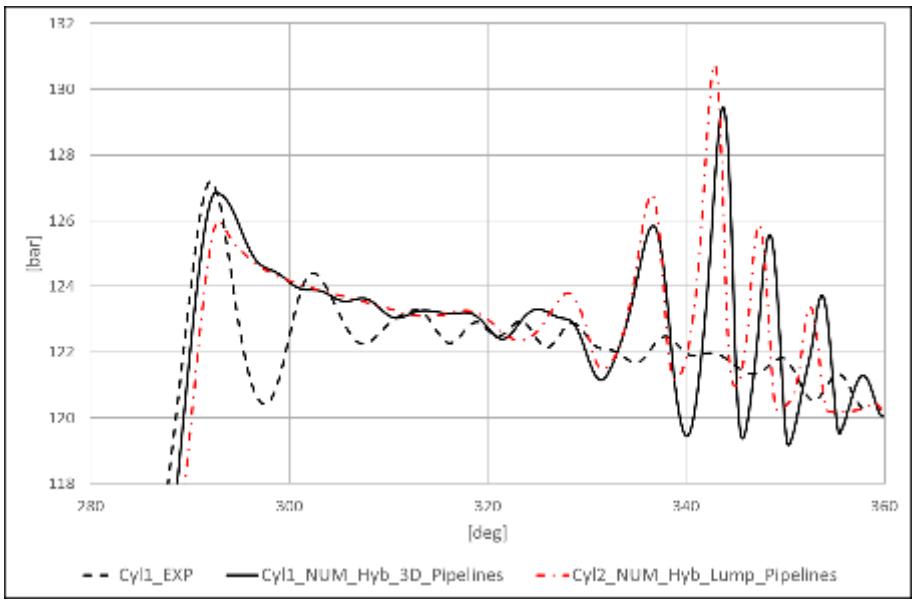

Figure 4.11 Discharge phase pressures of the two hybrid models with pipelines. Comparison between numerical (NUM) and experimental (EXP) data.

In Figure 4.12 the suction plenum pressure comparison is shown. The introduction of the duct with ambient termination on the pipeline side of the plenum leads to a good matching with experimental data in terms of plenum pressure. In the simulation results of the hybrid model with acoustic FEM characterization, it can be noticed that the main pressure oscillation (i.e. six times in a period of 360 degree) agrees with the experimental data. The other main pressure oscillation that occurs at a higher frequency, is present also in the experimental data, even if with a lower amplitude. The higher amplitude of the oscillation in the numerical data is addressed to a resonance due to the interaction between the plenum and the duct. Such resonance, in the acoustic linear equations at the basis of the acoustic modelling, is not attenuated by the average flow and fluid viscosity damping and leads to the propagation of pressure oscillations that in the experimental data have a lower amplitude. Conversely, the hybrid model with lumped elements simulates an acoustic response inside the plenum that doesn't match well the experimental data, due to the presence of a strong oscillating wave at a frequency that is not measured in the real test case. All the above considerations are underlined by the FFT analysis of the signals, as shown in Figure 4.12. It can be noticed that, while for the hybrid model with acoustic

FEM characterization there is an almost good agreement for all the frequencies, the lumped elements model shows oscillation amplitudes at 198.1 Hz, 222.8 Hz and 247 Hz that are higher than the same harmonics of the experimental data. This is addressed to the interaction of the lumped volume and the duct with anechoic termination that, due to the linearity of the acoustic modelling, propagates without any attenuation.

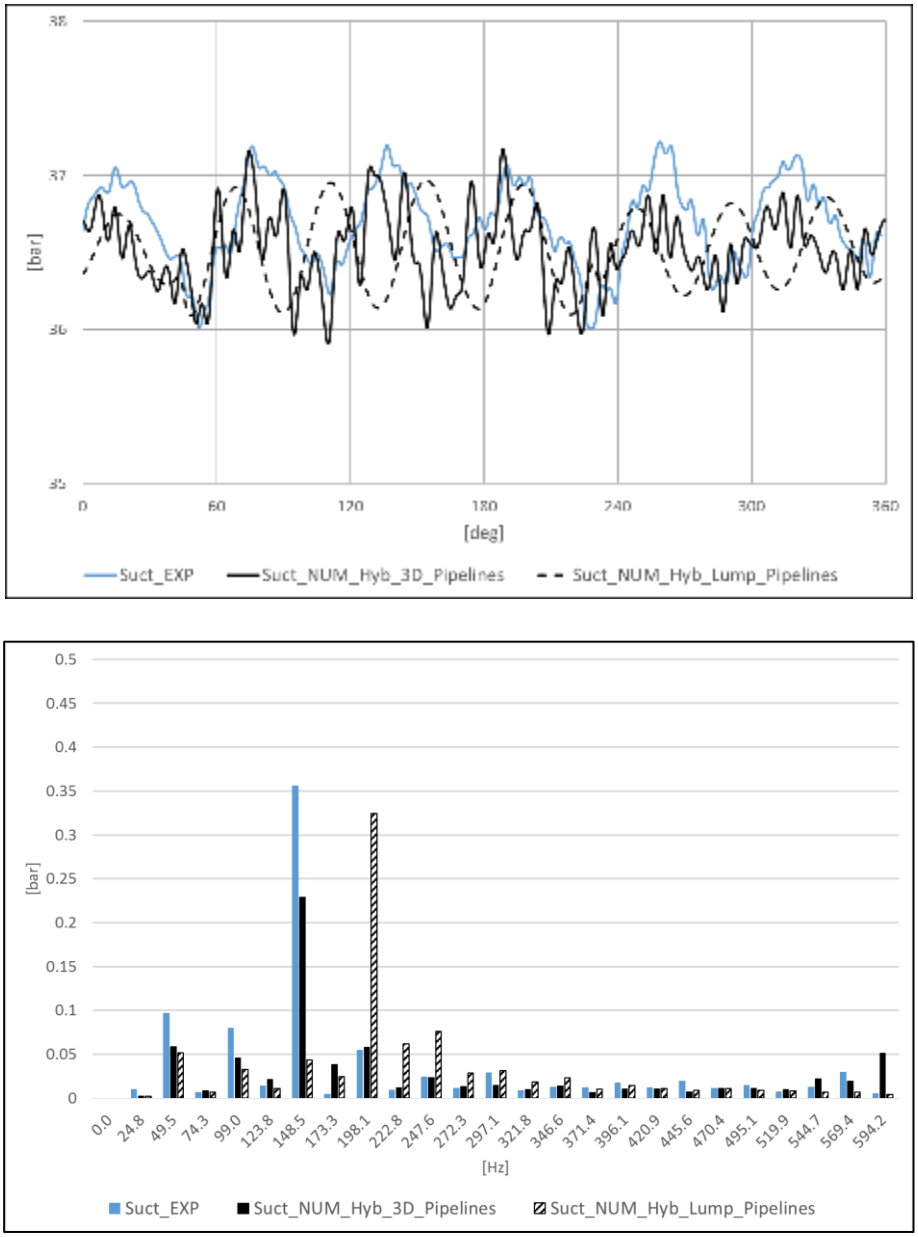

Figure 4.12 Suction plenum pressure profile of the hybrid models with pipelines. Comparison between numerical (NUM) and experimental (EXP) data. Results are expressed on the crank angle (up) and by the FFT (down).

The comparison of the pressure inside the discharge plenum (Figure 4.13) shows a very good agreement between numerical and experimental data for the hybrid model with acoustic FEM characterization. The small differences also in this case are addressed to the linear acoustic model that do not allow considering the effects of average flow. The FFT analysis of the pressure profiles highlights the reliability of the hybrid model with acoustic FEM characterization respect to the lumped elements model.

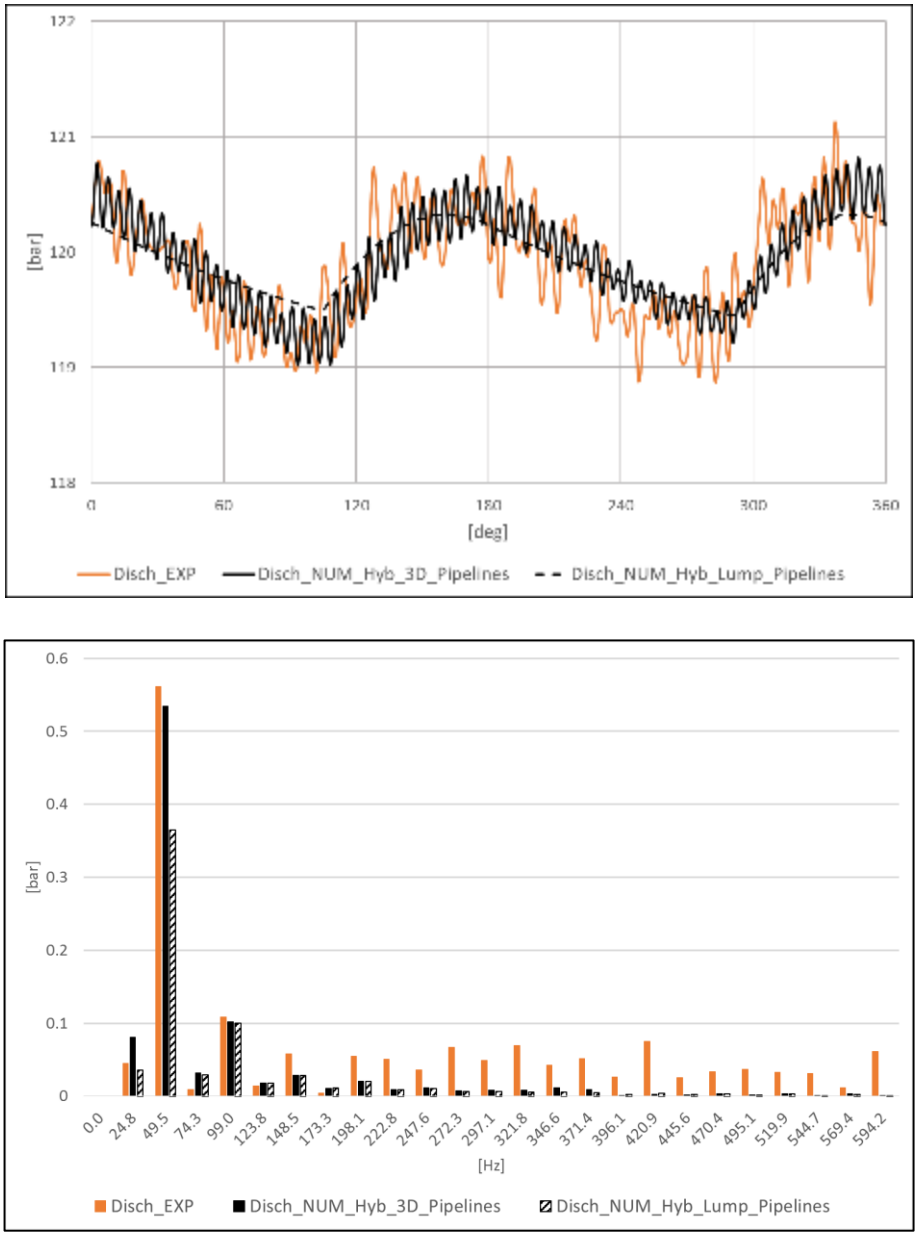

Figure 4.13 Discharge plenum pressure profile of the hybrid models with pipelines. Comparison between numerical (NUM) and experimental (EXP) data. Results are expressed on the crank angle (up) and by the FFT (down).

4.2 Hybrid model and Re.Co.A. comparison

In order to show the differences between the hybrid model with acoustic FEM characterization and the stand-alone compressor simulation with constant pressure boundary conditions, a comparison between the hybrid model with FEM acoustic characterization and the Re.Co.A. sub-model with constant boundary pressure is carried out.

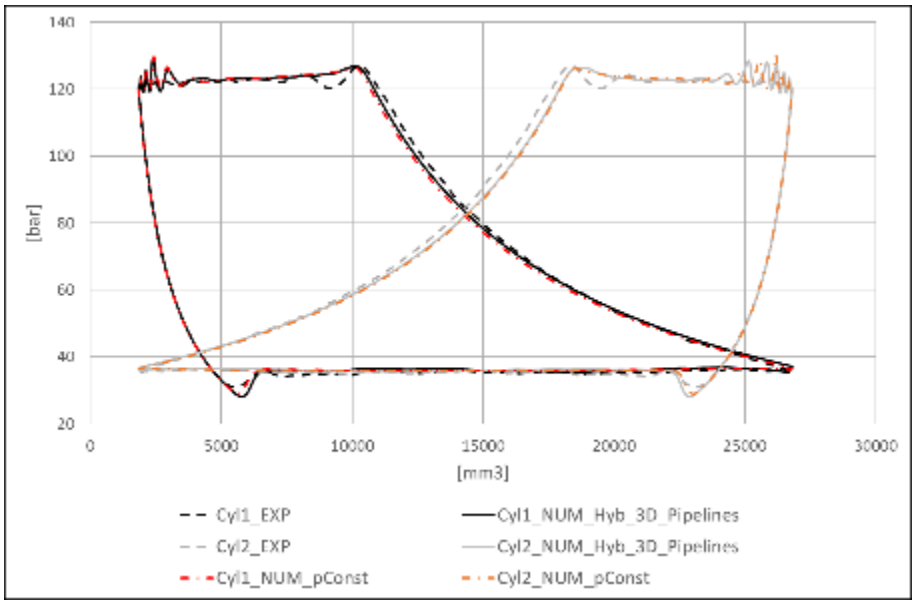

Figure 4.14 Compressor thermodynamic cycles of the hybrid 3D model and the Re.Co.A. model with constant boundary pressures. Comparison between numerical (NUM) and experimental (EXP) data.

As shown in Figure 4.14, the thermodynamic compressor cycles of both the simulations are in good agreement with experimental data. A deep analysis of the suction (Figure 4.15) and discharge (Figure 4.16) phases of the in-cylinder pressure highlight the higher details of the hybrid simulation with respect to the Re.Co.A. in terms of pressure fluctuations during both the abovementioned phases of the thermodynamic cycle.

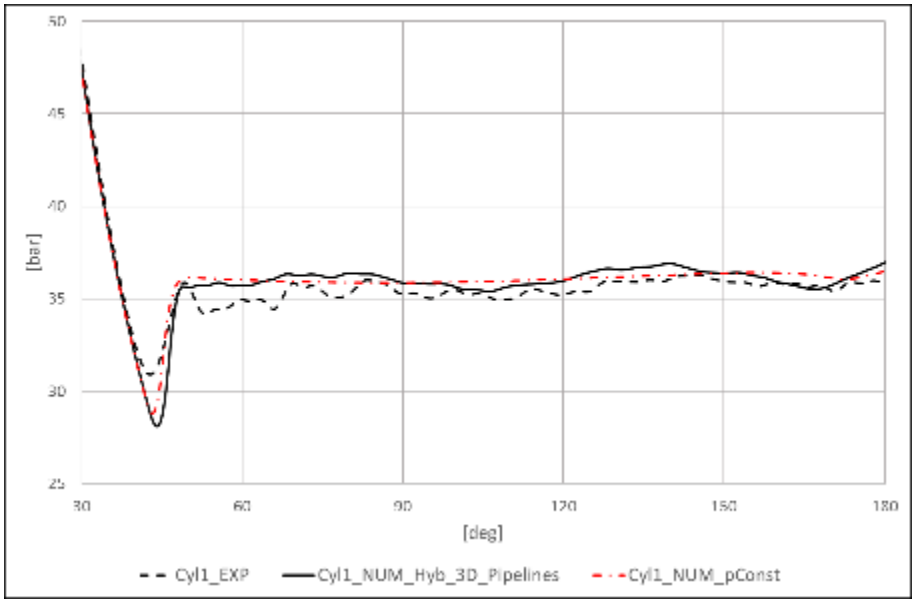

Figure 4.15 Suction phase pressures of the hybrid 3D model and the Re.Co.A. model with constant boundary pressures. Comparison between numerical (NUM) and experimental (EXP) data.

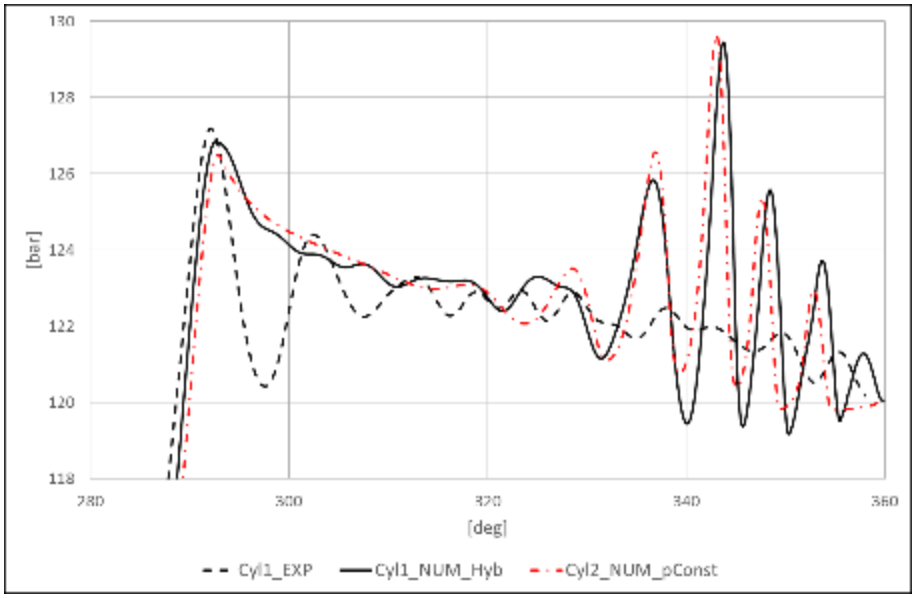

Figure 4.16 Discharge phase pressures of the hybrid 3D model and the Re.Co.A. model with constant boundary pressures. Comparison between numerical (NUM) and experimental (EXP) data.

A comparison between the results of the two models in terms of absorbed power and percent work absorbed per cycle is carried out. The percent absorbed work is computed respect to the experimental value, and is defined as follows:

$$\Delta\% = \frac{W_{sim} - W_{exp}}{W_{exp}} \qquad \textbf{[4.1]}$$

The comparison in terms of global parameters highlights the reliability of the hybrid model with acoustic characterization respect to the conventional simulation of the compressor with constant pressures at the boundaries. It is important to notice that there are not big differences (both of the models have a percentage difference less than the 3% respect to the experimental data), but it is a consequence of the experimental test case simulated. The fundamental aspect of this analysis is that the hybrid model computes results that are nearer to the experimental data, and have the potential to do the same in case of more particular test cases (e.g. different size compressors, high amplitude pressure oscillations in the plena) for which the stand-alone compressor with constant pressures at the boundaries could computes the thermodynamic cycle with bigger differences compared to the experimental one.

Moreover, the hybrid model with acoustic FEM characterization have a more detailed mass flow oscillation with respect to the compressor model with constant pressures at the boundaries. This differences between the two models in terms of suction mass flow (Figure 4.18) are stronger than the one of the discharge mass flow (Figure 4.19), due to the differences in valves oscillation. While the suction valves displacement do not have any oscillations and the mass flow is strongly affected by the pressure oscillations inside the plena, the discharge valves have high fluctuations and the mass flow is mainly conditioned by the valves displacement, except for the phase shift between the two simulations that depends on the pressure oscillations inside the plena. A more detailed mass flow profiles is an advantage for the pulsation analysis of the pipelines because lead to a complete simulation of the oscillating phenomena. As a consequence, a more detailed analysis in terms of vibration and noise can be carried out.

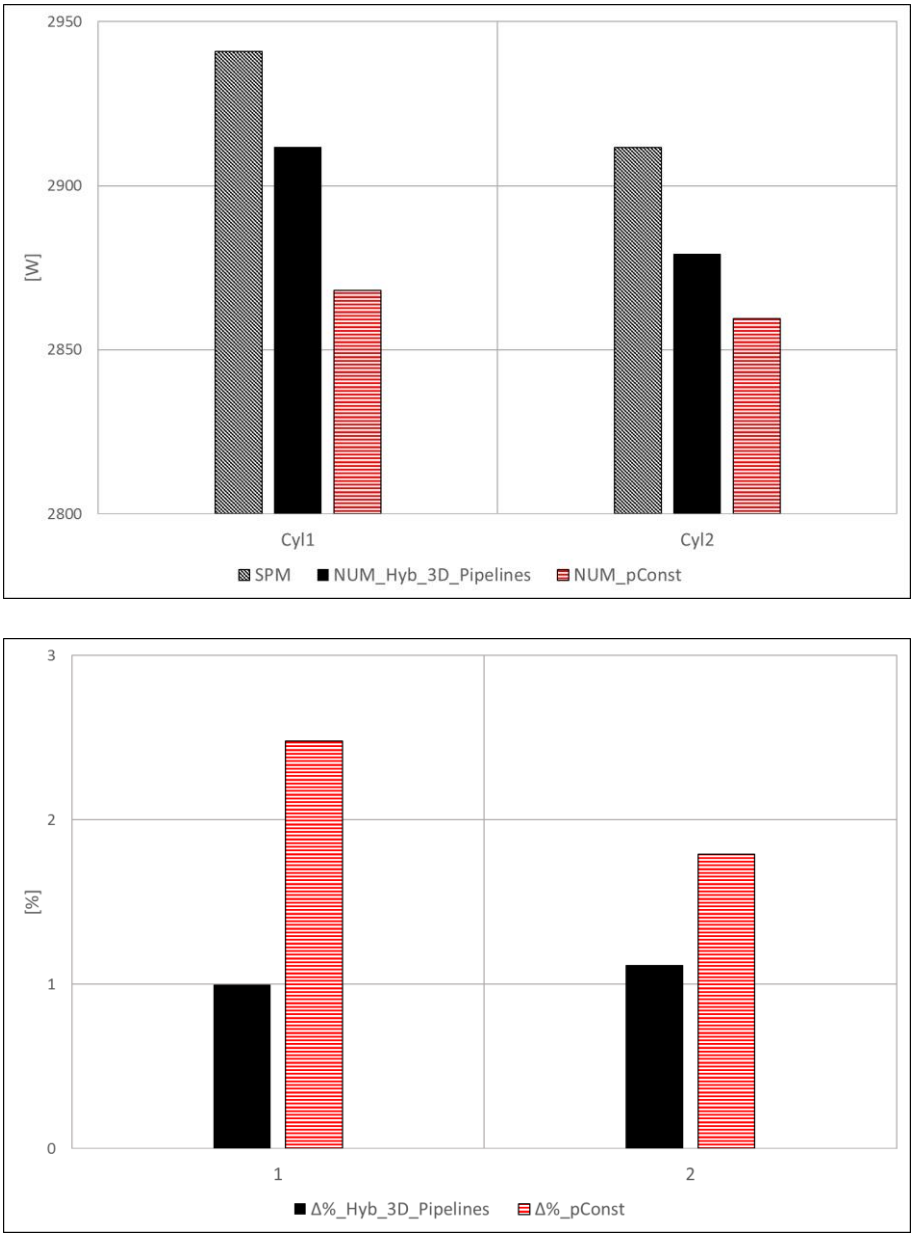

Figure 4.17 Absorbed power (up) and percent power (down) absorbed by the compressor of the hybrid 3D model and the Re.Co.A. stand-alone model with constant boundary pressures. Comparison between numerical (NUM) and experimental (EXP) data.

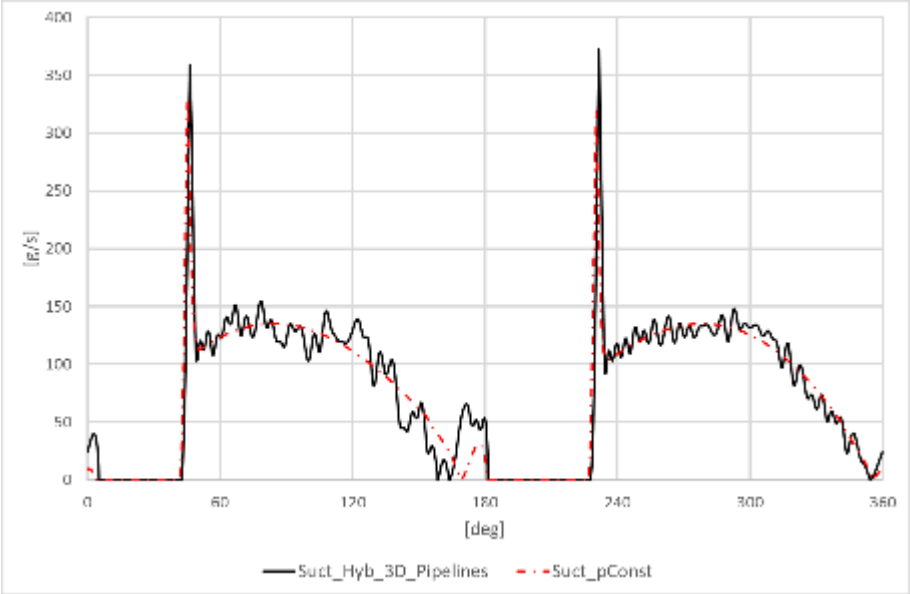

Figure 4.18 Suction mass flow profile of the hybrid 3D model and the Re.Co.A. model with constant boundary pressures.

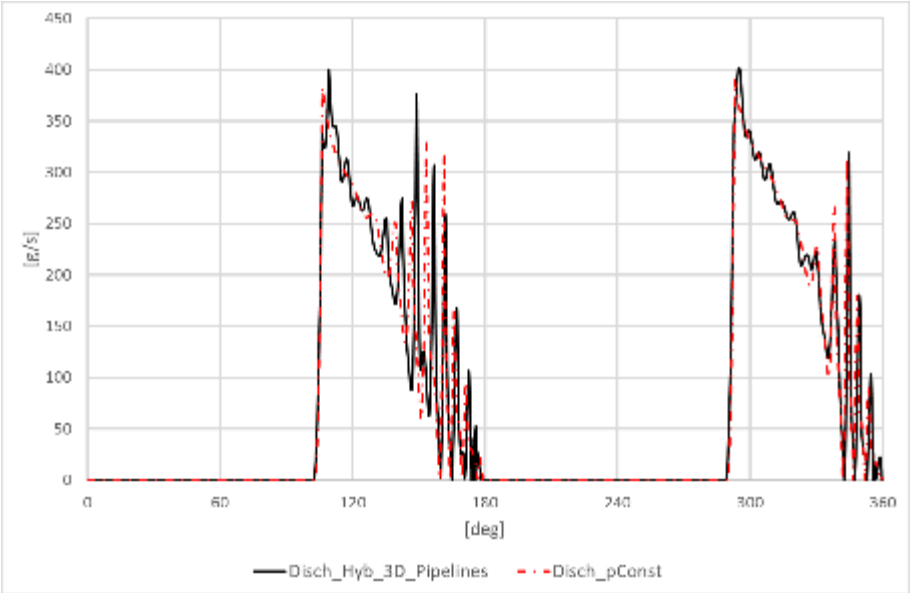

Figure 4.19 Discharge mass flow profile of the hybrid 3D model and the Re.Co.A. model with constant boundary pressures.

Conclusions

The large diffusion of reciprocating compressors and their high maintenance costs, together with the increasing worldwide demand for higher efficiency, lead to more accurate and detailed design processes, which are oriented both to performance optimization and reliability increase. In the design of reciprocating compressors and their plants, numerical simulations have an important role in the preliminary phases. In order to increase the design accuracy, the design tools used in the earliest phases of the design play a key role. These tools need to be as accurate as possible and meet the demands of engineers for usability and short computation times.

The work presented in this PhD Thesis is focused on the development and validation of a reciprocating compressor numerical model for predicting performance in the preliminary phases of design. The model allows simulating the whole compressor-pipelines system, with the advantage of analysing both the thermodynamic cycle of the compressor and the pressure waves pulsation in the pipelines. Also the interaction between the compressor and the pipelines is modelled, in order to analyse their mutual influence. The model is developed on a hybrid time-frequency domain approach. The compressor thermodynamic cycle is simulated by using a quasi-steady 0D time-domain sub-model, meanwhile the pipelines system is simulated by using an acoustic frequency-domain sub-model. The former solves the mass and energy conservation equation and the differential equation of the mass-spring-damper system that simulates the valve dynamics. The latter is based on the electroacoustic analogy and, by using transfer matrix method, solves the linear acoustic equation that describe the pressure wave propagation inside the geometrically defined fluid domain. The two sub-models interact by means of the FFT and inverse FFT of the numerical signals through which the compressor and

pipelines (i.e. mass flow and boundary pressure profiles) achieve the mutual interaction. In the past, hybrid models were developed, which simulated the compressor-pipeline interaction evaluation by simplifying strongly the pipeline complex geometries, especially concerning compressor plena. In some cases this led to approximated results that required the use of corrective terms to better match the experimental data.

In order to simulate the whole compressor system with a higher level of detail and to consider the interaction influence on both the compressor thermodynamic cycle and the pressure wave propagation in the pipelines, a numerical hybrid model integrated with a numerical acoustic FEM characterization is defined. By using the acoustic characterization it is possible to compute the transfer matrix of fluid domains with any geometry. Subsequently, the transfer matrix is used in the acoustic simulation of the hybrid model. It follows that the quasi-steady compressor model computes in details the thermodynamic cycle and valve dynamics for each step of the compressor cycle. Moreover, the acoustic approach allows simulating the acoustic response of complex geometry elements after their numerical or experimental acoustic characterization, which is previously carried out to define the element transfer matrix. This approach leads to a more detailed and generally applicable model of the compressor with particular attention to the typical complex geometry elements (mainly the compressor plena) without increasing the computational costs of the numerical simulations.

With the aim of validating the hybrid model approach, an experimental activity on a reciprocating compressor for refrigeration applications was carried out. The hybrid model accuracy was assessed through the comparison of numerical results with experimental data. The comparison is made in terms of both the compressor thermodynamic cycle and the pressure profiles inside the compressor suction and discharge plena.

In order to assess the reliability of the hybrid model with the acoustic FEM characterization with respect to the conventional acoustic modelling, the test case reciprocating compressor was simulated by using both the acoustic complex elements characterized through acoustic FEM simulations and the equivalent simplified geometries elements (i.e. acoustic lumped elements). The compressor experimental test circuit was simulated by the hybrid model with two different configurations of the suction and

discharge pipelines. One is the compressor and plena with anechoic terminations (i.e. no wave reflections) on the pipeline side of each plenum, the other one is the compressor with experimental test circuit pipelines. In the former case, the comparison between the numerical and experimental pressure profiles inside the plena did not show a good agreement with experimental data. On the contrary, in the second configuration, the elements on the pipeline side of each plenum were introduced in the pipeline configuration of the hybrid model in order to consider the acoustic reflection effects. In this case, a very good match with experimental data was achieved.

The results of the more detailed complex elements simulation show a better agreement with experimental data respect to the lumped elements configuration results. Both the pressure fluctuations in the plena and the thermodynamic cycle of the compressor confirm the accuracy of the hybrid model with FEM acoustic characterization in simulating the phenomena concerning the thermodynamic cycle and the pressure wave propagation in the plena and the pipelines.

The comparison between the two hybrid models highlighted the improvement of results accuracy due to the use of the acoustic FEM characterization for modelling the compressor plena. Moreover, the numerical results of the two different pipelines configurations underlined the sensitivity of the model to different boundary conditions, and the influence of the different boundary conditions on both the compressor thermodynamic cycle and plena pressure profiles. Conversely, the hybrid model with lumped elements led to a less accurate matching with the experimental pressure profiles inside the plena, both in terms of frequencies and amplitude highlighted by the FFT of the results.

In the final part of the sensitivity analysis of the hybrid model, a numerical comparison between the hybrid model with acoustic FEM characterization and the stand-alone compressor model with constant pressure boundary conditions was also carried out. The comparison in terms of power, percent work absorbed per cycle and mass flow profiles highlighted the improvement on numerical results due to the simulation with the hybrid model with acoustic FEM characterization.

The hybrid compressor model using acoustic FEM characterization is innovative and can overcome the limitation of mono-dimensional modelling, which cannot simulate geometrical complex elements, without increasing the computational costs that need to be maintained as low as possible in the first phases of the design process.

References

[1] K. H. An, J. H. Lee, I. W. Lee, I. S. Lee and S. C. Park, "Performance prediction of reciprocating compressor," in *International Compressor Engineering Conference,* 2002.

[2] F. Balduzzi, "Development of a CFD approach for the performance prediction of reciprocating compressors," PhD Thesis, , Florence, 2012.

[3] R. Aigner, "Internal flow and valve dynamics in a reciprocating compressor," PhD Thesis, Wien, 2007.

[4] E. Winandy, C. Saavedra and J. Lebrun, "Simplified modelling of an open type reciprocating compressor," *International journal of thermal sciences and signal processing,* vol. 41, pp. 183-192, 2002.

[5] M. Elhaja, "Numerical and experimental study of a two-stage reciprocating compressor for condition monitoring," *Mechanical systems and signal processing,* vol. 22, pp. 374-389, 2008.

[6] D. Deffenbaugh, "Advanced reciprocating compression technology," Pittsburgh, 2005.

[7] M. Nored, D. Tweten and K. Brun, "Compressor station piping noise: noise mechanisms and prediction methods," Gas Machinery Research Council - South West Research Institute, 2011.

[8] A. B. Tramschek and J. F. T. MacLaren, "Simulation of a reciprocating compressor accounting for interaction between valve movement and plenum chamber pressure," in *International Compressor Engineering Conference*, 1980.

[9] R. Singh and W. Soedel, "Mathematical modeling of multicylinder compressor discharge system interactions," *Journal of Sound and Vibration*, vol. 1, no. 63, pp. 125-143, 1979.

[10] K. Novak and J. Sauls, "Comparing FEM transfer matrix simulated compressor plenum pressure pulsations to measured pressure pulsations and to CFD results," in *International Compressor Engineering Conference*, 2012.

[11] W. A. Griffith and E. B. Flanagan, "Online continuous monitoring of mechanical condition and performance for critical reciprocating compressors," in *Proceeding of the 30th Turbo-machinery Symposium*, Texas A&M University, Houston, 2001.

[12] Nuovo Pignone, "Cylinder valve training".

[13] Nuovo Pignone, "Calcolo delle pulsazioni di pressione negli impianti dotati di compressori alternativi mediante simulatore analogico".

[14] L. Romani, "Advanced methodology for the characterization of reciprocating compressors," PhD Thesis, Florence, 2013.

[15] M. Costagliola, "Theory of spring loaded valves for reciprocating compressors," *Journal of Applied Mechanics*, vol. 4, no. 17, 1950.

[16] H. Bukac, "Understanding valve dynamics," in *International Compressor Engineering Conference*, 2002.

[17] B. G. S. Prasad, "Regenerative haet transfer in reciprocating compressors," Dresser Rand, Painted Post, New York.

[18] W. J. D. Annand, "Heat transfer in the cylinders of reciprocating internal combustion engines," *Journal of Mechanical Engineering,* no. 117, pp. 973-986, 1963.

[19] A. Almasi, "Pulsation suppression device design for reciprocating compressor," World Academy of Science, Engineering and Technology, 2009.

[20] M. L. Munjal, ACoustic of ducts and mufflers, New York: Wiley Interscience, 1987.

[21] T. W. Wu and P. Zhang, "Boundary element analysis of mufflers with an improved emtod for deriving the four-pole parameters," *Journal of Sound and Vibration,* vol. 217, no. 4, pp. 767-779, 1998.

[22] N. Bilal, D. Adams, K. Novak and J. Sauls, "General case for derifing four pole coefficients for gas pulsation," in *International Compressor Engineering Conference*, 2010.

[23] A. Fioravanti, G. Lenzi, G. Ferrara, G. Vichi, S. Ricci and L. Bagnoli, "Assessment and experimental validation of a 3D acoustic model of a motorcycle muffler," *SAE International Journal of Engines,* 2015.

[24] W. Desmet and D. Vandepitte, "Finite Element Modeling for Acoustics," in *International seminar on Applied Acoustics,* Leuven, 2002.

[25] X. Lin, "Simulation of valve dynamics in a large reciprocating compressor," Master Degree Thesis, New Brunswick, 1994.

[26] E. Giacomelli, "Simulation of cylinder valves for reciprocating compressor," in *ASME Conference of Engineering System Design and Analysis*, Torino, 2006.

[27] Y. Sathyanarayana and M. L. Munjal, A hybrid approach for aeroacoustic analysis of the exhaust systems.